The Fucino 250-170 ka tephra record: new insights on peri-Tyrrhenian explosive volcanism, central Mediterranean tephrochronology, and timing of the MIS 8-6 climate variability

Lorenzo Monaco[a, b], Niklas Leicher[c], Danilo. M. Palladino[d], Ilenia Arienzo[e], Fabrizio Marra[f], Maurizio Petrelli[g], Sebastien Nomade[h], Alison Pereira[i], Gianluca Sottili[d], Sandro Conticelli[j], Massimo D'Antonio[k], Alessandro Fabbrizio[l], Brian R. Jicha[m], Giorgio Mannella[a], Paola Petrosino[k], Polychronis C. Tzedakis[n], Bernd Wagner[c], Giovanni Zanchetta[a], Biagio Giaccio[b, f, *]

Affiliations
a Dipartimento di Scienze della Terra, University of Pisa, Pisa, Italy
b Istituto di Geologia Ambientale e Geoingegneria, CNR-IGAG, Monterotondo, Rome, Italy
c Institute of Geology and Mineralogy, University of Cologne, Cologne, Germany
d Dipartimento di Scienze della Terra, "Sapienza" - University of Rome, Rome, Italy
e Istituto Nazionale di Geofisica e Vulcanologia, Osservatorio Vesuviano, Naples, Italy
f Istituto Nazionale di Geofisica e Vulcanologia, INGV, Rome, Italy
g Dipartimento di Fisica e Geologia, University of Perugia, Perugia, Italy
h Laboratoire de Sciences du Climat et de l'Environnement, UMR 8212, CEA-UVSQ, IPSL and Université de Paris-Saclay, Gif-sur-Yvette, France
i Université Paris-Saclay, CNRS, UMR 8148, Laboratoire GEOPS, Orsay, 91405, France
j Dipartimento di Scienze della Terra, Università degli Studi di Firenze, Florence, Italy
k Dipartimento di Scienze della Terra, dell'Ambiente e delle Risorse, Università degli Studi di Napoli Federico II, Naples, Italy
l Institute of Petrology and Structural Geology, Faculty of Science, Charles University, Albertov 6, 12843 Prague, Czech Republic
m Department of Geoscience, University of Wisconsin-Madison, Madison, Wisconsin, USA
n Environmental Change Research Centre, University College London, London, UK
** Corresponding author*

ABSTRACT

The Fucino Basin, central Italy, with its long and continuous history of Quaternary sediment accumulation, is one of the richest Mediterranean Middle Pleistocene tephra records. Here, we present a new detailed investigation of tephra layers of the 250-170 thousand years before present (ka) interval, corresponding to the entire Marine Isotope Stage (MIS) 7 and parts of the MIS 8 and MIS 6. The investigated tephra layers have been characterised in terms of major, minor and trace elements, Sr-Nd isotopic compositions and $^{40}Ar/^{39}Ar$ ages. For correlation purposes, glass compositions and several new $^{40}Ar/^{39}Ar$ ages of selected proximal pyroclastic units spanning the same temporal interval from Vulsini (Latera Volcanic Complex), Sabatini, and Vico volcanic systems, central Italy, were measured. The late MIS 8-early MIS 6 Fucino tephras were backtracked to their corresponding volcanic sources, which include the Vulsini, Vico, Sabatini, Roccamonfina, Ischia and Campi Flegrei volcanic systems. While some of these tephra layers have been correlated to specific eruption units, other layers are currently not documented or described in near-vent sections, thus highlighting previously unrecognised events generated by these volcanic systems. Furthermore, the new high precision $^{40}Ar/^{39}Ar$ ages provide improved temporal constraints for Fucino making

it one of the most detailed and chronologically best constrained tephra records for central Mediterranean MIS 7 tephrochronology. The Fucino record thus provides new integrative information for reconstructing the explosive history of Italian volcanoes during the investigated time interval. Furthermore, the geochronological constrains provide the basis for future paleoclimatic investigations at local and regional scale.

1. Introduction

Past changes in the Earth's climate system are being explored in ever greater temporal detail to obtain a better understanding of the role of the orbital forcing and the interaction dynamics among its different components (e.g., cryosphere and oceanic-atmospheric circulation, and their regional expression and impact). Simultaneous to the advent of this high- to ultrahigh-resolution investigation approach, the urgency of precise and accurate chronologies becomes crucial. However, for changes before 55 ka, i.e., the current limit of the radiocarbon dating (e.g., Reimer et al., 2020), the chronology of the proxy records often is still limited by relatively high uncertainties, assumptions, and circular reasonings (e.g., astronomical tuning procedures). Reducing the uncertainties in dating and correlations, as well as making the chronology of the proxy series independent of any assumptions, are therefore becoming an urgent issue in paleoclimate studies.

In this framework, tephrostratigraphy and tephrochronology, that constitute the methods through which sedimentary successions can be synchronized and dated via geochemical and geochronological tephra fingerprinting (e.g., Davies et al., 2010), are now considered an outstanding tool for addressing several topics of the Quaternary sciences (Lowe, 2011; Lane et al., 2017), such as paleoclimatology (Lane et al., 2013; Blockley et al., 2014; Kutterolf et al., 2019), archaeology (Giaccio et al., 2008, 2017a; Lane et al., 2014; Pereira et al., 2018; Zanchetta et al., 2018; Villa et al., 2020), and paleogeographic-tectonic evolution (e.g., Giaccio et al., 2012a; Galli et al., 2017; Bini et al., 2020). Distal tephrostratigraphy is also increasingly being exploited for volcanological purposes, becoming a fundamental and integrative tool for a detailed reconstruction of the history, dynamics, and timing of explosive volcanism (e.g., Thorarinsson, 1944, 1981a, 1981b; Giaccio et al., 2014; Ponomareva et al., 2015; Albert et al., 2019; Wulf et al., 2020; Monaco et al., 2021).

However, such a great potential strongly depends on the completeness and quality of the available tephra geochemical and geochronological datasets that allow their unambiguous identification through diagnostic features, among which the geochemical glass composition is one of the most powerful (e.g., Smith and Westgate, 1968; Hayward, 2011; Lowe et al., 2017; Pearce et al., 2019).

Although tephrochronology can be applied to all regions of the Earth characterised by intense and frequent volcanism (e.g., Shane, 2000; de Fontaine et al., 2007; Wastegård et al., 2013; Albert et al., 2018; De Maisonneuve & Bergal-Kuvikas, 2020; Chen et al., 2022; Sunyé-Puchol et al., 2022), the Mediterranean area (Fig. 1a) is as an ideal region for its development and application. This is due to the complex geodynamic setting of the region, the widespread and geochemically diverse Quaternary magmatism (e.g., Wilson and Bianchini, 1999), and the abundant continental and marine basins acting as fundamental traps for sediments and tephra layers (e.g., Paterne et al., 1986, 1988, 2008; Wulf et al., 2004, 2008, 2012; Bourne et al., 2010, 2015; Satow et al., 2015; Petrosino et al., 2016; Giaccio et al., 2017a, 2019; Leicher et al., 2019, 2021; Vakhrameeva et al., 2021). Furthermore, the alkaline magmas feeding the peri-Tyrrhenian potassic Quaternary volcanoes (e.g., Peccerillo, 2017) generated products bearing K-rich minerals (e.g., sanidine and leucite), which are ideal for direct $^{40}Ar/^{39}Ar$ dating. The significant technological developments of noble gas mass spectrometers over the last decade, such as the introduction of the multi-collector spectrometer Isotopx NGX-600 (Mixon et al., 2022), have improved the effectiveness of the method and the possibility of getting direct, high-precision $^{40}Ar/^{39}Ar$ dating of fine-grained distal tephra (e.g., Albert et al., 2019; Monaco et al., 2022).

The lacustrine succession hosted in the Fucino Basin, central Italy (Fig. 1c), with its long and continuous Quaternary sediment accumulation history, combined with its downwind position relative to the preferential axis of volcanic ash dispersion in the region and the numerous tephra layers hosted in its sediments, proves to be the richest Mediterranean Middle Pleistocene tephra record (Giaccio et al., 2017a, 2019; Di Roberto et al., 2018; Del Carlo et al., 2020; Monaco et al., 2021). Here we present a detailed investigation of the tephra succession spanning the ~250-170 ka interval from the Fucino lake sediments recovered in the F4-F5 core documenting the last 430 kyr (Giaccio et al., 2019; Monaco et al., 2021). The selected interval spans from the late MIS 8 to the early MIS 6 glacial periods, ~250-170 ka, and thus encompasses the whole MIS 7 interglacial complex. Current knowledge on this interval is still incomplete in terms of both regional pyroclastic succesions, either from the proximal or distal archives, and of the wider Mediterranean tephrochronology, as only few archives in this region cover this particular interval (Fig. 1). Therefore, the detailed investigation of the MIS 7 tephra from Fucino lake succession offers the opportunity of improving our knowledge on the regional explosive volcanism for this interval. Ultimately, this will also allow setting the basis for extending the use of the tephrochronology for any application in Quaternary Sciences, such as paleoclimatology, paleogeography, tectonics, and archaeology, in the central Mediterranean region for the late MIS 8-early MIS 7 period.

To achieve these results, here we have analysed 21 Fucino tephra layers, in terms of major, minor and trace elements, Sr-Nd isotope ratios and provided new $^{40}Ar/^{39}Ar$ ages. Furthermore, to improve the reference geochemical dataset required for establishing reliable correlations of the Fucino tephra with the corresponding near-vent volcanic deposits and other distal archives, we also studied some proximal pyroclastic successions from Vulsini, Vico, and Sabatini volcanoes, and one distal tephra from the Lake Ohrid succession, both spanning the same temporal interval of the investigated Fucino tephra. The results of this study are discussed both in terms of the volcanic histories and recurrence time intervals at the peri-Tyrrhenian Quaternary volcanoes and of tephrochronological constraints for the Mediterranean MIS 7 sedimentary archives.

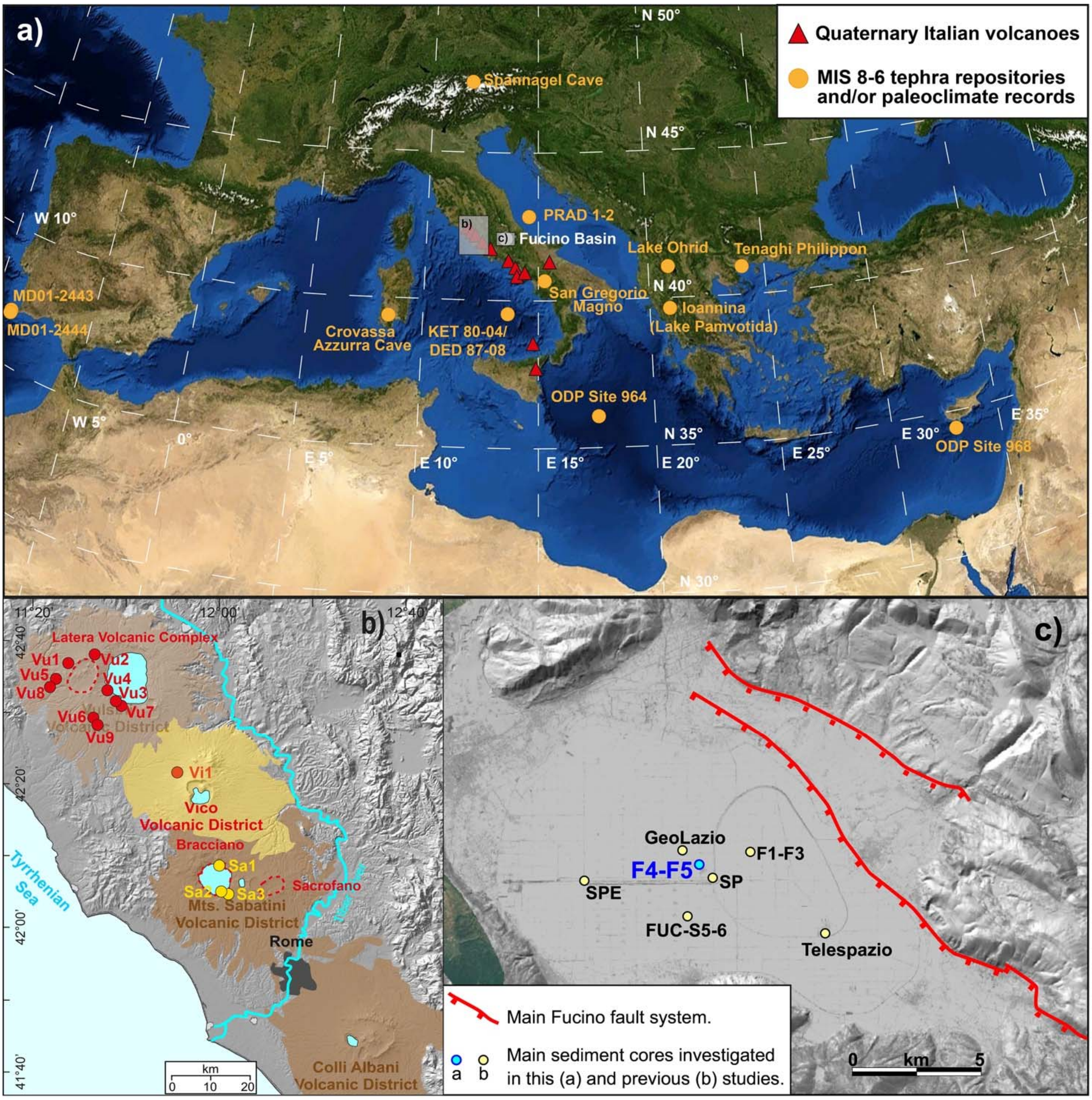

Figure 1. Reference maps. **a)** Map of the Central Mediterranean with the location of the Fucino Basin, the continental and insular Quaternary Italian volcanic districts and other sites cited in the text. **b)** Location of the Latera Volcanic Complex (LVC), Vico volcano, and Bracciano and Sacrofano of Sabatini Volcanic District (SVD) centres, along with locations of investigated sections. **c)** Fucino Plain with the locations of the F4-F5 and other drilling sites.

2. Geological setting and tephrochronological framework of the Fucino Basin

The Fucino Basin is one of the largest intermountain tectonic basins in central Italy (Fig. 1c) and formed during the extensional stretching of the Apennine chain following the opening of the Tyrrhenian Basin (e.g., Doglioni et al., 1996). Starting in the Late Pliocene-Early Pleistocene, extensional tectonics, mainly acting along E-W, NE-SW, and NW-SE oriented high-angle normal faults, caused the stretching of the mountain chain (e.g., D'Agostino et al., 2001) and opening of several intermountain basins, including the Fucino Basin (Galadini and Galli, 2000; Boncio et al., 2004; Giaccio et al., 2012b; Amato et al., 2014). The Plio-Quaternary tectonic and sedimentary evolution of the Fucino Basin was driven by the *Fucino Fault System* (Galadini and Galli, 2000; Fig. 1c), which depicts a semi-graben architecture where the thickness of the Plio-Quaternary sedimentary infilling increases up to ~900 m from west to east toward the depocenter (Cavinato et al., 2002; Patacca et al., 2008). The Fucino Basin was likely characterised by continuous sedimentation (Giaccio et al., 2017a, 2019; Mannella et al., 2019) since the Plio-Pleistocene and hosted a lake, *Lacus Fucinus*, until the 19th century CE, when it was drained by the Torlonia family.

Two cores were recovered at the F4-F5 drilling site in the central area of the basin (42°00'06" N, 13°32'18" E, Fig. 1c) and combined into a 98 m-long composite profile based on optical information and geochemical data obtained from XRF scanning (Giaccio et al. 2019). Drilling site selection strategy and recovery procedure are reported in Giaccio et al. (2019). The F4-F5 composite profile contains at least 130 visible tephra layers (Giaccio et al., 2019; Fig. 2). The sediment succession from F4-F5 was ascribed to the last 430 kyr (Fig. 2; Giaccio et al., 2019) based on correlations with tephra layers from the nearby F1-F3 record covering the last 190 kyr (Giaccio et al., 2017a), and on a detailed geochemical and geochronological characterisation of 32 tephra layers from the lowermost portion of the F4-F5 record, spanning the 430-365 ka time interval or the MIS 11 period (Monaco et al., 2021; Fig. 2). Tephra layers from this MIS 11 interval were attributed to the Vulsini, Vico, Sabatini, Colli Albani, and Roccamonfina volcanic districts (Fig. 1), providing new detailed chronological constraints for the frequent explosive activity of these volcanoes.

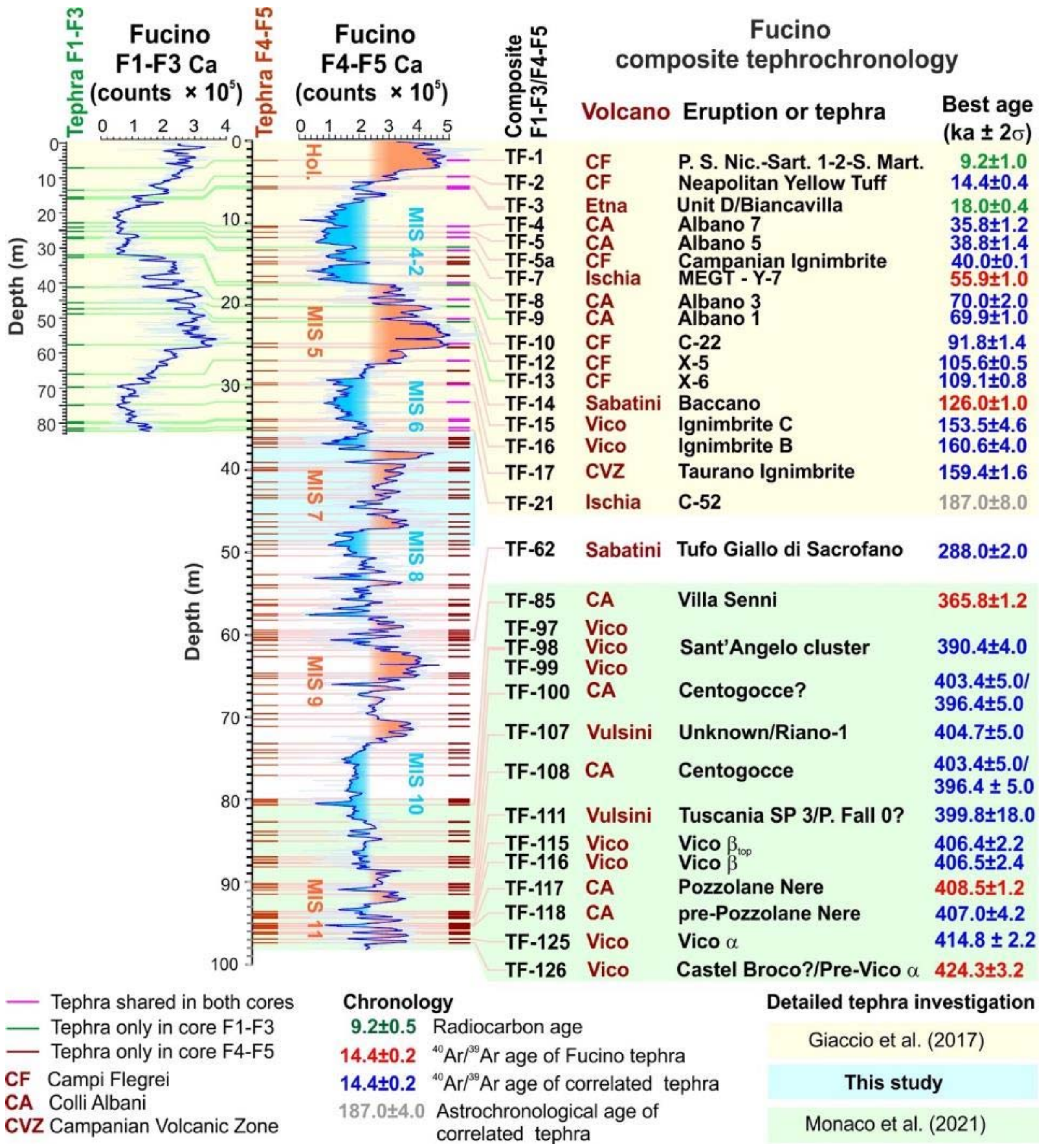

Figure 2. Composite F1-F3/F4-F5 tephra record. Data source: Giaccio et al. (2017a, 2019), Monaco et al. (2021) and references therein.

3. Materials and methods

In this study, 21 Fucino (visible) tephra layers covering the MIS 6-8 period (Fig. 3), 1 Ohrid tephra (OH-DP-0725) and 13 proximal units, from the Vulsini, Sabatini and Vico volcanic systems, have been characterised in terms of major (n=35) and trace (n=15) element compositions, Sr-Nd isotopes (n=17) and $^{40}Ar/^{39}Ar$ dating (n=9; Canino unit was dated twice). The Fucino tephra have been sampled directly from the cores retrieved at a depth of 31-49 m (below ground level), and have been washed with tap water and sieved to isolate the desired fraction of 250-60 μm. Some of the Fucino F4-F5 tephra were also pre-treated with HCl (i.e., tephra layers TF-21a, TF-23, TF-35b), sieved at 25 μm (TF-21a, TF-23, TF-33, and TF-35b) and density separated. Labelling of the Fucino tephra follows that of previous studies (i.e., Giaccio et al., 2019; Monaco et al., 2021), i.e., continuous numbering from the top (uppermost tephra = TF-1) to the bottom. Tephra layers discovered after the primary sampling have the number followed by a letter (e.g., TF-35b) to avoid renaming tephra layers from previous works.

Major element analysis has been performed with the Electron Probe Micro Analyser (EPMA) at three different institutes: 1) Institute of Petrology and Structural Geology (Charles University, Prague, Czech Republic); 2) *Istituto di Geologia Ambientale e Geoingegneria* of the Italian National Research Council (IGAG-CNR, Rome, Italy); 3) University of Cologne (Cologne, Germany). The quality and reproducibility of the data has been verified through the employment of the same secondary standards and by replicting the analysis on some tephra layers (i.e., TF-19, -21, -22, -24, -25, -26, -27, -28, -31, and -32) in all three laboratories.

Trace element analysis has been performed at the Earth and Physics Department, University of Perugia (Perugia, Italy), using the laser ablation-inductively coupled plasma-mass spectrometry (LA-ICP-MS). Sr-Nd isotope ratios have been determined at the Radiogenic Isotope Laboratory (RIL) of the *Istituto Nazionale di Geofisica e Vulcanologia, Osservatorio Vesuviano* (INGV-OV). Finally, $^{40}Ar/^{39}Ar$ age determinations have been performed at two laboratories, i.e., at *Laboratoire des Sciences du Climat et de l'Environnement* (LSCE - CEA, Gif-sur-Yvette, France) and at University of Wisconsin-Madison (UVM) dating facilities.

A summary of the performed analysis is reported in Table 1, while detailed information on the sample processing, the instruments utilized and applied settings is provided in Supplementary Materials-1.

Table 1. Data summary of the investigated F4-F5 Fucino tephra, along with Ohrid tephra OH-DP-0725 and proximal LVC, Vico and SVD pyroclastic units.

Distal tephra							
Location	**Tephra**	**Core section and depth (cm)**	**Composite Bottom**	**Type of analysis**			
				Major	**Trace**	**Sr and Nd**	**$^{40}Ar/^{39}Ar$**

			Depth (m)	elements (EPMA-WDS)	elements (LA-ICP-MS)	isotopes (TIMS)	dating
Fucino Basin (F4-F5)	TF-17a[b]	F4-22 60.00-62.00	31.74	Yes	No	No	No
	TF-18[a,b]	F4-23 107.8-111.0	33.79	Yes	Yes	Yes	No
	TF-19[a,b]	F5-23 61.50-67.00	34.01	Yes	Yes	Yes	No
	TF-21[a,b]	F4-24 45.50-48.93	34.83	Yes	Yes	No	No
	TF-21a[b]	F4-24 79.50-81.50	35.15	Yes	No	No	No
	TF-22[a,b]	F5-25 111.5-114.7	36.04	Yes	No	Yes	Yes
	TF-23[b]	F5-24 130.8-134.3	36.24	Yes	No	No	No
	TF-24[b]	F4-25 66.20-68.50	36.59	Yes	Yes	No	No
	TF-25[b]	F4-25 78.90-87.70	36.78	Yes	Yes	No	No
	TF-26[b]	F4-25 127.0-129.0	37.20	Yes	No	Yes	No
	TF-27[b]	F4-26 136.0-142.0	39.05	Yes	Yes	Yes	Yes
	TF-28[b]	F4-27 28.00-33.00	39.66	Yes	No	No	No
	TF-29[b]	F4-27 59.00-60.20	39.94	Yes	No	No	No
	TF-30[b]	F5-27 03.00-07.50	40.07	Yes	No	No	No
	TF-31[b]	F4-28 42.00-43.80	41.41	Yes	No	Yes	No
	TF-32[b]	F4-28 132.0-136.0	42.30	Yes	Yes	Yes	Yes
	TF-33[b]	F4-29 45.70-47.70	43.00	Yes	No	No	No
	TF-35[b]	F5-29 71.20-71.80	43.70	Yes	No	No	No
	TF-35b[b]	F4-30 79.96-97.45	45.24	Yes	No	No	No
	TF-37[b]	F4-31 20.23-22.76	46.23	Yes	No	No	No
	TF-43[b]	F4-32 149.8-151.5	49.02	Yes	No	Yes	No
Lake Ohrid	OH-DP-0725[b,c]	1D-32H-2 1.25-3.75	72.50	Yes	No	No	No
Proximal volcanic units							
Volcanic system	**Unit**	**Section location**	**Coordinates**				
LVC	Pitigliano[b]	Case Collina quarry (Vu1)	42°38'31"N 11°43'54"E	Yes	Yes	Yes	No
	Onano[b]	Grotte di Castro-Onano road cut (Vu2) Poggio Falchetto-Bonini (Vu3)	42°40'41"N 11°51'10"E 42°35'08"N 11°51'24"E	Yes	Yes	Yes	Yes
	Grotte di Castro[b]	Poggio delle Forche (Vu4)	42°33'11"N 11°53'02"E	Yes	Yes	Yes	Yes
	Sorano[b]	Rio Maggiore road cut (Vu5)	42°37'07"N 11°40'13"E	Yes	Yes	Yes	No
	Sovana[b]	Rio Maggiore road cut (Vu5)	42°37'07"N 11°40'13"E	Yes	No	No	Yes
	Farnese[b]	Arlena di Castro-Tessenanno road cut (Vu6) Rio Maggiore road cut (Vu5)	42°27'46"N 11°48'18"E 42°37'07"N 11°40'13"E	Yes	Yes	Yes	Yes
	Stenzano[b]	Rio Maggiore road cut (Vu5)	42°37'07"N 11°40'13"E	Yes	No	No	No
	Canino[b]	Monte di Marta (Vu7) Fosso la Nova road cut (Vu8) Pian di Vico (Vu9)	42°32'05"N 11°54'56"E 42°35'54"N 11°38'46"E 42°25'08"N 11°48'41"E	Yes	Yes	Yes	Yes (twice)
SVD	TR-CR-2[b]	Trevignano Romano-Centro Rapaci (Sa1)	42°10'23"N 12°14'47"E	Yes	Yes	Yes	No
	TR-CR-1[b]			Yes	Yes	Yes	No
	Vigna di Valle[b]	Anguillara Sabazia (Sa2)	42°05'29"N 12°16'16"E	Yes	No	Yes	No
	Pizzo Prato[b]	Anguillara Sabazia-Mola Vecchia (Sa3)	42°05'25"N 12°16'55"E	Yes	No	No	No
Vico	Farine Formation	San Martino al Cimino train station (Vi1)	42°22'58"N 12°06'26"E	Yes	No	No	No

[a]: Giaccio et al. (2017a); [b]: this study; [c]: Leicher et al. (2021). Abbreviations: LVC = Latera Volcanic Complex; SVD = Sabatini Volcanic District, EPMA-WDS = Electron Probe Micro Analyser-Wavelenght Dispersive System, LA-ICP-MS = Laser Ablation-Inductively Coupled Plasma-Mass Spectrometry, TIMS = Thermal Ionization Mass Spectrometry.

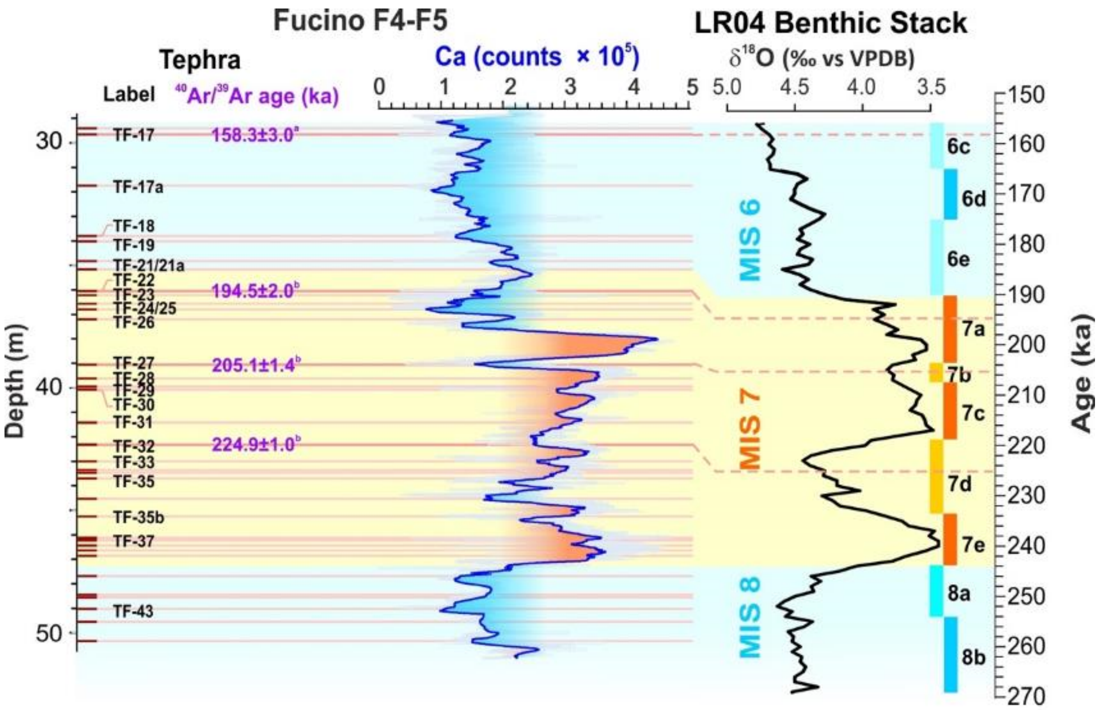

Figure 3. Detailed tephrostratigraphy and Ca counts from XRF scanning (Giaccio et al., 2019) of the investigated MIS 8-MIS 6 interval from Fucino F4-F5 core compared with LR04 Benthic Stack (Lisiecki and Raymo, 2005). The available ([a] Giaccio et al., 2017a) and new ([b] this study) direct $^{40}Ar/^{39}Ar$ age determinations of the Fucino tephra are also shown. Note: Fucino data are plotted against the depth, whilst the LR04 against the age.

4. Results

4.1. Major and minor element glass composition

The glass chemical composition of the analysed Fucino tephra layers and proximal units are shown in the *Total Alkali vs Silica* classification diagram (TAS, Le Maitre et al., 2002; Fig. 4a). We noticed that a variable amount of the glass shards from the tephra layers from an interval hosting a small methane reservoir (between ~46 and ~49 m depth) appear morphologically modified, with a fibrous shape. These altered shards also yielded odd compositions, with anomalous high Al_2O_3, very low K_2O and other anomalies in the element concentrations and ratios, likely resulting from a devitrification processes. However, in some layers (e.g., TF-35b, TF-37 and TF-43), a part of the glass shards appears pristine in their shape and microtexture and yielded chemical composition fully consistent with those expected for the unaltered glass. Thus, we consider these compositions as reliable and keep them as representative of the original unaltered glass.

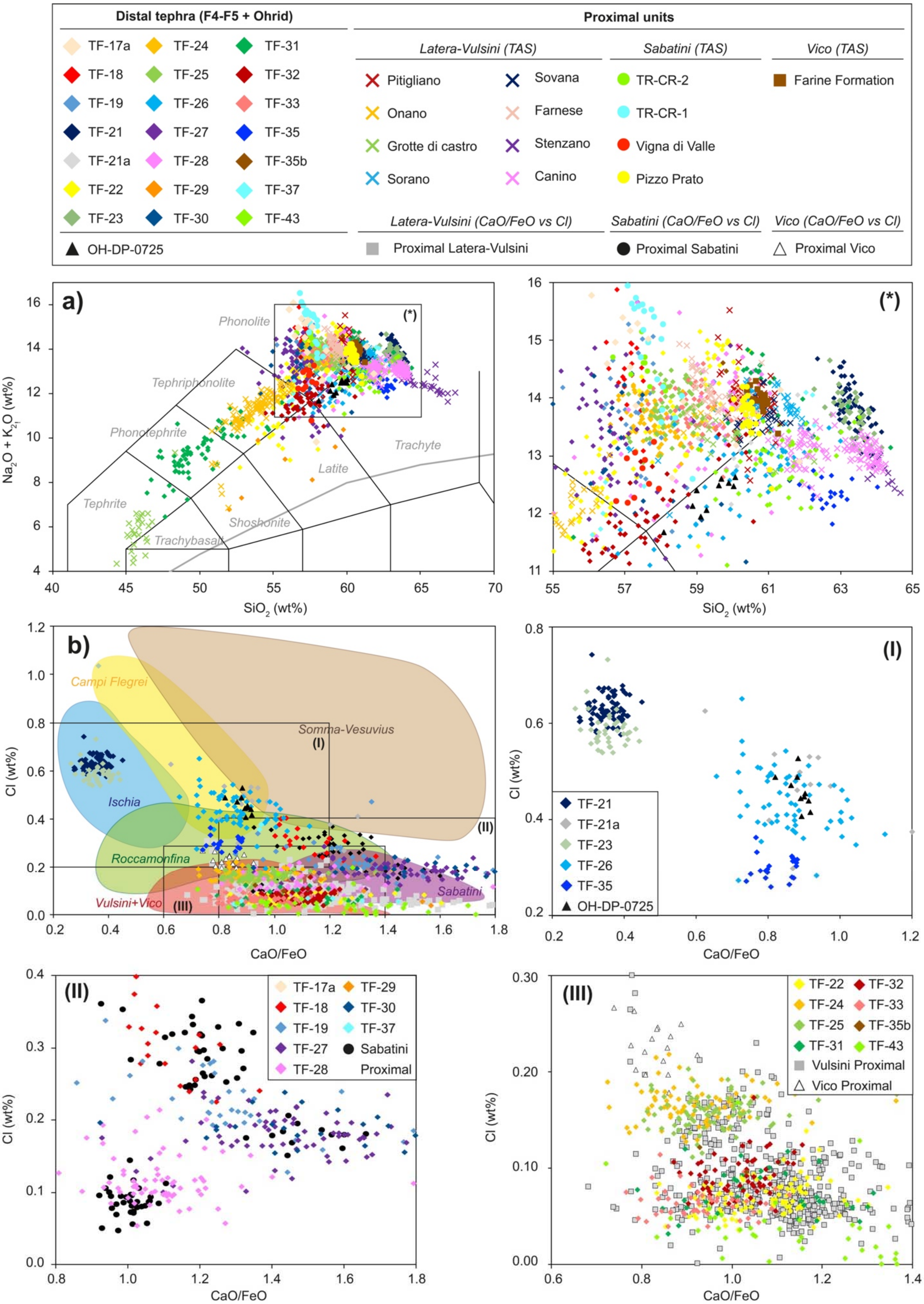

Figure 4. Classification and discrimination diagrams for Fucino MIS 8-6 investigated tephra, the proximal pyroclastic units of Latera Volcanic Complex (LVC), Vico volcano (Farine Formation unit), and Sabatini Volcanic District (SVD), and Ohrid tephra OH-DP-0725. **a)** *Total Alkali vs Silica* (TAS; Le Maitre et al., 2002); the grey line represents the limit that divides the sub-alkaline and alkaline series (Irvine and Baragar, 1971). **b)** CaO/FeO vs Cl (Giaccio et al., 2017a).

All 21 Fucino tephras plot within the fields of the high-K series (Appleton, 1972), and can be classified as potassic tephrites, phonotephrites, tephriphonolites, phonolites and trachytes, but also as latites and shoshonites (e.g., tephra layers TF-22, TF-27, and TF-29; Table 2). Most Fucino tephras are mainly phonolithic and trachytic in composition (Fig. 4a; Supplementary Fig. S1a), with variable amounts of alkali contents and ratios, all with $K_2O/Na_2O \geq 1$, except for TF-21 and TF-23 where $K_2O/Na_2O < 1$ (Fig. S3a).

Table 2. Lithological and mineralogical features, and *Total Alkali vs Silica* (TAS, Le Maitre et al., 2002) classification of the twenty-one tephra layers deposited at the F4-F5 site in the Fucino Basin during the MIS 8-6 interval.

Tephra	Thickness (cm)	Lithology		TAS classification (main rock type)
		Juvenile clasts	Minerals	
TF-17a	2.00	White and grey pumice	Kfs>cpx>bmca	Ph
TF-18	3.20	Grey pumice	Kfs>cpx	Ph
TF-19	5.50	Grey pumice	Kfs>cpx>bmca	Ph
TF-21	3.43	White pumice	Kfs>bmca	Tr
TF-21a	2.00	transparent-white – brownish shards and pumice	Kfs>cpx>bmca	Ph-Tr
TF-22	3.20	White pumice and grey scoria	Kfs>bmca	Ph-Tph-Lat
TF-23	3.50	Transparent shards white pumice	Kfs>plg >bmca>cpx	Tr
TF-24	2.30	White pumice	Kfs>bmca	Ph
TF-25	8.80	White pumice	Kfs>bmca	Ph
TF-26	2.00	White and grey pumice	Kfs>cpx>bmca	Tr-Ph
TF-27	6.00	White pumice	Bmca>kfs	Ph-Tph-Tr-Lat
TF-28	5.00	White pumice	Bmca>kfs	Ph-Tph-Tr-Lat
TF-29	1.20	Grey pumice	Bmca>kfs	Sho-Lat
TF-30	4.50	White and grey pumice	Kfs>bmca>cpx	Ph-Tr
TF-31	1.80	White and grey pumice	Kfs>bmca>cpx	Ph-Tr-Tph-Pht
TF-32	4.00	Grey pumice	Kfs>bmca>cpx	Tph-Ph-Tr-Lat
TF-33	2.00	white and grey pumice, transparent shards	Kfs>cpx>bmca	Ph
TF-35	0.60	White pumice	Kfs>bmca	Tr
TF-35b*	17.5	Very few material	No	Ph
TF-37	2.53	white and grey pumice, grey-black scoria	Kfs>cpx>bmca	Pht-Tph-Ph-Tr
TF-43	1.70	White pumice	Bmca>kfs	Tr

*: Bioturbated layer, real tephra thickness is not quantifiable. Rock type abbreviations: Ph = phonolite; Tr = trachyte; Tph = tephriphonolite; Pht = phonotephrite; Lat = latite; Sho = shoshonite. Mineral abbreviations: Kfs = K-feldspar; bmca = black mica; cpx = clinopyroxene; plg = plagiocase.

Table 3. Lithological and mineralogical features and TAS (Le Maitre et al., 2002) classification of the LVC, Vico and SVD investigated proximal units.

Unit	Sub-unit/ sample	Lithology		TAS classification (main rock type)
		Juvenile clasts	Free crystals	
Pitigliano	Tuff	Black scoria	Kfs	Ph-Tr
	Basal pumice fall	White pumice	Kfs	Ph-Tr
Onano	Spatter flow	Black spatter	Kfs	Sho
	Lower sillar-mid	Grey and white pumice	Cpx>kfs	Ph-Tph-Pht
	Lower sillar-base	Grey and white pumice	Kfs>bmca>cpx	Ph-Tph
Grotte di Castro	Basal fall-top	White pumice	Kfs	Ph-Tr
	Basal fall-base	Dark grey scoria	Cpx	Pht-Te-Trb
Sorano	Ash flow-main body	White pumice	Kfs>bmca	Ph-Tr
	Ash flow-base	White pumice	Bmca>cpx	Ph-Tr
Sovana*	Black pumice flow	Black scoria	Kfs>Lc	Ph
	“BUS”	White pumice	Kfs	Ph
Farnese	Pumice flow	Light grey pumice	Kfs>cpx	Ph
	Pumice fall F	White pumice	Kfs>cpx	Ph
Stenzano	Pyroclastic flow	White pumice	Kfs>bmca	Tr
Canino	Fall C	White pumice	Kfs>cpx>bmca	Tr
	Upper Flow	Black scoria	Kfs	Tr
	Main Flow	Light grey-pink pumice	Kfs>cpx	Tr
	Upper Fall B	White pumice	Kfs>cpx	Tr
	Lower Fall B	White pumice	Kfs>cpx	Tr
TR-CR-2	TR-CR-2	White pumice	Kfs	Ph
TR-CR-1	Scoria Fall	Grey scoria	Kfs>cpx	Ph
	Top	White pumice	Kfs>cpx	Ph
	Base	White pumice	Kfs	Ph
Vigna di Valle	Surge-pumice layer	White pumice	Kfs>cpx	Ph-Lat
	Surge-base	White pumice	Kfs>cpx	Ph
Pizzo Prato	Lower Flow	White pumice	Kfs>cpx	Ph
	Fall Top	White pumice	Kfs>bmca>cpx	Ph-Tr
	Fall Base	White pumice	Kfs>cpx	Ph-Tr
Farine Formation	Pyroclastic flow	White-brownish pumice	Kfs>cpx>bmca	Ph-Tr

*Palladino et al., 2014. Rock type abbreviations: Tr = trachyte; Ph = phonolite; Tph = tephriphonolite; Pht = phonotephrite; Lat = latite; Sho = shoshonite; Te = tephrite; Trb = trachybasalt. Mineral abbreviations: Kfs = K-feldspar; bmca = black mica; cpx = clinopyroxene; Lc = leucite. Other abbreviations: TAS = Total Alkali vs Silica; LVC = Latera Volcanic Complex; SVD = Sabatini Volcanic District.

The eight proximal LVC units are classified as K-phonolites and K-trachytes (Table 3), but also as potassic tephriphonolites (Onano unit) and tephrites-trachybasalts (Grotte di Castro Basal Fall sub-unit; Fig. 4a, Supplementary Fig. S1b). The four proximal SVD units are all phonolitic in composition (Fig. 4a, Supplementary Fig. S1b), with similar amounts of K_2O and Na_2O ($K_2O/Na_2O = 1$), except for Pizzo Prato unit where K_2O/Na_2O is > 2 (Fig. S3b). The Farine Formation unit from Vico volcano has a fairly homogeneous phonolitic-trachytic composition (Fig. 4a, Supplementary Fig. S1b), with 60-62 wt.% SiO_2, 13-15 wt.% alkali sum and mean K_2O/Na_2O ratio of 1.58 ± 0.18 (2 s.d.; Fig. S3b). Finally, Ohrid tephra OH-DP-0725 is trachytic in composition (Fig. 4a), with $K_2O/Na_2O > 1$ (mean = 1.81 ± 0.13 [2 s.d.]). Leicher et al. (2021) reported both a phonolitic and a rhyolitic component, the latter not observed in the sample analysed in this study. Full analytical data can be found in Supplementary Materials-2.

4.2. Trace element glass compositions

Seven out of the eight Fucino tephras and all eight proximal LVC and SVD units selected for trace element analysis, provided sufficient analytical points (i.e., > 10-15) for their characterisation, whereas only 1 point could be obtained for TF-43 (not shown in Fig. 5), preventing us from determining its trace element composition.

The analysed Fucino tephras form three distinguished clusters (Fig. 5a-b). TF-18, -19, -27 and -32 form a common cluster, but have different Th concentrations if compared with other incompatible trace elements (Fig. 5a-b). Indeed, tephra layers TF-18 and TF-19 are more enriched in Th (Th = 140-173 ppm and 122-200 ppm respectively), with respect to TF-27 (58-115 ppm) and TF-32 (50-68 ppm). Tephra TF-21 forms a cluster less enriched in Th (75-93 ppm, amongst the lowest concentrations) whilst being more enriched in Zr (869-1113 ppm, Fig. 5a), Nb (98-121 ppm, Fig. 5b) and Ta (4.3-5.3 ppm) with respect to all the other Fucino tephra. Furthermore, it displays the highest ratios of High Field Strength Elements (HFSE) and Light Rare-Earth Elements (LREE) to Th (e.g., Ta/Th = 0.05-0.07; Nb/Th = 1.17-1.47 [Fig. 5c]; La/Th = 2.22-2.91 [Fig. 5d]; Ce/Th = 4.07-4.97). Finally, phonolitic tephra TF-24 and TF-25 form a separate cluster, being the most enriched in Th, ranging respectively from 208-285 ppm and 214-264 ppm, compared to all the other Fucino tephra having ≤ 200 ppm of Th (Fig. 5a-b). TF-24 and TF-25 are also characterised by similar, and basically indistinguishable from one another, ratios of HFSE and LREE to Th (e.g., Nb/Th = 0.24-0.29 for TF-24 and 0.23-0.31 for TF-25 [Fig. 5c]; La/Th = 0.89-0.99 for TF-24 and 0.85-0.98 for TF-25 [Fig. 5d]; Ce/Th = 1.50-1.72 for TF-24 and 1.41-1.59 for TF-25).

The LVC pyroclastic units are characterised by very similar incompatible trace element contents, overlapping with those of Fucino tephra (Fig. 5a-b). Overall, Th ranges between 55-155 ppm, Zr between 364-899 ppm (Fig. 5a), Nb between 21-48 ppm (Fig. 5b), and Ta between 1-3 ppm for the LVC units. Ratios of HFSE and LREE to Th overlap with those of TF-32 and partially with TF-18 and TF-19 (Fig. 5c-d).

SVD pyroclastic units show a similar variation of incompatible trace element contents, with higher Th (i.e., 129-236 ppm) with respect to LVC units, overlapping only with tephra layers TF-18 and TF-19 (Fig. 5a-b).

However, when employing ratios of HFSE and LREE to Th, a good overlap is observed also for TF-27 (Fig. 5c-d). Full analytical data can be found in Supplementary Materials-2.

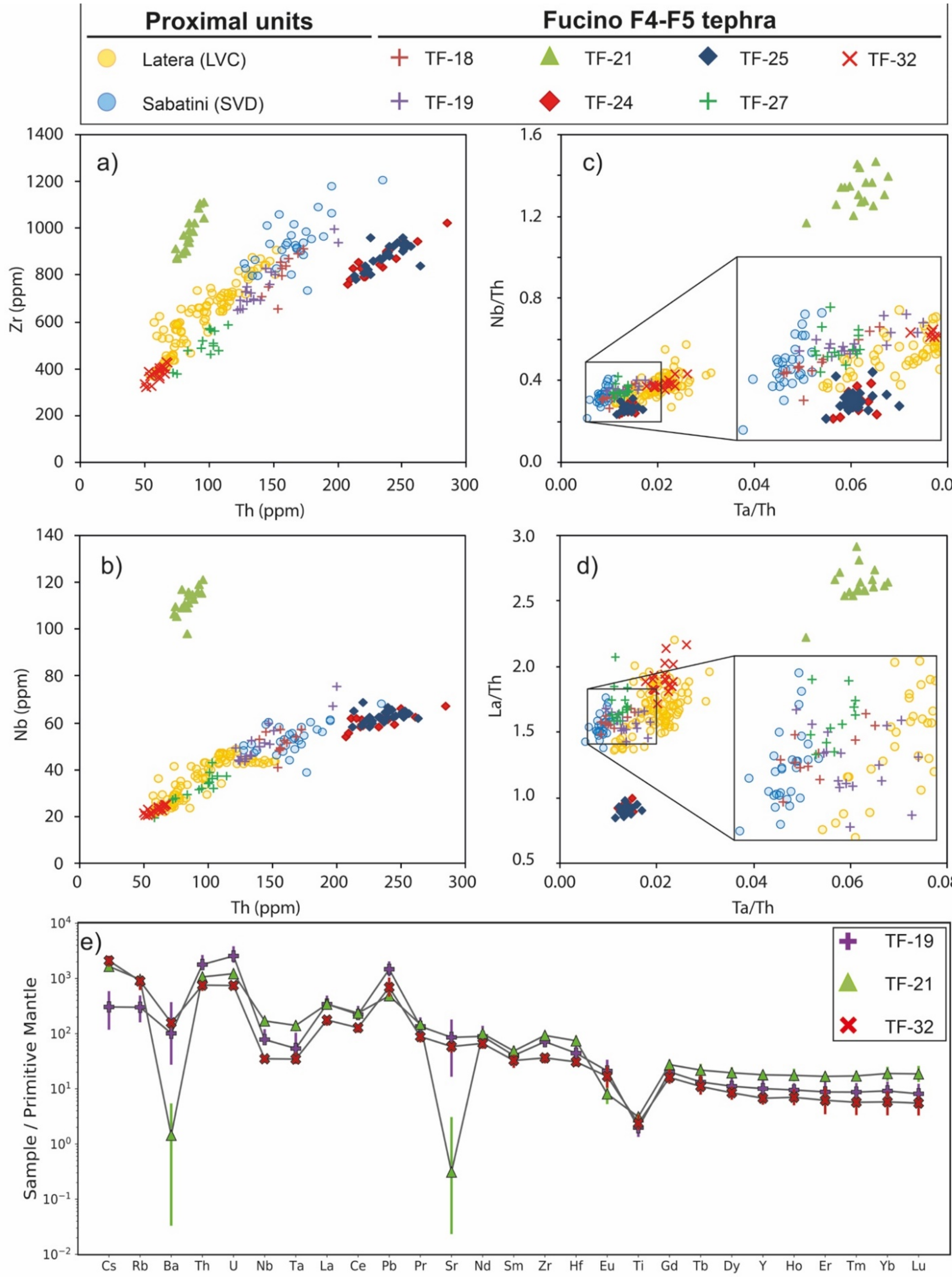

Figure 5. Trace element representative bivariate (a to d) and spider diagrams (e; normalized to the primitive mantle; McDonough and Sun, 1995) of the selected Fucino F4-F5 tephra and proximal LVC and SVD pyroclastic units.

4.3. *Sr and Nd isotopic composition*

$^{87}Sr/^{86}Sr$ ratios (Fig. 6a) of the Fucino F4-F5 tephra range from 0.70623 (TF-26) to 0.71056 (TF-43), with most of the samples (i.e., excluding TF-26) having $^{87}Sr/^{86}Sr > 0.710$ (Table 4). TF-22, TF-31, TF-32, and TF-43 show $^{87}Sr/^{86}Sr > 0.7103$. Feldspar and light and dark glass fraction of TF-22 display the same Sr isotopic composition (0.71038). TF-31 is characterised by a small Sr isotope variation, with respect to the analytical error, between feldspar and glass fraction (0.7105). Pyroxene, feldspar, biotite, and glass fraction from TF-32 have Sr isotopic composition ranging from 0.71036 to 0.71055. Feldspar from TF-43 has $^{87}Sr/^{86}Sr$ of 0.71056. TF-18, TF-19, and TF-27 show similar $^{87}Sr/^{86}Sr$ (Table 4), all < 0.7103. The lowest values among these three samples are recorded by TF-27 pyroxene and glass fraction, both being characterised by Sr isotope ratios of ~0.7101. TF-26 mineral and glass fractions display $^{87}Sr/^{86}Sr$ ranging from 0.70623 (feldspar) to 0.70656 (pyroxene), significantly lower with respect to all the other Fucino tephra. $^{143}Nd/^{144}Nd$ (Fig. 6b) have been determined for four Fucino tephra (i.e., TF-22, TF-26, TF-27, and TF-32). They are compatible with those of the proximal samples with the exception of tephra TF-26, which displays the highest $^{143}Nd/^{144}Nd$ value among all samples (i.e., 0.51255). Full analytical data can be found in Table 4.

From the SVD, the units Vigna di Valle, Trevignano Romano Centro Rapaci (TR-CR-1, 2), and Pizzo Prato (the latter analysed in Sottili et al., 2019) are characterised by Sr isotope ratios from 0.7101 to 0.7103. $^{143}Nd/^{144}Nd$ measured for TR-CR-2 is 0.5121. Glass fractions and related feldspar are in isotopic equilibrium (Table 4; Fig. 6).

The Pitigliano, Onano, Grotte di Castro, Sorano, Farnese, and Fall-C units from LVC have $^{87}Sr/^{86}Sr$ ranging from 0.7103 to 0.7108. The lowest ratios belong to the Farnese glass fraction, whilst the highest to the Canino Fall-C. Farnese glass and feldspar are in isotopic disequilibrium and are characterised by Sr isotope compositions ranging from 0.7101 and 0.7103. The possible occurrence of antecrysts can explain such a difference, as often happen when considering large magma chambers, producing high magnitude eruptions. The $^{143}Nd/^{144}Nd$ is 0.5121 for all samples (Table 4; Fig. 6b). Samples from the LVC (i.e., Pitigliano, Onano, Grotte di Castro, Sorano, Farnese, and Canino Fall-C) are featured by $^{87}Sr/^{86}Sr \geq 0.7103$ (Table 4) and overlap with the Fucino tephra TF-22, TF-31, TF-32, and TF-43. Finally, TR-CR-2, TR-CR-1, and Vigna di Valle units from the SVD, display similar $^{87}Sr/^{86}Sr$ ratios (Table 4), overlapping with those of the Fucino tephra TF-18, TF-19, and TF-27.

Table 4. Individual $^{87}Sr/^{86}Sr$ and $^{143}Nd/^{144}Nd$ isotope ratios for the investigated F4-F5 Fucino tephra, and proximal Vulsini and Sabatini pyroclastic units.

Tephra/Unit	Sub-sample	$^{87}Sr/^{86}Sr$	Error	$^{143}Nd/^{144}Nd$	Error
Fucino Tephra					
TF-18	Feldspar	0.71029	0.000019		0.00001
TF-19	Feldspar	0.71028			
TF-22	Feldspar	0.71038			
	Pyroxene	0.71038		0.51212	
	Glass fraction	0.71038			
TF-26	Feldspar	0.70623			
	Pyroxene	0.70657			
	Glass fraction	0.70635		0.51255	
TF-27	Feldspar	0.71027			
	Pyroxene	0.71013			
	Glass fraction	0.71014		0.51210	
TF-31	Feldspar	0.71052			
	Glass fraction	0.71046			
TF-32	Feldspar	0.71044			
	Pyroxene	0.71055			
	Biotite	0.71050			
	Glass fraction	0.71036		0.51212	
TF-43	Feldspar-rich	0.71056			
Proximal Vulsini					
Pitigliano	Feldspar	0.71039			
	Glass fraction	0.71039		0.51211	
Onano	Glass fraction	0.71033		0.51211	
Grotte di Castro	Feldspar	0.71043			
	Glass fraction	0.71041		0.51211	
Sorano	Feldspar	0.71046			
	Glass fraction	0.71038			
Farnese	Feldspar	0.71029			
	Glass fraction	0.71010		0.51212	
Fall-C	Feldspar	0.71077			
	Pyroxene	0.71079		0.51211	
	Glass fraction	0.71079		0.51211	
Proximal Sabatini					
TR-CR-2	Feldspar	0.71025			
	Glass fraction	0.71023		0.51211	
TR-CR-1	Feldspar	0.71026			
	Glass fraction	0.71024			
Vigna di Valle	Feldspar	0.71015			
	Glass fraction	0.71012			

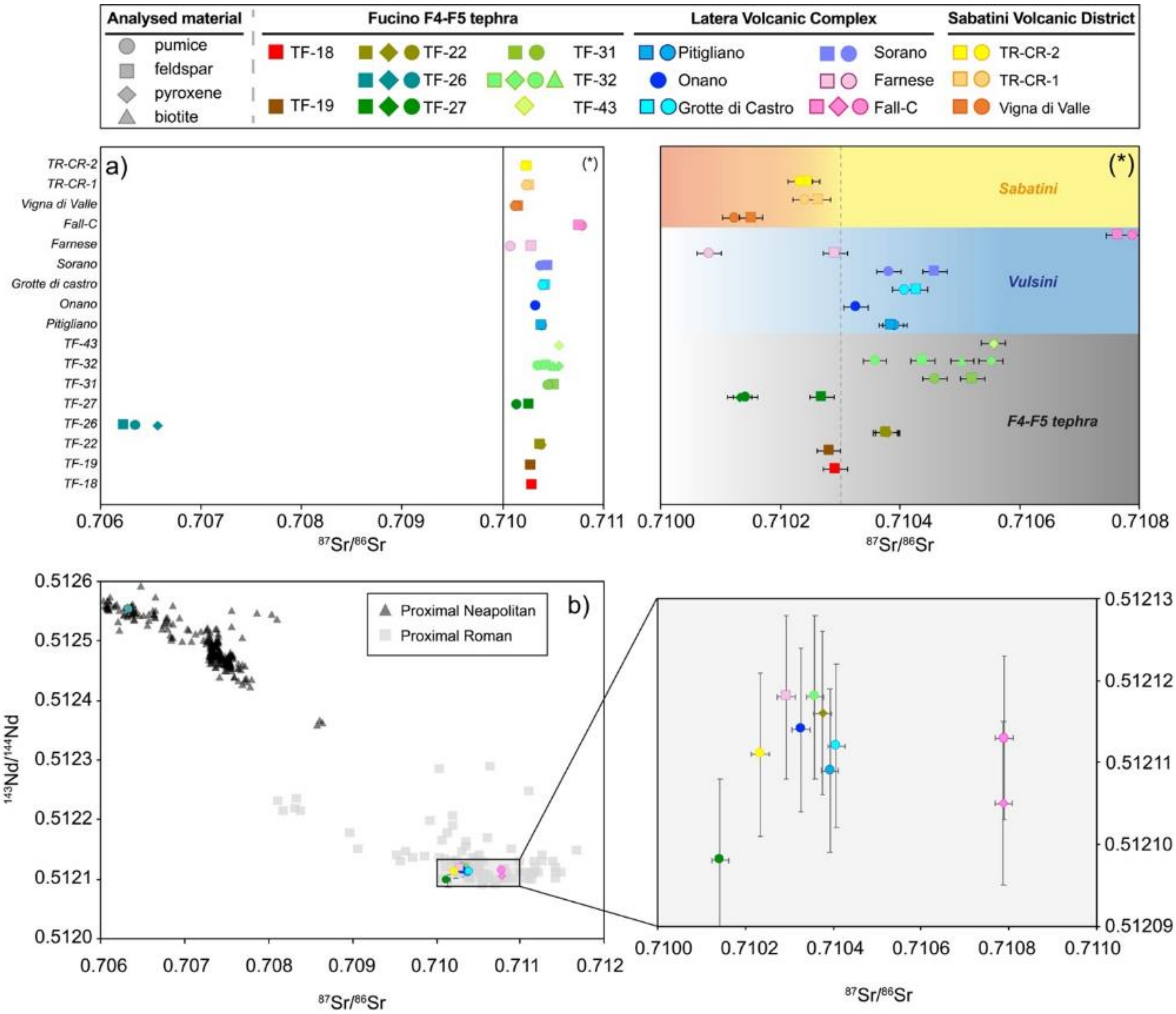

Figure 6. $^{87}Sr/^{86}Sr$ **(a)** and $^{87}Sr/^{86}Sr$ vs $^{143}Nd/^{144}Nd$ **(b)** isotopic composition of the selected Fucino F4-F5 tephra and proximal LVC and SVD pyroclastic units. $^{87}Sr/^{86}Sr$ vs $^{143}Nd/^{144}Nd$ literature data from Neapolitan (i.e., Campi Flegrei and Ischia) and Roman (i.e., Vulsini, Vico, Sabatini and Colli Albani) volcanoes are displayed in **b)** as a comparison. Literature data source: Neapolitan = Arienzo et al. (2009, 2010, 2015, 2016), Brown et al. (2014), Casalini et al. (2018), D'Antonio et al. (2007, 2013), Di Renzo et al. (2011), Pabst et al. (2007), Pelullo et al. (2020), Tonarini et al. (2009); Roman = Di Battistini et al. (1998), Gaeta et al. (2016), Gasperini et al. (2002), Perini et al. (2004), Sottili et al. (2019).

4.4. $^{40}Ar/^{39}Ar$ ages

LSCE (Laboratoire de Sceinces du Climat et de l'Environnement) - $^{40}Ar/^{39}Ar$ dating results for individual tephra layers are presented as probability diagrams in Figure 7. Weighted mean age uncertainties are reported at 2σ, including J uncertainty and were calculated using Isoplot 4.0 (Ludwig, 2012). For each sample, inverse isochrones have $^{40}Ar/^{36}Ar$ initial intercepts that are within uncertainty of that of the atmosphere suggesting that the dated crystals do not contain abundant trapped excess argon.

TF-22 – Sanidine crystals extracted from this tephra layer range in length from 200 to 250 μm, which makes them less suitable for single-crystal fusion dating and thus the detection of potential xenocrysts as the argon beam sizes are very small (2 times the ^{40}Ar blank). Despite the low precision of these 8 single crystal fusion dates (Fig. 7), we did not detect any obvious older crystals. We improved the precision by fusing two (6 measurements), and four crystals (6 measurements) at the same time. All experiments with multiple crystals share a similar age within uncertainty, which proves that we were not able to detect any significant older crystal within the analytical uncertainties. These findings agree with the isotopic evidence which suggest isotopic equilibrium between glass and mineral fractions. Finally, to obtain a more precise age, the remaining crystals were analyzed in a small population of 10 to 15 crystals. Including all experiments, we obtained a total of 24 similar ages, allowing us to calculate an accurate and precise weighted mean age of 194.5 ± 2.0 ka (MSWD = 0.3, p = 1.0).

TF-27 - A total of 15 individual sanidine crystals were dated. Excluding 4 older crystals, interpreted as xenocrysts (red bars in Fig. 7), a main population constituted by 11 crystals allowed calculation of a weighted mean age of 205.1 ± 1.4 ka (MSWD = 1, p = 0.43) for this tephra. The possible occurrence of xenocrysts or antecrysts is confirmed by the relatively high $^{87}Sr/^{86}Sr$ obtained for the feldspar with respect to pyroxene and glass fractions.

TF-32 - 19 single sanidine crystal ages were obtained for this tephra layer. The probability diagram is complex, multimodal with at least 5 modes with crystals as old as 275 ka (Fig 7). Remarkably, this evidence agrees well with the results of the Sr isotopic investigations performed on different mineral fractions and the related glass. At least three distinct $^{87}Sr/^{86}Sr$ ratios have been recognized based on the isotopic composition of $^{87}Sr/^{86}Sr$ of glass, feldspar, and pyroxene-biotite, which suggest the occurrence of different crystals populations. The youngest feldspar population includes 9 crystals sharing the same age within uncertainties. Using these crystals, we calculated a weighted mean age of 224.9 ± 1.0 ka (MSWD = 0.8, p = 0.60) that we interpret as the age of deposition of this tephra.

Farnese - 15 individual sanidine crystals were analysed. All of them share the same age within uncertainties as shown by the corresponding almost Gaussian probability diagram (Fig. 7). Using these crystals, we calculated a weighted mean age of 235.6 ± 0.6 ka (MSWD = 0.7, p = 0.8) that we interpret as the age of the Farnese eruption.

Canino Fall-B - we analysed 15 individual sanidine crystals for this sub-unit. Excluding one crystal that shows a significantly older age and is thus interpreted as a xenocrystal (red bar), all the 14 remaining ones have the same age within uncertainties (Fig. 7). This main population, here interpreted as juvenile crystals, allows us to propose an age of 253.8 ± 0.8 ka (MSWD = 1.1, p = 0.4) for the Canino Fall-B sub-unit.

Canino Fall-C - 11 sanidine crystals were individually dated for this sub-unit. Like Canino Fall-B, beside one xenocryst with a low $^{40}Ar^*$ dated at 276 ka, all remaining crystals display a similar age within uncertainties (Fig. 7) in agreement with the results of the isotopic investigations. Using this main and younger juvenile population of crystals, we have calculated a weighted mean age of 253.1 ± 0.8 ka (MSWD = 1.4, p = 0.8) for the Canino Fall-C sub-unit. This age is undistinguishable from the one we obtained for Canino Fall-B, which makes sense as both sub-units belong to the same eruptive cycle (Palladino and Agosta, 1997). The weighted mean age of the Canino eruption, given by both Fall-B and Fall-C sub-units, is thus 253.4 ± 0.8 ka.

UWM (University of Wisconsin-Madison) - $^{40}Ar/^{39}Ar$ dating results for all individual tephra layers are presented as probability diagrams in Figure 7.

Onano - 36 sanidine crystals were dated for the Onano unit. Of these, 32 were interpreted as juvenile crystals and yielded a weighted mean age of 224.7 ± 2.6 ka (MSWD = 1.1, 2 σ; Fig. 7).

Grotte di Castro - for this unit, 39 sanidine crystals were dated, but only 26 were interpreted as juveniles and yielded a weighted mean age of 225.3 ± 1.2 ka (MSWD = 1.2, 2 σ), the remaning 13 crystals being interpreted as older xenocrysts (red squares in Fig. 7).

Sovana - 23 sanidine crystals were dated for this unit. Of these, 16 crystals yielded a weighted mean age of 226.4 ± 0.7 ka (MSWD = 0.4, 2 σ; Fig. 7), while the remaining 7 crystals were interpreted as older xenocrysts.

Full analytical data can be found in Supplementary Materials-3.

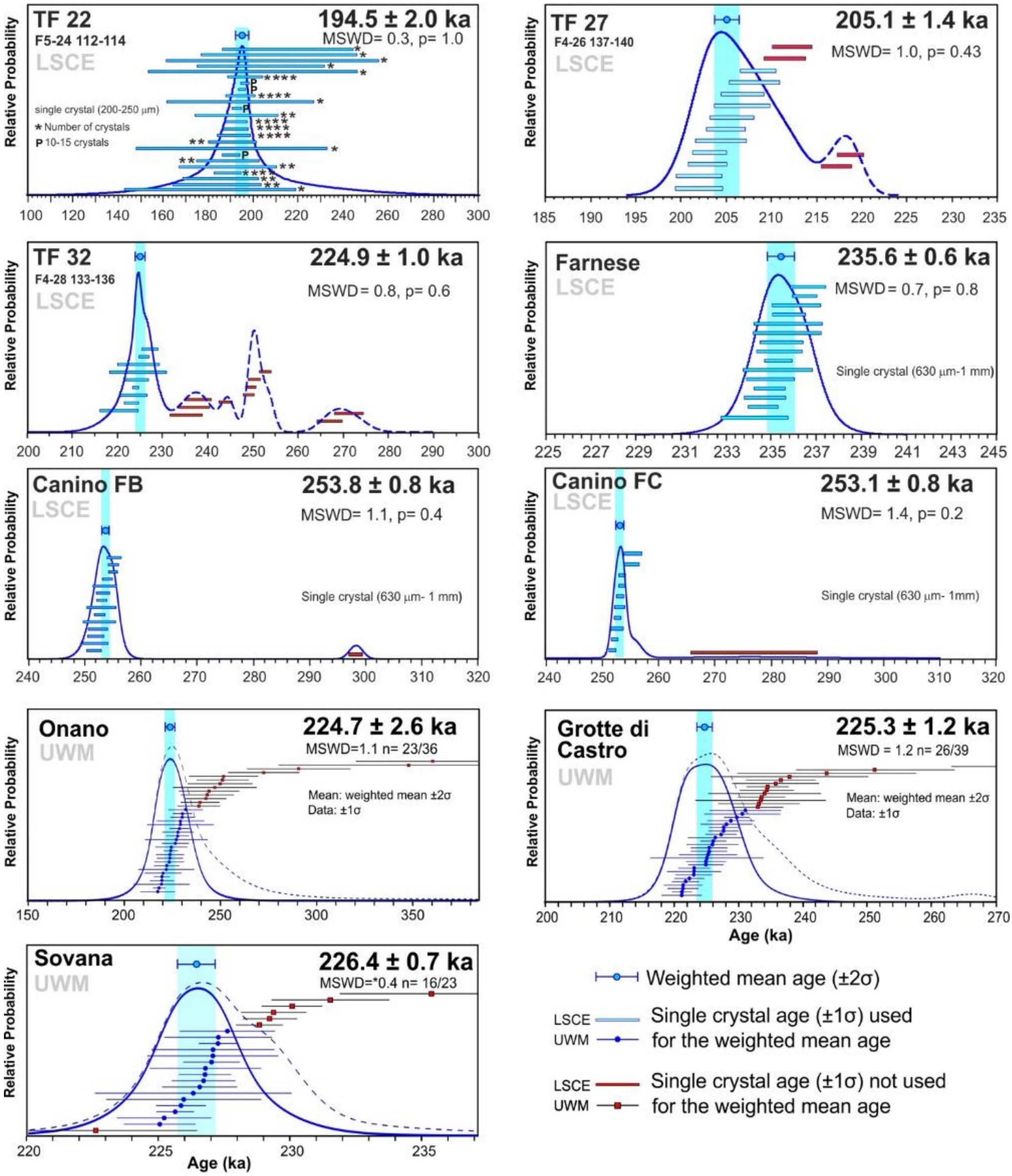

Figure 7. Age probability diagrams of tephra layers TF-22, TF-27, and TF-32, and of proximal LVC pyroclastic units Onano, Grotte di Castro, Sovana, Farnese, Canino Fall-B, and Canino Fall-C.

5. Discussion

5.1. Volcanic sources of the Fucino tephras

5.1.1. Active volcanoes over the investigated timespan

Volcanoes belonging to the Quaternary potassic peri-Tyrrhenian volcanic region (Fig. 1b) are the most probable sources of all investigated tephra. Indeed, previous investigations (Giaccio et al., 2017a, 2019; Monaco et al., 2021) showed that, to a great extent, the majority of the Fucino tephra documented so far were sourced from these volcanic systems along with products from the Aeolian Islands (Di Roberto et al., 2018) and Etna volcano (Giaccio et al., 2017a; Del Carlo et al., 2020). Furthermore, almost all these volcanic systems were active in the time interval 250-170 ka (e.g., Peccerillo, 2017).

Between ~250 ka and 160 ka, the Latera Caldera (LVC; Vulsini volcanic district; Fig. 1b) produced several Plinian-fall (Palladino and Agosta, 1997) and pyroclastic flow (Sparks, 1975; Palladino and Valentine, 1995) deposits, some of them associated to caldera-forming eruptions (Palladino et al., 2010). These eruptions include, from the oldest to the youngest, those of Canino, Stenzano, Farnese, Sovana, Sorano, Grotte di Castro, Onano, and Pitigliano, the deposits of which were all geochemically characterised in this study. Also, Plinian activity in the eastern Vulsini (Nappi et al., 1994) partially overlapped with the study period.

At Vico volcano (Fig. 1b), after a period of ~50 kyr dominated by effusive activity (Lago di Vico lava Formation, 305-258 ka, e.g., Perini et al., 2004), which built up the stratovolcano, a series of explosive, caldera-forming eruptions, i.e., Ignimbrite A/Farine Formation (here analysed), the Ignimbrite B/Ronciglione Formation, and the Ignimbrite C/Sutri Formation (Bertagnini and Sbrana, 1986; Perini et al., 1997; Bear et al., 2009), occurred.

At Sabatini (Fig. 1b), two volcanic centres were simultaneously active, i.e., the Sacrofano (~300-200 ka) and Bracciano (~325-200 ka) calderas (Sottili et al., 2019; Marra et al., 2020), both of which had major Plinian (e.g., Magliano Romano Plinian Fall, 312 ± 2 ka; Sottili et al., 2010), caldera-forming eruptions (e.g., Tufo Giallo di Sacrofano, Tufo di Bracciano, Tufo di Pizzo Prato; Sottili et al., 2010, 2019), and minor explosive activity associated to pyroclastic surges, strombolian eruptions and lava flows at parasite cones along the rims of the two calderas.

At Colli Albani, the long Tuscolano-Artemisio Phase (de Rita et al., 1988), also known as the Vulcano Laziale period (Giordano and the CARG Team, 2010), spanned the interval 608-351 ka (Marra et al., 2009; Gaeta et al., 2016). It was followed by the Mt. Faete Phase (now Tuscolano-Artemisio-Faete; Giordano and the CARG Team, 2010), characterised by strombolian activity from several edifices coupled to the emplacement of peripheral lava flows in the interval 308-250 ka (Marra et al., 2003; Gaeta et al., 2016), before switching to the Late Hydromagmatic Phase (200-36 ka; Marra et al., 2016), or Via dei Laghi period (Giordano and the CARG Team, 2010), during which the Ariccia (~200 ka), Nemi (~150 ka), Valle Marciana (~100 ka), and Albano (~70-36 ka) maars were active (e.g., Freda et al., 2006; Giaccio et al., 2009; Marra et al., 2016).

Products of the Colli Albani volcano are generally characterised by K-foiditic compositions (e.g., Peccerillo, 2017), which are not observed for any of the investigated tephra layers, thus allowing us to exclude this volcanic system as a possible source of the investigated F4-F5 tephra.

At Roccamonfina (Fig. 1b), the Upper White Trachytic Tuff (UWTT, ~234 ka; Giannetti and De Casa, 2000) and Yellow Trachytic Tuff (YTT, ~231 ka; Giannetti, 1996) were emplaced, followed by central activity at Mt. Lattani-Mt. Santa Croce latitic scoria cones (173-152 ka; Ruchon et al., 2008).

In the Campanian Plain, activity is documented by a series of ignimbrite deposits, including the Seiano (~250 ka), Moschiano (~188 ka) and Taurano (~160 ka) ignimbrites (De Vivo et al., 2001; Rolandi et al., 2003), and other pyroclastic deposits (i.e., Taurano Layered Tuff Series, 207-188 ka; De Vivo et al., 2001; Belkin et al., 2016). Such a Middle Pleistocene activity in the Campania area is referred to the diffused, so-called Campanian Volcanic Zone (CVZ) by Rolandi et al. (2003), although younger pyroclastic deposits (92-109 ka), similarly spread in the Campanian Plain, have been recently confidently ascribed to the Campi Flegrei activity (Monaco et al., 2022). Therefore, rather than ascribing this Middle Pleistocene activity to a poorly defined zone of diffused volcanism, we prefer to identify its source within the Neapolitan volcanic area (NVA), i.e., an area that roughly envelops the present volcanic centers of the Campi Flegrei, Ischia and Procida. Finally, at Ischia, southern Italy, several Plinian Fall deposits emplaced by this volcano are documented in the island itself and neighbouring areas. The deposits better preserved on the island date back to 75 ka (e.g., Brown et al., 2008, 2014), but with evidence in distal settings of an activity as old as at least 150 ka, and lasting up to historical times (e.g., Poli et al., 1987; Sbrana et al., 2018).

5.1.2. Geochemical signatures and volcanic sources

Potassic tephrites, phonotephrites, tephriphonolites, phonolites, trachytes, shoshonites, and latites compositions (Fig. 4a) are quite common to all the peri-Tyrrhenian Quaternary potassic volcanoes (e.g., Peccerillo, 2017). To identify and discriminate the volcanic sources of the Fucino tephras, we employed the CaO/FeO vs Cl classification diagram (Fig. 4b; Giaccio et al., 2017a), which allows discrimination of products with 52-67 wt.% of SiO_2 of the Roman (i.e., Vulsini, Vico and Sabatini), Roccamonfina and Campanian (i.e., Ischia, Campi Flegrei and Somma-Vesuvius) volcanoes from each other. In Figure 4b (see also Supplementary Fig. S2a), the 21 Fucino tephra can be divided as follows.

Tephra layers TF-21 and TF-23, which are distinguished from all the others by a K_2O/Na_2O ratio < 1 (Fig. S3a), are both characterised by a CaO/FeO ratio < 0.5 and Cl ranging between 0.54-0.74 wt.%, compatible with products from Ischia volcano (Fig. 4b; Fig. S2a). An origin from Ischia for TF-21 was already pointed out by Giaccio et al. (2017a) and is also suggested by the high ratios of HFSE and LREE to Th (Fig. 5c-d), and the anomaly of Ba and Sr (Fig. 5e).

Tephra TF-21a and TF-26 have CaO/FeO ratios ranging between 0.6 and 1.3, and Cl contents of 0.27-0.63 wt.% and 0.27-0.65 wt.%, respectively (Fig. 4b; Fig. S2a), which would suggest a NVA origin for both and specifically in Campi Flegrei. Indeed, TF-26 $^{87}Sr/^{86}Sr$ and $^{143}Nd/^{144}Nd$ values (Fig. 6a-b) are compatible with literature data on old volcanic rocks from the Neapolitan volcanoes.

TF-35 has an intermediate CaO/FeO ratio of 0.74-0.88 and Cl content of 0.26-0.36 wt.% (Fig. 4b; Fig. S2a), which is compatible with either a Roccamonfina or NVA origin.

Tephra layers TF-17a, TF-18, TF-19, TF-27, and TF-30 have a wider CaO/FeO range, generally ≥ 1, and variable Cl content comprised between 0.01 and 0.47 wt.%, which is compatible with products from Sabatini. Indeed, data of the newly acquired TR-CR-2, TR-CR-1 and Vigna di Valle Sabatini units sampled in proximal outcrops perfectly overlap with TF-17a, TF-18, TF-19, TF-27, and TF-30 (Fig. 4b; Fig. S2). TF-28, TF-29 and TF-37 show similarly high CaO/FeO ratios (e.g., TF-28 up to 1.79) and low Cl contents (TF-28 = 0.05-0.21 wt.%; TF-29 = 0.02-0.14 wt.%; TF-37 = 0.04-0.37 wt.%), thus lying at the intersection between the Sabatini and Vulsini-Vico fields (Fig. 4b). Nevertheless, these Cl contents are compatible with that of Pizzo Prato unit (i.e., 0.05-0.14 wt.%), which extends the field of the Sabatini products in the CaO vs Cl diagram (Fig. 4b; Fig. S2b). Hence, one of the possible sources for these samples could be the SVD. Finally, the measured $^{87}Sr/^{86}Sr$ and $^{143}Nd/^{144}Nd$ values (Fig. 6a-b) for TF-18, TF-19, and TF-27 samples are compatible with isotopic variation displayed by SVD proximal samples (Sottili et al., 2019) and overlap with those of the SVD units TR-CR-2, TR-CR-1, and Vigna di Valle, confirming their attribution to the SVD.

Tephra layers TF-22, TF-31, TF-32, TF-33, TF-35b, and TF-43 are characterised by variable CaO/FeO ratios (overall between 0.70-1.50) and low Cl contents, generally $\leq$ 0.10 wt.% (Fig. 4b), overlapping with products of the LVC here investigated, thus suggesting an origin from this volcano. Furthermore, $^{87}Sr/^{86}Sr$ and $^{143}/^{144}Nd$ ratios (Fig. 6a-b) measured for TF-22, TF-31, TF-32, and TF-43 match those of the proximal LVC units (i.e., Pitigliano, Onano, Grotte di Castro, Sorano, Farnese, and Canino Fall-C).

Finally, the two phonolitic tephra TF-24 and TF-25 are characterised by very similar CaO/FeO ratios (0.72-1.43 and 0.81-1.37 respectively) and Cl contents (0.13-0.22 and 0.11-0.20 wt.%), which are compatible with products of both Vico and Vulsini volcanoes. However, considering that LVC products of this period have Cl contents generally $\leq$ 0.10 wt.% (Fig. 4b; Fig. S2b), we are more inclined to consider Vico as the source of these two tephra layers. This is also suggested by the peculiar trace element composition of TF-24 and TF-25 which is clearly distinguished from that of the LVC (Fig. 5). For instance, ratios of Ta to Th for TF-24 and

TF-25 range respectively from 0.012 to 0.015 ppm, and from 0.011 to 0.017 ppm (Fig. S6a), whilst LVC units have Ta/Th ratios generally > 0.020 ppm (Fig. S6b). These trace elements concentrations, however, are compatible with those of Vico Period I units (Fig. 9d), supporting an origin from this volcano.

5.2. Other tephra repositories spanning the late MIS 8-early MIS 6 interval

Only few tephra records, both in continental and marine sedimentary environments, covering the 250-170 ka time interval here considered are documented in the literature. In southern Italy, the lacustrine succession of San Gregorio Magno Basin (Fig. 1a) covers the ~240-15 ka interval (Munno and Petrosino, 2007; Petrosino et al., 2019), with the uppermost tephra (i.e., tephra layer S21) correlated to the Neapolitan Yellow Tuff eruption (NYT, 14.9 ± 0.4 ka; Deino et al., 2004) whilst tephra S4 was directly $^{40}Ar/^{39}Ar$ dated by Ascione et al. (2013) at 239.0 ± 8.0 ka, thus implying that the lowermost three tephra (i.e., S3, S2, and S1) are all older than 240 ka.

In the Adriatic Sea, marine core PRAD 1-2 (Fig. 1a) hosts tephra layers dated back to ~200 ka (Bourne et al., 2010, 2015). Of these, PRAD-3225 was confidently correlated to Ohrid tephra OH-DP-0624 (Leicher et al., 2016) and Fucino tephra TF-17 (Giaccio et al., 2017a). This leaves only the lowermost two tephra (i.e., PRAD-3586 and PRAD-3666) as potential correlatives to the F4-F5 Fucino tephra.

In the Tyrrhenian Sea, the marine core KET 80-04/DED 87-08 (Fig. 1a) spans the 200-90 ka time interval (Paterne et al., 2008) and hosts several tephra layers ascribed to eruptive activity of Italian volcanoes. Giaccio et al. (2017a) proposed a tentative correlation between either C-52 or C-54 (~189-192 ka) with the Ischian-like tephra TF-21.

The long succession of Lake Ohrid (Albania, North Macedonia; Fig. 1a) hosts a rich tephra sequence that continuously spans the last 1.36 Myr (Wagner et al., 2019). Leicher et al. (2016, 2019, 2021) presented data relative to the last 630 kyr, and identified at least 8 tephra layers, attributed to the NVA, Pantelleria and Roccamonfina volcanic systems, covering the time interval of ~241-160 ka, based on the Lake Ohrid age-depth model.

In Greece, the peatland sequence of Tenaghi Philippon (Fig. 1a) is reported to span also the last 1.36 Ma (Tzedakis et al., 2006), but so far detailed tephra studies are available only for the MIS 1-MIS 5 (Wulf et al., 2018), MIS 9-MIS 7e (Vakhrameeva et al. 2019) and MIS 10-MIS 12 (Vakhrameeva et al., 2018), thus covering only marginally the interval of interest of this study. Specifically, Vakhrameeva et al. (2019) reported four tephra layers (i.e., TP05-50.05, TP05-50.45, TP05-50.55, and TP05-50.75) with a modelled age between 240-235 ka. However, these four tephra layers have a peculiar rhyolitic composition of an unknown source, which is not observed in any of the Fucino tephra presented in this study, thus ruling out any possible counterpart candidate from this sequence.

Finally, in the Ionian Sea, cryptotephra investigations from ODP Site 964 (Fig. 1a; Vakhrameeva et al., 2021) allowed land-to-sea correlation for the last 800 kyr. Two visible tephra layers, with an orbital age of ~168 ka (964A-2H-3-78) and ~238 ka (964A-2H-5-59a and 964A-2H-5-59b), were tentatively correlated with tephra from the above-mentioned Lake Ohrid and San Gregorio Magno successions, but discarded based on TE data. Of these, tephra layers 964A-2H-3-78 and 964A-2H-5-59a both have a Pantelleria-like composition (Vakhrameeva et al., 2021), which is not observed among the Fucino tephra and can thus be confidently discarded as potential correlatives. Instead, tephra layer 964A-2H-5-59b has a Campanian like composition that can be tentatively correlated to one of the Fucino tephra. All the other cryptotephra have an age older than 300 ka (Vakhrameeva et al., 2021) and can thus be discarded as well.

To summarize, potential F4-F5 tephra counterparts could be hosted at San Gregorio Magno, PRAD 1-2, DED-87-08, Lake Ohrid, and ODP Site 964 successions.

5.3. Individual tephra correlation

5.3.1. Correlation of Fucino tephra found in F4-F5 and F1-F3 cores

The uppermost interval of the investigated F4-F5 core overlaps with the lowermost interval of the previously investigated shorter F1-F3 core (Giaccio et al., 2017a). In fact, based on the stratigraphic order and features, tephra layers TF-18, TF-19, TF-21, and TF-22 from the F4-F5 core can be confidently linked to the equivalent tephra from F1-F3 core, which were attributed to a Roman-undefined source (TF-18/TF-19, TF-20, and TF-22) and Ischia volcano (TF-21) (Giaccio et al., 2017a). Direct comparison between the F1-F3 and F4-F5 tephra shows consistent geochemical data between the two sets of tephra, corroborating their correlation (Figs. 8a, 9a, 10a).

5.3.2. F4-F5 tephra correlation

5.3.2.1. Tephra from Vulsini-Latera Volcanic Complex

TF-22 - Vulsini unknown. This Vulsini tephra (Fig. 4b) has a variable geochemical composition, with a silica content ranging from 52 wt.% to 61 wt.%, an alkali sums of 8-15 wt.%, and a variable alkali ratio (i.e., K_2O/Na_2O) of 1.3-3.9 (Fig. S3a). In the TAS diagram (Fig. 4a) it occupies various fields and can be classified as a potassic tephriphonolite, phonolite, and latite. Sr and Nd isotope ranges (Fig. 6a-b) indicate a Roman origin as well, corroborating this attribution. None of the analysed Vulsini units has an age compatible with that of TF-22 (i.e., 194.5 ± 2.0 ka; Fig. 7), thus it can be attributed to an undefined Vulsini unit yet to be identified in proximal settings.

A comparison between TF-22 and Adriatic Sea core PRAD 1-2 (Fig. 1a) tephra PRAD-3586 shows a good geochemical match (Fig. 8a). This layer was originally correlated with V-2/Sutri Formation (Bourne et al., 2015) dated at 151 ± 3 ka (Laurenzi and Villa, 1987). However, this correlation is stratigraphically and geochronologically inconsistent with the convincing correlation of the younger PRAD-3225 with TF-17/Taurano Ignimbrite dated at 158.3 ± 3.0 ka proposed by Giaccio et al. (2017a), who also correlate the Vico-C/Sutri eruption to the overlying TF-15. Therefore, the correlation of PRAD-3586 with TF-22 appears fully supported by geochemical data and in agreement with tephrostratigraphical evidence, which places it below PRAD-3225 correlated to TF-17/Taurano Ignimbrite.

In the Tyrrhenian Sea core DED-87-08 (Fig. 1a), Paterne et al. (2008) reported the occurrence of five tephra layers with Roman and/or Campanian like composition, characterised by a High and Low Alkali Ratio, with an age comprised between ~205-183 ka. Of these, C-56 occurs just after the end of MIS 7 (~196 ka in Paterne et al., 2008), with an estimated age of 196.4 ka, which corresponds to that of TF-22 (194.5 ± 2.0 ka). The EDS geochemical composition, reported as mean and standard deviation values, provided for this tephra by Paterne et al. (2008) is consistent whit that of TF-22 and PRAD-3586 (Fig. 8a). However, the lack of individual WDS glass composition prevents us from any conclusive correlation between C-56 and TF-22/PRAD-3586.

TF-31 - Onano. This tephra falls in the middle of the period of increasing Ca content recorded by the Fucino sediments correlated to the MIS 7 period (Giaccio et al., 2019; Fig. 3), a climatostratigraphic position that allows us to estimate its age around 220 ka (Fig. 3), in agreement with its position between TF-27 and TF-32, here $^{40}Ar/^{39}Ar$ dated at 205.1 ± 1.4 ka and 224.9 ± 1.0 ka, respectively (Fig. 7).

TF-31 displays a very heterogeneous composition, ranging from tephrite to phonolite-trachyte with a compositional gap separating a less evolved tephritic-phonotephritic-tephriphonolitic population from a more evolved phonolitic-trachytic component (Fig. 4b). Among the LVC proximal pyroclastic units, the Onano eruption (Palladino and Simei, 2005) similarly consists of a heterogeneous composition (Fig. 4a), and comparison between TF-31 and Onano shows a good geochemical match (Fig. 8b). Here the Onano unit is $^{40}Ar/^{39}Ar$ dated at 224.7 ± 2.6 ka, in agreement with the climatostratigraphic position of TF-31 and thus corroborating this correlation.

TF-32 - Grotte di Castro. This tephra is located ~1 m below TF-31/Onano and is directly dated by $^{40}Ar/^{39}Ar$ at 224.9 ± 1.0 ka, i.e., an age indistinguishable from that of TF-31/Onano (Fig. 7). It is characterised by a peculiar composition that occupies various fields of the TAS diagram (Fig. 4a), classifiable as a tephriphonolite-phonolite-trachyte-latite. In terms of TE composition, TF-32 shows REE concentrations (e.g., Y = 23-34 ppm, Fig. S4a; La = 95-128 ppm; Ce = 184-234 ppm) similar to Grotte di Castro (Y = 26-40 ppm, Fig. S4b; La = 105-184 ppm; Ce = 183-286 ppm), although the composition of the latter is more enriched in incompatible elements. Based on these stratigraphic, geochronological, and geochemical constraints, the Grotte di Castro unit (Colucci et al., 2013) arises as the best correlation candidate for TF-32. Major element bivariate diagrams (Fig. 8b) show a good geochemical match between TF-32 and Grotte di Castro. Furthermore, in proximal settings, Grotte di Castro is overlain by deposits of Onano (e.g., Palladino et al., 2010; Colucci et al., 2013), here correlated with TF-31. Finally, the $^{40}Ar/^{39}Ar$ date of 224.9 ± 1.0 ka for TF-32 matches very well that of 225.3 ± 1.2 ka of Grotte di Castro (Fig. 7). Therefore, the stratigraphic position and the geochemical and geochronological data consistently confirm this correlation.

TF-33 - Sovana. TF-33 is found less than one meter below TF-32/Grotte di Castro and thus should be slightly older than 224.9 ± 1.0 ka, which places it in the middle of the MIS 7 period (Fig. 3). This phonolitic tephra is characterised by a homogeneous composition, with SiO_2 ranging between 57-61 wt.% and alkali sum of 12-15 wt.% (Fig. 4a), falling at the boundary with the trachyte field. The LVC units of Sorano and Sovana, which in proximal settings underlie the Grotte di Castro unit (Palladino and Taddeucci, 1998; Palladino et al., 2010, 2014; Valentine et al., 2019), here correlated to TF-32, represent the two most likely candidates for a correlation with TF-33, and the comparison with the Sovana glass data shows a good geochemical match with TF-33 (Fig. 8c). Here, the Sovana unit is $^{40}Ar/^{39}Ar$ dated at 226.4 ± 0.7 ka (Fig. 7), thus in agreement with the immediately overlying TF-32 correlated to Grotte di Castro, here $^{40}Ar/^{39}Ar$ dated at 224.9 ± 1.0 ka and 225.3 ± 1.2 ka (weighted mean age: 225.1 ± 0.8 ka), respectively (Fig. 7). In proximal settings, the Sovana unit was dated at 215 ± 6.0 ka (Turbeville, 1992), highlighting that previous age determinations of some Latera units were substantially underestimated.

TF-35b - Farnese. This LVC tephra falls at the end of the first peak of Ca content in Fucino’s sediments, likely corresponding to the end of the MIS 7e sub-stage (Fig. 3), astronomically dated between ~244 and ~234 ka (Lisiecki and Raymo, 2005). For this tephra, due to its low glass shard concentration, we managed to acquire only 3 analytical points, which likely are insufficient for expressing the full geochemical variability of the tephra. Among the remaining LVC units, the only one with a similar phonolitic composition and a chronology consistent with TF-35b is the Farnese unit (Figs. 4a, 8d; Palladino and Valentine, 1995). Here, the Farnese unit is $^{40}Ar/^{39}Ar$ dated at 235.6 ± 0.6 ka, which is consistent with the climatostratigraphic position of TF-35b, thus supporting the correlation. The new age we obtained for Farnese is also consistent with the less precise age of 242 ± 8 ka previously determined for this unit (Turbeville, 1992). The correlation allows us to transfer the new high precision $^{40}Ar/^{39}Ar$ age of Farnese to the Fucino succession.

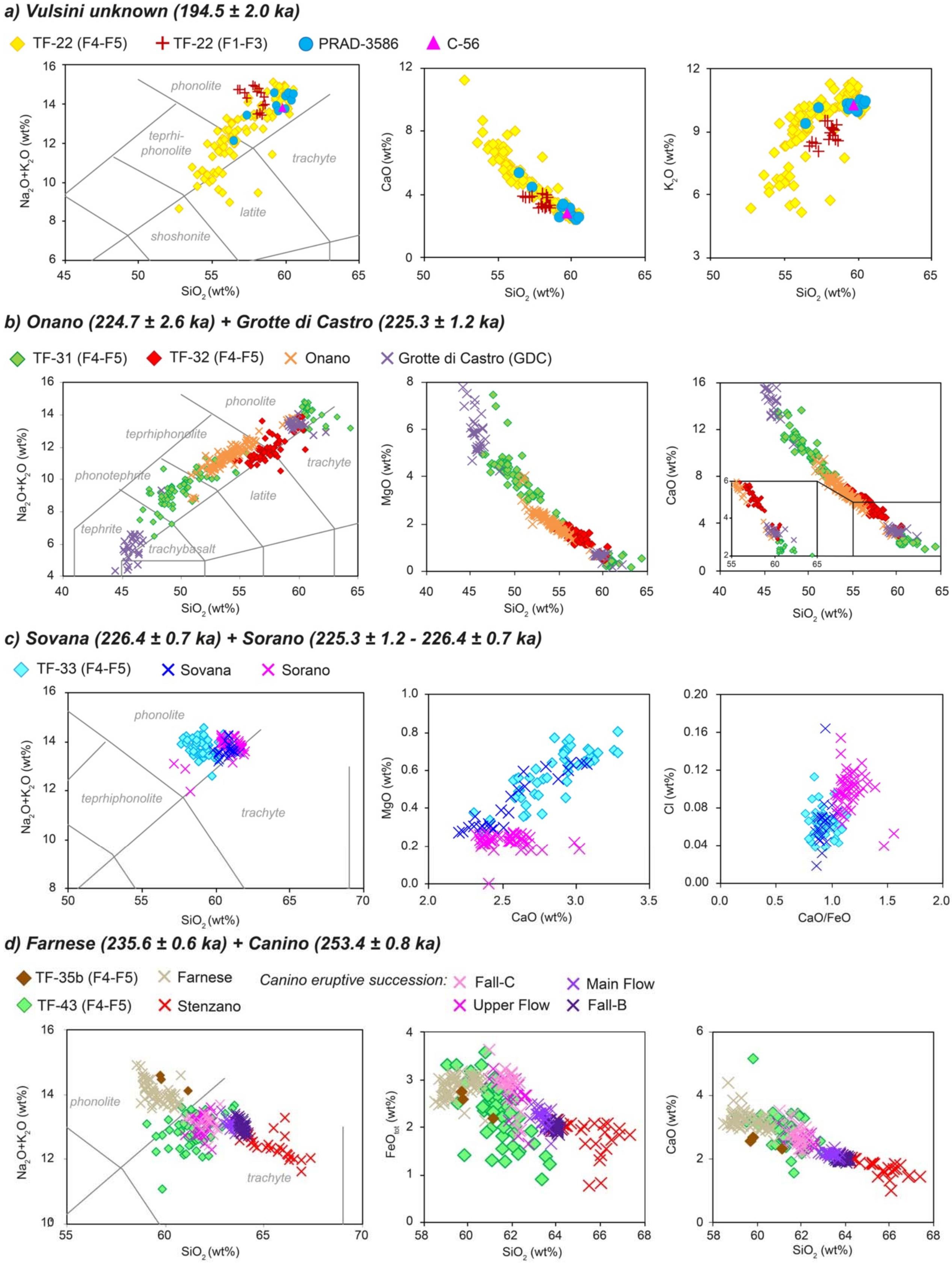

Figure 8. *Total alkali vs silica* (TAS) classification diagram (Le Maitre et al., 2002) and representative major element biplots for TF-22, TF-31, TF-32, TF-33, TF-35b, and TF-43 from the F4-F5 record compared with proximal Latera Volcanic Complex (LVC) units. Data source: WDS glass composition of TF-22, TF-31, TF-32, TF-33, TF-35b, TF-43 (F4-F5), Onano, Grotte di Castro, Sorano, Sovana, Farnese, Stenzano, and Canino (Fall-C, Upper Flow, Main Flow and Fall-B): this study; TF-22 (F1-F3): Giaccio et al. (2017a); PRAD-3586: Bourne et al. (2015); whole-rock mean composition of DED-87-08 C-56 tephra: Paterne et al. (2008); $^{40}Ar/^{39}Ar$ age of TF-22, TF-32, Onano, Grotte di Castro, Sovana, Farnese, and Fall-C: this study.

TF-43 - Canino. This LVC tephra, the lowermost investigated in this study, falls towards the end of an interval of low Ca sediment concentrations (Fig. 3), which is interpreted as the expression of the MIS 8 glacial period (Giaccio et al., 2019) and thus has an estimated climatostratigraphic age of ~250 ka. It is mainly characterised by a slightly variable trachytic composition, with 59-64 wt.% SiO_2 and 11-14 wt.% alkali sum (Fig. 4a). Among the LVC units, both the Stenzano (Taddeucci and Palladino, 2002) and Canino (Palladino and Agosta, 1997; Palladino et al., 2010) units are characterised by a trachytic composition (Fig. 4a) and are chronostratigraphically compatible with TF-43. A comparison with these units reveals a convincing geochemical match between Canino and TF-43 (Fig. 8d). The $^{87}Sr/^{86}Sr$ ratio obtained for TF-43 (i.e., 0.7106), although being perfectly in line with the values of the other Vulsini units (Fig. 6a), is somewhat lower than the values obtained for Canino (i.e., 0.7108). This discrepancy can be attributed to either an isotopic variability within the feeding system that fed the eruption or a not completely clean feldspar fraction. Here, Canino Fall-C has been dated at 253.1 ± 0.8 ka, an age virtually indistinguishable from that of Canino Fall-B (253.8 ± 0.8 ka; Fig. 7) and fully in agreement with previous $^{40}Ar/^{39}Ar$ age of 253 ± 6.0 ka (Turbeville, 1992), which has been recalibrated in this study. The Canino chronology is also consistent with the late MIS 8 climatostratigraphic position of TF-43. The correlation of Canino with TF-43 allows us to transfer its high-precision $^{40}Ar/^{39}Ar$ age to the Fucino succession, providing an age control point for the lower part of the studied interval.

5.3.2.2. Tephra from Sabatini

TF-17a - Trevignano Romano TR-CR-2. This Sabatini tephra occurs **~**2 m below TF-17, $^{40}Ar/^{39}Ar$ dated at 158.8 ± 3.0 ka (Giaccio et al., 2017a), and in the early part of the MIS 6 glacial (Fig. 3). It is phonolitic in composition (Fig. 4a) with variable silica concentrations (56.1-61.3 wt.%) and alkali sums (14.1-16.1 wt.%). It has a major element geochemical composition similar to the newly investigated TR-CR-2 unit from Trevignano Romano (Tables 1, 3; Fig. 9a). In proximal settings, TR-CR-2 is stratigraphically located under deposits of the S. Bernardino Maar (Sottili et al., 2010; Sottili et al., 2012), which has an inferred age of ≤172 ka, compatible with the stratigraphic position of TF-17a. Thus, here we correlate TF-17a with TR-CR-2, based on geochemical and stratigraphic evidence.

TF-18/TF-19 - Trevignano Romano TR-CR-1. This couplet of Sabatini tephras, like TF-17a, occurs in the early part of the period characterised by low Ca content correlated to the MIS 6 glacial (Fig. 3) and are bracketed between tephra TF-17 and TF-22, $^{40}Ar/^{39}Ar$ dated at 158.8 ± 3.0 ka (Giaccio et al., 2017a) and 194.4 ± 2.0 ka (this study; Fig. 7), respectively. They stratigraphically match the couplet of the geochemically indistinguishable tephra TF-18/TF-19 found in the F1-F3 core that was ascribed to an undefined Roman source (Giaccio et al., 2017a). Here, we correlate TF-18/TF-19 to the TR-CR-1 unit from Trevignano Romano (Tables 1, 3; Fig. 1), which displays similar major and trace element compositions (Figs. 5, 9a). For instance, TF-18 and TF-19 have HFSE ratios to Y (i.e., Nb/Y = 0.89-1.22 [TF-18] and 1.02-1.34 [TF-19]; Zr/Y = 14.34-19.75 [TF-18] and 14.41-20.22 [TF-19]; Fig. S5a) similar to TR-CR-1 (Nb/Y = 0.99-2.58; Zr/Y = 18.15-42.23; Fig. S5b). $^{87}Sr/^{86}Sr$ and $^{143}Nd/^{144}Nd$ ratios determined on TF-18 and TF-19 overlap with those of TR-CR-1 and the other SVD units (Fig. 6a-b), corroborating these correlations. In proximal settings, TR-CR-1 occurs below TR-CR-2, consistent with the correlation of TF-17a with TR-CR-2.

TF-27 - Vigna di Valle. This Sabatini tephra occurs in a stadial pulsation of the late MIS 7, likely corresponding to the MIS 7b sub-stage dated at ~205 ka in LR04 Benthic Stack (Fig. 3), and just below the Iceland Basin geomagnetic excursion (Giaccio et al., 2019). It is characterised by a variable composition, mainly phonolitic, and can be classified as tephriphonolite-phonolite-latite-trachyte according to the TAS diagram (Fig. 4a). $^{87}Sr/^{86}Sr$ and $^{143}Nd/^{144}Nd$ ratios determined on TF-27 support an origin from Sabatini, as these values overlap with those of the other SVD units (Fig. 6a-b). Comparisons with the proximal SVD pyroclastic units show a convincing geochemical match with the Vigna di Valle unit (Fig. 9b), dated at 193.0 ± 7.0 ka (FCt 28.02; Sottili et al., 2010), equivalent to 195.0 ± 7.0 using FCt at 28.294 Ma or ACs at 1.1891 Ma (Niespolo et al., 2017), thus in disagreement with the age of 205.1 ± 1.4 ka (Fig. 7) detetermined here for TF-27. However, in Sottili et al. (2010), only 4 crystals were used for calculating the weighted mean age of Vigna di Valle, whilst other 4 crystals were excluded, being interpreted as xenocrysts. However, 3 of these supposed xenocrysts have ages that overlap with those of the 4 accepted ones if we consider the 1-sigma. Thus, by reintegrating these 3 previously rejected but consistent crystals, the weighted mean age of Vigna di Valle becomes 205.9 ± 5.0 ka, i.e., in agreement with the more precise $^{40}Ar/^{39}Ar$ age of 205.1 ± 1.4 ka we obtained for TF-27 (Fig. 7), which supports our correlation and substantially reduces the chronological uncertainty for the Vigna di Valle eruption.

TF-28 - Sabatini unknown. This tephra occurs in the second half of the MIS 7, at the end of a period of high Ca content likely corresponding to the end of MIS 7c, and thus has an estimated age of ~210 ka (Fig. 3). It is characterised by a dominant phonolitic composition (Fig. 4a; Fig. S1b), with a SiO_2 content of 55-63 wt.%

and alkali sum of ~11-16 wt.%. According to the CaO/FeO vs Cl classification diagram, TF-28 falls between the Vulsini+Vico and Sabatini fields, making its attribution to one of these three potential volcanic sources challenging. However, the newly acquired glass-WDS data from proximal Pizzo Prato unit perfectly overlaps with TF-28, allowing it to be ascribed to the Sabatini volcano (Figs. 4b, 9c). However, the age of 251 ± 16 ka available for the Pizzo Prato unit (Sottili et al., 2010), although associated with a large error, appears not compatible with the position of TF-28, which occurs less than 1 m below TF-27/Vigna di Valle, dated at 205.1 ± 1.4 ka. This large age discrepancy would suggest either a correlation with another, currently undocumented, Sabatini unit younger than Pizzo Prato, or a substantial age overestimate (due to xenocryst contamination?) of the Pizzo Prato unit. In lack of a new age determination, we propose for now a correlation of TF-28 tephra with an undocumented Sabatini unit.

TF-30 - Sabatini unknown. This tephra is located closely below the above-mentioned TF-28 tephra and thus shares with it a similar climatostratigraphc position and age (Fig. 3). Its phonolitic composition (Fig. 4a) does not match that of the Pizzo Prato unit (Fig. 9c) or those of other geochronologically compatible known Sabatini units (e.g., Sottili et al., 2019; Marra et al., 2020). Nevertheless, the geochemical composition of TF-30, similar to those of the other Sabatini units here investigated, suggests an origin from this volcano and this tephra is therefore here ascribed to an undefined Sabatini eruption.

5.3.2.3. Tephra from Vico

TF-24 and TF-25 - Vico unknown. These two chemically related tephra layers are climatostratigraphically associated to the early stage of MIS 6 (Fig. 3). They are characterised by a similar and homogeneous phonolitic composition, with SiO_2 ranging between 56-60 wt.% (TF-24) and 57-60 wt.% (TF-25) and an alkali sum of 12-15 wt.% (both; Fig. 4). Despite their almost identical composition, reworking processes can be excluded because they are separated by ~10 cm of lacustrine sediment and do not show any of the lithological feature indicating reworking (i.e., graded basl boundary, normal grading, admixture with no-volcanic sediment). TF-24 and TF-25 are positioned between TF-22 and TF-27, dated at 194.4 ± 2.0 ka and 205.1 ± 1.4 ka respectively, collocating them between the caldera-forming eruptions of Vico Ignimbrite A (or Farine Formation, ~250 ka; Sollevanti, 1983) and Ignimbrite B (or Ronciglione Formation, 157 ± 3 ka; Laurenzi and Villa, 1987). Comparison with the newly acquired glass-WDS composition of Vico-A/Farine Formation unit (Fig. 9d) shows geochemical similarities with the two Fucino tephra (i.e., similar CaO/FeO ratio), which further supports an origin from Vico volcano. However, so far, no eruption is reported between the Vico-A and Vico-B Ignimbrites (e.g., Perini et al., 2004), preventing us from any tentative correlation and suggesting that the two Fucino tephra represent deposits of an explosive activity currently undocumented in proximal settings.

However, in distal settings we find a good geochemical match between TF-24/TF-25 and the Adriatic tephra PRAD-3666 (Fig. 9d). The layer PRAD-3666 was originally attributed to an undefined Roman volcano (Bourne et al., 2015) and was geochronologically poorly constrained between 181 and 156 ka. However, as already discussed above (see section 5.3.2.1.) and in previous studies (e.g., Giaccio et al., 2017a), the age model for the Middle Pleistocene section of PRAD 1-2 is biased by errouneus correlations. Here, we propose PRAD-3666 as a correlative tephra for TF-24 and/or TF-25 tephra, which is fully consistent with the above proposed correlation of PRAD-3586 with TF-22 (see section 5.3.2.1).

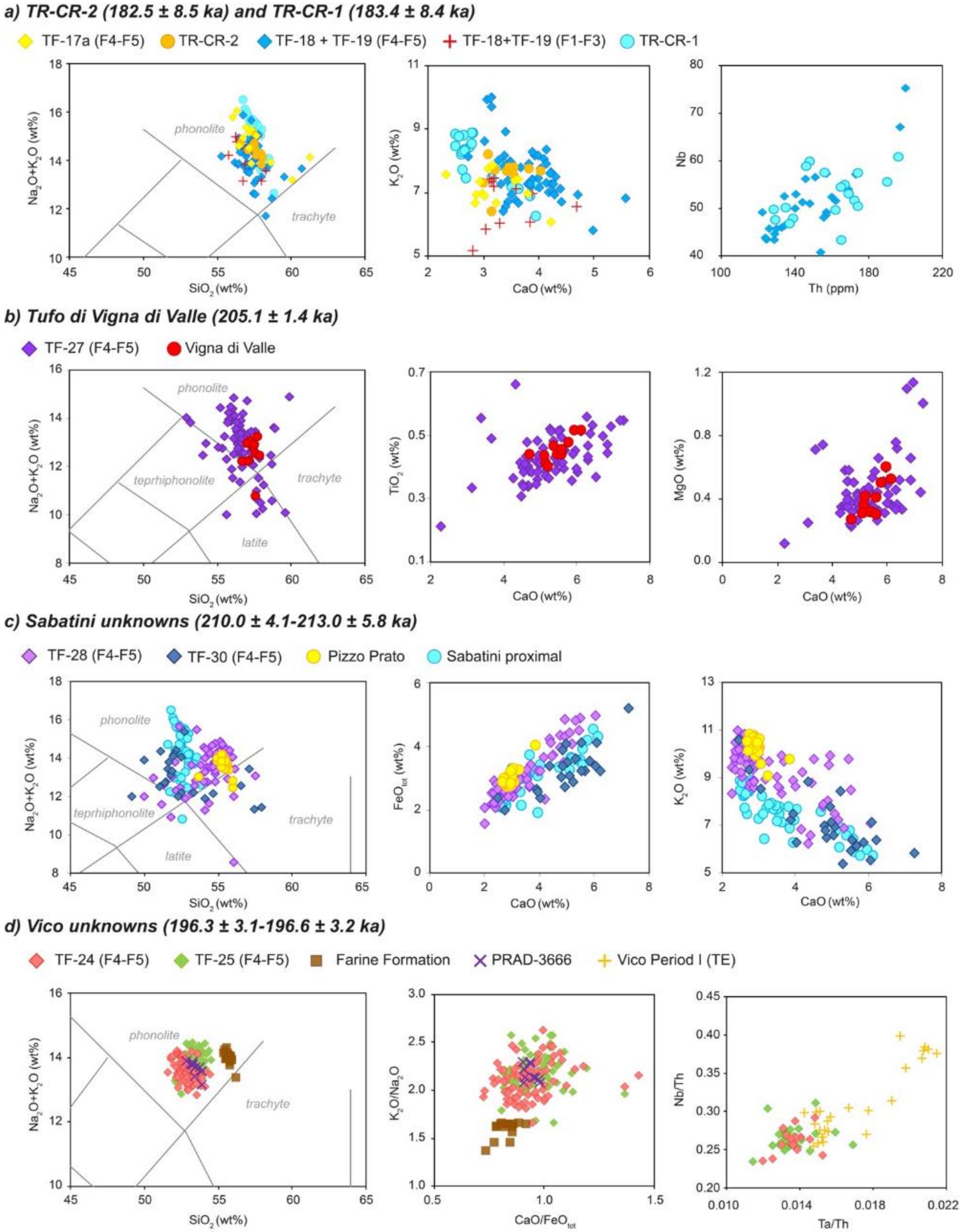

Figure 9. *Total alkali vs silica* (TAS) classification diagram (Le Maitre et al., 2002) and representative major and trace element bivariate diagrams for TF-17a, TF-18, TF-19, TF-24, TF-25, TF-27, TF-28, and TF-30 from the F4-F5 record compared with proximal Sabatini Volcanic District (SVD) and Vico (i.e., Farine formation) units. Data source: WDS glass composition of TF-17a, TF-18, TF-19, TF-24, TF-25, TF-27, TF-28, TF-30 (F4-F5), TR-CR-2, TR-CR-1, Vigna di Valle, Pizzo Prato (Sabatini proximal data), and Farine Formation (Vico): this study; TF-18 + TF-19 (F1-F3): Giaccio et al. (2017a); PRAD-3666: Bourne et al. (2015); TE glass composition of TF-18+TF-19, TF-24, and TF-25: this study; TE glass composition of Vico Period I: Monaco et al. (2021); $^{40}Ar/^{39}Ar$ age of TF-27: this study. $^{40}Ar/^{39}Ar$ age of TR-CR-2, TR-CR-1, TF-28/Sabatini, TF-30/Sabatini, TF-25 and TF-25/Vico = age depth model of this study.

5.3.2.4. Roman-undefined tephra

TF-29 and TF-37. TF-29, deposited in the late part of the MIS 7 period (Fig. 3), is characterised by a latitic-trachytic composition, with SiO_2 values ranging from 55 to 65 wt.% and alkali sums of 9-12 wt.%. TF-37 has a polymodal composition (Fig. 4a; Fig. S1a), ranging from phonotephrite to phonolite-trachyte, with increasing alkali sum at increasing SiO_2. The limited number of analytical points obtained for these two tephra layers (9 and 11 respectively) makes their attribution to one of the peri-Tyrrhenian volcanic sources challenging. In the CaO/FeO vs Cl classification diagram (Fig. 4b) they fall at the Sabatini and Vulsini+Vico boundary. The low Cl content of TF-29 (mean of 0.08 wt.%) and TF-37 (mean of 0.11 wt.%) surely point out a Roman origin, the specific source of which is however not confidently determinable. For these reasons, these two tephras will be ascribed to a Roman-undefined volcanic source.

5.3.2.5. Tephra from Ischia

TF-21 and TF-23. Both Ischia tephra TF-21 and TF-23 are climatostratigraphically placed in the early MIS 6 glacial period and are located respectively above and below TF-22, here $^{40}Ar/^{39}Ar$ dated at 194.4 ± 2.0 ka. They are characterised by a homogeneous trachytic composition (Fig. 4a), with SiO_2 contents ranging between 62-64 wt.% (TF-21) and 62-65 wt.% (TF-23) and identical alkali sums (~13-15 wt.%). In Giaccio et al. (2017a), tephra layer TF-21 was tentatively correlated to either the C-52 or C-54 tephra layers from the Tyrrhenian marine core KET 80-04/DED-87-08 of Paterne et al. (2008). Although the geochemical composition of TF-21 and TF-23 is compatible with that of the Tyrrhenian layers C-52 and C-54 (Fig. 10a), the lack of individual glass analysis for these marine tephras still leaves this potential correlation uncertain.

5.3.2.6. Tephra from Roccamonfina/Neapolitan volcanic area?

TF-35. This tephra is characterised by a homogeneous trachytic composition, with 61-64 wt.% SiO_2, 11-13 wt.% alkali sums, and mean K_2O/Na_2O ratios of 1.63 ± 0.25 (2σ; Fig. 4). The relatively high Cl content (up to 0.36 wt.%) and CaO/FeO ratio of 0.74-0.88 suggest either a Roccamonfina or NVA origin for this tephra (Fig. 4b-l). It is located between TF-33/Sovana (226.4 ± 0.7 ka) and TF-35b/Farnese (235.6 ± 0.6 ka). In proximal settings, deposits of the Roccamonfina caldera-forming eruptions of the Upper White Trachytic Tuff (UWTT, Subunit G of Giannetti and De Casa, 2000) and Yellow Trachytic Tuff (YTT) were respectively dated at 234.0 ± 9.0 ka (recalculated age from Giannetti and De Casa, 2000) and 231 ± 6.0 ka (recalculated age from Giannetti, 1996), which are compatible with that of ~230 ka estimated for TF-35. Rouchon et al. (2008) provided whole-rock composition of two WTT samples (i.e., RMF96 and RMF11), both trachytic in composition. However, it is not specified by the authors to which sub-units the two samples refer, preventing us from any tentative correlation with these units. Nevertheless, based on chronological constraints, TF-35 might represent one of the two above-mentioned eruptions of the UWTT-YTT.

At Lake Ohrid (Fig. 1a), Leicher et al. (2019) reported the occurrence of some tephra with uncertain Campi Flegrei (NVA)/Roccamonfina-like (i.e., OH-DP-0997, OH-DP-1055) or Campi Flegrei geochemical signature (OH-DP-1006). Of these, the older OH-DP1055 (241.2 ± 6.2 ka) is roughly consistent with the oldest activity documented in the Campanian area, which relates to the Seiano Ignimbrites dated beween ~250 ka and ~290 ka (Rolandi et al., 2003) and which precedes the Taurano-Moschiano phase (~190-160 ka; Rolandi et al., 2003). The younger OH-DP-0997 and OH-DP-1006 tephras, with modelled ages of 228.9 ± 5.7 and 230.9 ± 6.3 ka, respectively (Leicher et al., 2021), are chronologically compatible with TF-35. The comparison between TF-35 and these two Ohrid tephra, however, shows remarkable geochemical differences with OH-DP-0997, while some degree of similarity with OH-DP-1006 can be noted, although OH-DP-1006 shows a wider compositional variability (Fig. 10b). Leicher et al. (2021) correlated OH-DP-1006 to the S2 tephra from San Gregorio Magno (Munno and Petrosino, 2007), which, like TF-35, shows a more homogenous composition, and thus TF-35 and S2 are more similar to each other than to OH-DP-1006 (Fig. 10b). The S2 tephra at San Gregorio Magno directly underlies tephra S4, $^{40}Ar/^{39}Ar$ dated at 239 ± 8 ka (Ascione et al., 2013), and thus within 2 sigma age uncertainty of the ages obtained for TF-35 and the Ohrid tephras. However, due to the vague geochemical match, we consider only a tentative correlation of all these tephras.

5.3.2.7. Tephra from NVA

TF-21a and TF-26. Both TF-21a and TF-26 are MIS 6 tephra, that were emplaced at the very onset of this glacial period and have an estimated age of ~200-190 ka (Fig. 3). They are characterised by a phonolitic-trachytic composition (Fig. 4a), with a similar increase of the alkali content at increasing silica, which ranges between 58-62 wt.% (TF-21a) and 56-63 wt.% (TF-26). The relatively high and variable Cl content (TF-21a = 0.23-0.63 wt.%; TF-26 = 0.19-0.65 wt.%), the CaO/FeO ratios (Fig. 4b, Fig. S2a) and the Sr-Nd isotope composition (Fig. 6b) clearly point to a NVA origin for both tephras. Specifically, the low $^{87}Sr/^{86}Sr$ (0.706-0.707) and simultaneously high $^{143}Nd/^{144}Nd$ ratios (i.e., 0.5126) for TF-26 are typical features of the older Campi Flegrei products (e.g., D'Antonio et al., 2007; Monaco et al., 2022) preceding the Campanian Ignimbrite eruption (39.85 ± 0.14 ka; Giaccio et al., 2017b). The Moschiano Ignimbrite (Rolandi et al., 2003), with a poorly constrained age of 188.0 ± 7.4 ka, could represent a possible candidate for a correlation with TF-21a (Fig. 11, Table 5). So far, the only available glass composition of these late Middle Pleistocene units refers to the Taurano Ignimbrite (sample AF-Y1-13; Amato et al., 2018) dated at 160.2 ± 2.0 ka (recalculated; De Vivo et al., 2001) and correlated to the Fucino tephra TF-17, dated to 158.3 ± 3.0 ka, and other equivalent tephra layers in the Adriatic Sea and Lake Ohrid (Giaccio et al., 2017a). Overall, the compositions of TF-21a and TF-26 are consistent with that of Taurano Ignimbrite/TF-17, including all its distal equivalents (Fig. 10c-d). Thus, TF-21a and TF-26 can be similarly ascribed to a late Middle Pleistocene NVA activity, which in the Campanian Plain is sporadically documented by ignimbrites and ash-fall deposits occurring in suitable depositional settings. Here we propose a correlation of TF-21a to the Moschiano Ignimbrite, whilst we attribute TF-26 to a volcanic activity preceding the emplacement of the Taurano Ignimbrite, i.e., the pre-Taurano Ignimbrite unit.

In the Mediterranean area, late Middle Pleistocene Neapolitan-like tephra layers are reported in several repositories. At Lake Ohrid (Fig. 1a), at least seven tephra with Neapolitan-, Roccamonfina-like composition are recorded in the time interval of 241-160 ka (Leicher et al., 2019, 2021). Of these, Ohrid tephra OH-DP-0725 (Leicher et al., 2021; new glass-EPMA-WDS data presented also in this study) shows a good geochemical match with both TF-21a and TF-26 based on major element composition (Fig. 10c-d). However, OH-DP-0725 has a modelled age of 174.4 ± 5.2 ka (Leicher et al., 2021), which is geochronologically incompatible with both TF-21a and TF-26, therefore excluding a possible correlation.

A reliable geochemical match is also observed between Fucino tephra TF-21a and S7 tephra from San Gregorio Magno Basin (Munno and Petrosino, 2007), which occurs just below tephra S8, correlated to OH-DP-0710 (Leicher et al., 2019) and dated to 172.3 ± 5.6 ka (Leicher et al., 2021). TF-21a, with an estimated age of 190-180 ka, can be thus tentatively correlated with S7 (Fig. 10c). In the Tyrrhenian core DED-87-08 other Neapolitan-like tephra, chronologically compatible with TF-21a and TF-26, such as C-49/C-51 (178-183 ka) and C-53/C-55 (~189-196 ka) respectively, have been reported by Paterne et al. (2008), and show a composition similar to both TF-21a and TF-26 (Fig. 10c-d). Again, the lack of individual glass analysis prevents us from any definitive correlation. Notably, in core DED-87-08 a couple of younger tephra (C-41 and C-42; ~150 ka; Paterne et al., 2008) are geochronologically and geochemically roughly consistent with the Taurano Ignimbrite/TF-17 (Fig. 10c).

Finally, at ODP Site 964 (Vakhrameeva et al., 2021), tephra layer 964A-2H-5-59b has a Campanian like composition. However, both geochemical (major and minor elements) and geochronological (orbital age of ~238 ka) data rule out a correlation with any of the two Fucino tephra layers.

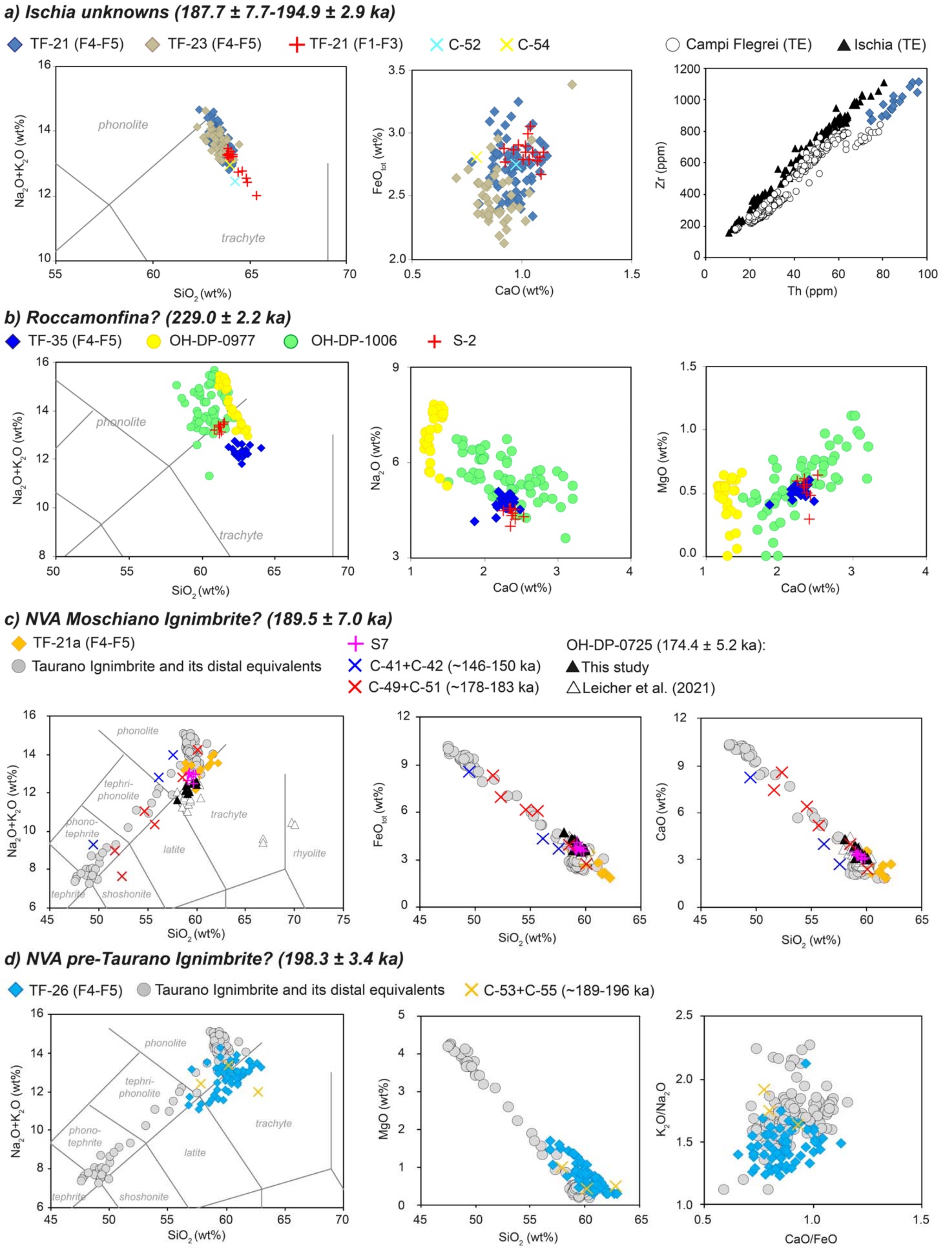

Figure 10. *Total alkali vs silica* (TAS) classification diagram (Le Maitre et al., 2002) and representative major and trace element bivariate diagrams for TF-21, TF-21a, TF-23, TF-26, and TF-35 from the F4-F5 record compared with OH-DP-0725, OH-DP-0977, OH-DP-1006 and tephra layers from the literature. Data source: WDS glass composition of TF-21, TF-21a, TF-23, TF-26, and TF-35 (F4-F5), and OH-DP-0725: this study; TF-21 (F1-F3): Giaccio et al. (2017a); OH-DP-0725, OH-DP-0977, OH-DP-1006: Leicher et al. (2021); EDS composition of S2 and S7: Munno and Petrosino (2007); whole-rock composition of C-41, C-42, C-49, C-51, C-52, C-53, C-54 and C-55: Paterne et al. (2008). Taurano Ignimbrite literature data: TF-17 (Giaccio et al., 2017a), OH-DP-0624 (Leicher et al., 2021), PRAD-3225 (Bourne et al., 2015), AF-Y1-13 and S11-PAUP (Amato et al., 2018). Trace element glass composition of TF-21 (F4-F5): this

study; trace element glass composition of proximal Ischia and Campi Flegrei pyroclastic units: Tomlinson et al. (2012, 2015). All the $^{40}Ar/^{39}Ar$ ages derive from the age-depth model.

5.4. Age model

Using the $^{40}Ar/^{39}Ar$ ages of the Fucino tephras (Fig. 7) and those derived from the above-discussed correlations of these tephras with the newly dated proximal counterparts (Fig. 7), we developed a Bayesian age-depth model for the interval of ~250-170 ka (Fig. 11a) using the Bacon software (Blaauw and Christen, 2011). Specifically, eleven $^{40}Ar/^{39}Ar$ ages related to eight tephra layers were used, as shown in Figure 11a. For three of them (TF-17, TF-27, and TF-32) we used the weighted mean ages resulting from both the direct dating of the Fucino tephra and the related proximal equivalents. In one case, only the direct $^{40}Ar/^{39}Ar$ age of the Fucino tephra (TF-22) was integrated, while for the remaining 4 tephra (TF-31, TF-33, TF35b and TF-43) only the age of the correlated proximal equivalents was used (Fig 11a).

The chronological constraints are quite well distributed along the succession, with a higher density of the control points between 224 ka and 235 ka (Fig. 11a). Overall, the resulting curve shows a quite constant sedimentation rate and history of sediment accumulation (Fig. 11b). The age-depth model allows us to reliably assess the age of each individual late MIS 8-early MIS 6 investigated tephras as modelled ages, with their own statistically significant uncertainty, as shown in Figure 11b and summarized in Table 5.

5.5. Implications for volcanology and Quaternary sciences

5.5.1. Mediterranean tephrochronology and peri-Tyrrhenian explosive activity during MIS 8-6 revaluated in light of the Fucino record

The detailed late MIS 8-early MIS 6 tephra record from Fucino basin significantly enriches the Mediterranean tephrochronology and allows a substantial refinement of the peri-Tyrrhenian eruptive history in the time interval of 250-170 ka (Fig. 11).

As summarized in section 5.2., very few Mediterranean records cover, totally or partially, the investigated interval and sometimes the related data are not provided as full geochemical dataset (e.g., core DED 87-08 from the Tyrrhenian Sea), thus currently limiting a full exploitation of the Fucino record for possible correlations.

Here, we propose two potential new correlations between the Adriatic Sea PRAD 1-2 and the F4-F5 Fucino tephras (i.e., TF-22=PRAD-3586 and TF-24/TF-25=PRAD-3666) that substantially improve the chronology for the lowermost interval of the PRAD 1-2 sediment core. Specifically, TF-22=PRAD-3586 is here precisely $^{40}Ar/^{39}Ar$ dated at 194.5 ± 2.0 ka, while the modelled age for TF-24/TF-25=PRAD-3666 is 196.3 ± 3.1-196.6

± 3.2 ka (Table 5). We also present a tentative correlation of tephra layer S7 from the San Gregorio Magno Basin succession (Munno and Petrosino, 2007; Petrosino et al., 2019) with the NVA-like Fucino tephra TF-21a, which has a modelled age of 189.5 ± 7.0 ka (Table 5). The former is also geochemically similar to Ohrid tephra OH-DP-0725, for which here we have provided new glass-WDS analysis. However, both the modelled age at 174.4 ± 5.2 ka and the climatostratigraphic position of OH-DP-0725 (Leicher et al., 2021) appear incompatible with a correlation with TF-21a (Fig. 12). A quite convincing correlation has instead been proposed between TF-35, with a modelled age of of 229.2 ± 2.2 ka (Table 5; Fig. 11b), and the likely NVA tephra S2/OH-DP-1006, from San Gregorio Magno Basin and Lake Ohrid, respectively. Therefore, for the 250-170 ka interval, in addition to TF-17/OH-DP-0624 (Fig. 12), which is correlated to the Taurano Ignimbrite (Giaccio et al., 2017a), TF-35/OH-DP-1006 might represent a second tie point for synchronizing Fucino and Ohrid lake successions (Fig. 12).

Finally, some possible correlations might exist between the Fucino and DED 87-08 tephra layers. However, the potential correlations (i.e., TF-21=C-52/C-54, TF-21a=C-53/55, TF-22=C-56, TF-26 = C-53/55) cannot be here definitively proposed due to the lack of individual WDS-glass compositions of the DED-87-08 tephra layers, leaving these correlations open to future investigations. Unfortunately, no tephra correlation has been determined between the Fucino paleolake sequence and Tenaghi Philippon or ODP Site 964 for this time interval. However, currently the MIS 6-7d interval at Tenaghi Philippon has not been investigated yet, thus correlations between the two tephra repositories might emerge in the future.

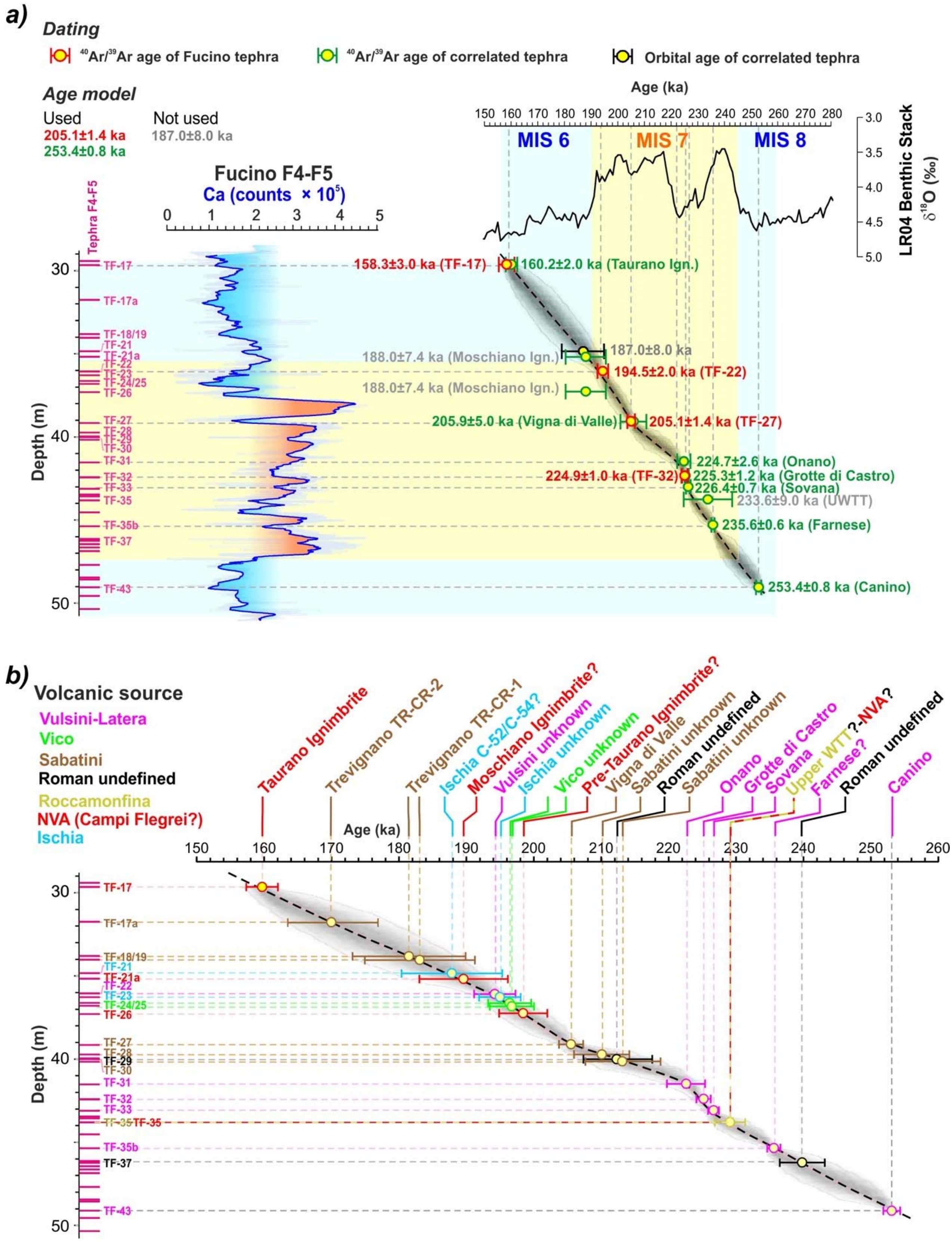

Figure 11. Summary of the tephrochronological constrains and results for the late MIS 8-early MIS 6 Fucino record. **a)** Age-depth model. For comparison, the resulting Fucino Ca time-series is showed together with the LR04 Benthic Stack (Lisiecki and Raymo, 2005). **b)** Volcanic sources, individual correlation, and modelled ages (2σ error) for the F4-F5 investigated tephra.

On the other hand, as far as the history of the peri-Tyrrhenian volcanism is concerned, our results provide further important insights. Notably, for the Latera caldera activity in the Vulsini volcanic district, we provide new $^{40}Ar/^{39}Ar$ dating for the eruptive succession of Sovana, Grotte di Castro and Onano (Fig. 7; Table 5). The $^{40}Ar/^{39}Ar$ dating method is unable to resolve the inter-eruptive intervals between these three closely spaced events, as the ages are statistically undistinguishable from each other. Instead, the Fucino record provides modelled ages that allow for an estimation of the time elapsed between these subsequent eruptions (Table 5; Fig. 11). Furthermore, the Vulsini-like TF-22 tephra, here $^{40}Ar/^{39}Ar$ dated at 194.5 ± 2.0 ka (Fig. 7), could provide a precise chronological constraint for the minor Latera activity between Onano and Pitigliano, which is documented in proximal settings, but still yet not fully characterised.

At Sabatini volcano, proximal deposits discontinuously document explosive activity between the eruptions of Vigna di Valle and Pizzo Prato (Sottili et al., 2019). At Fucino, at least two tephra layers (TF-28 and TF-30) with Sabatini like composition document so far unknown explosive activity at ~210-213 ka (210.0 ± 4.1 ka and 213.0 ± 5.8 ka). The Fucino record also provides a new, more precise $^{40}Ar/^{39}Ar$ age of 205.1 ± 1.4 ka for the previously poorly dated Vigna di Valle unit, and modelled ages of 171.1 ± 7.1 ka and 183.4 ± 8.4 ka/182.5 ± 8.5 ka for the undated Trevignano Romano units TR-CR-2 and TR-CR-1, respectively (Table 5; Fig. 11b).

At Vico volcano, a ~90 kyr interval is reported between the Vico Ignimbrite A (or Farine Formation, ca. ~250 ka; Sollevanti, 1983) and Ignimbrite B (or Ronciglione Formation, 157 ± 3 ka; Laurenzi and Villa, 1987) in the literature. However, at Fucino two tephra layers (i.e., TF-24 and TF-25) with a Vico-like geochemical composition occur in a time interval of 205.1 ± 1.4 ka (TF-27/Vigna di Valle) and 194.5 ± 2.0 ka (TF-22/Vulsini unknown; Table 5; Fig. 11b), thus halving (from ~90 to ~45 kyr) the proposed quiescence period.

At Ischia volcano, proximal deposits outcropping in the SE sector of the island are reported to date as far back as > 150 ka (e.g., Poli et al., 1987; Sbrana et al., 2018). At Fucino, the two Ischia tephra TF-21 and TF-23, with a modelled age of 187.8 ± 7.5 ka and 195.0 ± 3.1 ka, respectively (Table 5; Fig. 11), testify, in agreement with previous tephra studies (e.g., Paterne et al., 2008), that the island has been volcanically active at least since the late Middle Pleistocene period.

At NVA, explosive activity preceding the Campanian Ignimbrite eruption (39.85 ± 0.14 ka; Giaccio et al., 2017b) has been erased and/or covered by deposits of the most recent activity, and is still poorly documented (e.g., Pappalardo et al., 1999; De Vivo et al., 2001; Rolandi et al., 2003; Di Renzo et al., 2007; Di Vito et al., 2008; Belkin et al., 2016). However, recent investigations of relatively proximal sections in the Campania plain allowed the recognition of a relevant Campi Flegrei explosive activity between ~92 ka and

~109 ka (Monaco et al., 2022), also linking it to widespread tephra, such as the X-6, X-5 (Keller et al., 1978) and C-22 (Paterne et al., 1986), which act as relevant markers for the Mediterranean MIS 5 successions (e.g., Wulf et al., 2012, 2018; Giaccio et al., 2012a; Regattieri et al., 2015; Leicher et al., 2016; Petrosino et al., 2016). At Fucino, two or three Campi Flegrei-like tephra layers, i.e., TF-21a, TF-26 and, possibly, TF-35, represent activity at this volcano at ~189 ka, ~199 ka and ~230 ka (Table 5; Fig. 11). TF-21a in particular is chronologically consistent with the Moschiano Ignimbrite, dated at 188.0 ± 7.4 ka and attributed to the so-called CVZ (Rolandi et al., 2003). Although individual correlations currently are either hampered by the lack of glass geochemical data or not supported by geochronological-geochemical evidence, a chronologically and geochemically similar activity is documented in the Tyrrhenian Sea, at San Gregorio Magno Basin (Petrosino et al., 2019) and Lake Ohrid (Leicher et al., 2019, 2021; Table 5; Fig. 11). The abundance and wide dispersal of distal tephra deposits with similar, NVA-like geochemical compositions, including the Taurano Ignimbrite and its distal equivalents (e.g., from the Tyrrhenian Sea, San Gregorio Magno and Lake Ohrid) and older tephra layers (i.e., TF-21/Moschiano Ignimbrite, TF-26/pre-Taurano Ignimbrite) highlight a significant late Middle Pleistocene explosive activity at NVA, which calls for further detailed investigations in both proximal and distal settings.

Finally, in the time interval here considered, only one tephra layer with a potential Roccamonfina signature (TF-35) is documented at Fucino, possibly linked to the Upper White Trachytic Tuff eruptive cycle (e.g., Giannetti and De Casa, 2000). However, as the potential correlatives of TF-35 in Lake Ohrid (OH-DP-1006) and San Gregorio Magno Basin have been both attributed to Campi Flegrei/NVA (Leicher et al., 2021; Munno and Petrosino, 2007), the final attribuition to the actual source volcano of TF-35, i.e., to either Roccamonfina or NVA, is here left open to future investigations.

In conclusion, the tephra succession from the Fucino Basin presented here hosts deposits of explosive activity currently undocumented (or not yet correlated) at Vulsini (TF-22), Vico (TF-24, TF-25), Sabatini (TF-28, TF-30), and Ischia (TF-21, TF-23) volcanoes. The Fucino tephra sequence also confirms previous evidence of a conspicuous Middle Pleistocene activity at NVA (TF-21a, TF-26, TF-35). Our record also provides precise chronological constraints for many of the undated or poorly dated eruptions of the Middle Pleistocene peri-Tyrrhenian volcanoes identified in the Fucino record.

Table 5. Summary of the proposed correlations of the F1-F3 (Giaccio et al., 2017a) and F4-F5 Fucino tephra with tephra layers from other repositories across central-southern Italy and the Mediterranean.

Fucino tephra				Source		Distal archives			
Label	Age (ka±2σ) $^{40}Ar/^{39}Ar$ Direct	Age (ka±2σ) $^{40}Ar/^{39}Ar$ Correlated	Age (ka±2σ) Modelled	Volcano	Unit	PRAD1-2	Ohrid	SGM	DED-87-08
TF-17	158.8±3.0[1]	160.2±2.0[2]	159.6±2.4	CF/NVA*	Taurano Ignimbrite	PRAD-3225	OH-DP-0624		C-41/ C-42?
TF-17a			171.1±7.1	Sabatini	TR.CR-2				
TF-18			182.5±8.5	Sabatini	TR-CR-1				
TF-19			183.4±8.4						
TF-21			187.7±7.7	Ischia	Unknown				C-52/ C-54?
TF-21a		188.0±7.4[3]	189.5±7.0	NVA	Moschiano Ignimbrite?			S7	C-53/ C-55?
TF-22	194.5±2.0[4]		194.2±2.8	Vulsini	Unknown	PRAD-3586			C-56?
TF-23			194.9±2.9	Ischia	Unknown				
TF-24			196.3±3.1	Vico	Unknown	PRAD-3666			
TF-25			196.6±3.2	Vico	Unknown				
TF-26			198.3±3.4	NVA	Pre-Taurano Ignimbrite?				C-53/ C-55?
TF-27	205.1±1.4[4]	205.9±5.0[5]	205.5±1.8	Sabatini	Vigna di Valle				
TF-28			210.0±4.1	Sabatini	Unknown				
TF-29			212.2±5.2	Roman	Unknown				
TF-30			213.0±5.8	Sabatini	Unknown				
TF-31		224.7±2.6[4]	222.5±2.8	Vulsini	Onano				
TF-32	224.9±1.0[4]	225.3±1.2[4]	225.1±1.1	Vulsini	Grotte di Castro				
TF-33		226.4±0.7[4]	226.6±0.8	Vulsini	Sovana				
TF-35			229.0±2.2	Roccamonfina?-NVA?	Unknown/UWTT? Pre-Taurano Ignimbrite?		OH-DP-1006?	S2?	
TF-35b		235.6±0.6[4]	235.6±1.0	Vulsini	Farnese				
TF-37			240.0±3.4	Roman	Unknown				
TF-43		253.4±0.8[4]	253.1±1.3	Vulsini	Canino				

$^{40}Ar/^{39}Ar$ age data source: [1]: Giaccio et al. (2017a); [2]: De Vivo et al. (2001); [3]: Rolandi et al. (2003); [4]: this study; [5]: recalculated from Sottili et al. (2010). All $^{40}Ar/^{39}Ar$ are reported using the age for Alder Creek sanidine standard (ACs-2) at 1.1891 Ma (Niespolo et al., 2017).

5.5.2. *Tephra climatostratigraphy and MIS 7 paleoclimatic proxy record chronology*

Overall, the resulting Fucino Ca and Ti time series (depth series from Giaccio et al., 2019), which are proxies of the lake primary productivity and of the catchment erosion, respectively, and by extension of temperature and precipitation (e.g., Mannella et al., 2019), reflect the climate variability of the late MIS 8-early MIS 6 glacial-interglacial at both glacial-interglacial and millennial timescales (Fig. 12). The MIS 7 period includes three warm substages, MIS 7e, 7c and 7a. The first two have been assigned interglacial status, while the third is considered a 'continued interglacial' as it was not preceded by any substantial ice-sheet expansion during MIS 7b (Tzedakis et al., 2017). In terms of interglacial intensity, sea level and global surface temperature reconstructions suggest that MIS 7e, 7c and 7a were weaker compared to the MIS 5e, 9e, 11c and 1 interglacials (e.g., Past Interglacials Working Group, 2016; Snyder, 2016). The independent $^{40}Ar/^{39}Ar$ chronology of Fucino record places the beginning of MIS 7e at 243.6 ± 4.7 ka, i.e., very close to the maximum insolation at 243.5 ka, in line with the canonical view of Milankovitch forcing pacing the timing of interglacials (Hays et al., 1976; Tzedakis et al., 2012) (Fig. 12). The MIS 8-MIS 7e transition is marked by an abrupt decrease (increase) of Ti (Ca) and is preceeded by a late MIS 8 interstadial oscillation centered at

~245 ka (Fig. 12). Although the timing of the deglacial transition is bracketed by two high-precision $^{40}Ar/^{39}Ar$ ages of TF-43 (Canino, 253.4 ± 0.8 ka) and TF-35b (Farnese, 235.6 ± 0.6 ka) that are 18 kyr apart, the emerging chronology is in good agreement with astrochronologically-calibrated Mediterranean records (e.g., Lake Ohrid pollen: Sadori et al., 2016, 2018; Donders et al., 2021; Ioannina I-284 pollen: Roucoux et al., 2007) and the U/Th-dated stalagmites from continental Europe (Wendt et al., 2021).

According to the Ti and Ca data, the MIS 7e interglacial shows evidence of climate instability, which may have correlatives in other Mediterranean records (Fig. 12). Compared to other marine sequences, a number of terrestrial records indicate a shorter interglacial duration, ending around 236 ka (e.g., Tzedakis et al., 2004; Roucoux et al., 2007; Sadori et al., 2016; Wendt et al., 2021), though this is not as clear in the Fucino Ca and Ti timeseries (Fig. 12).

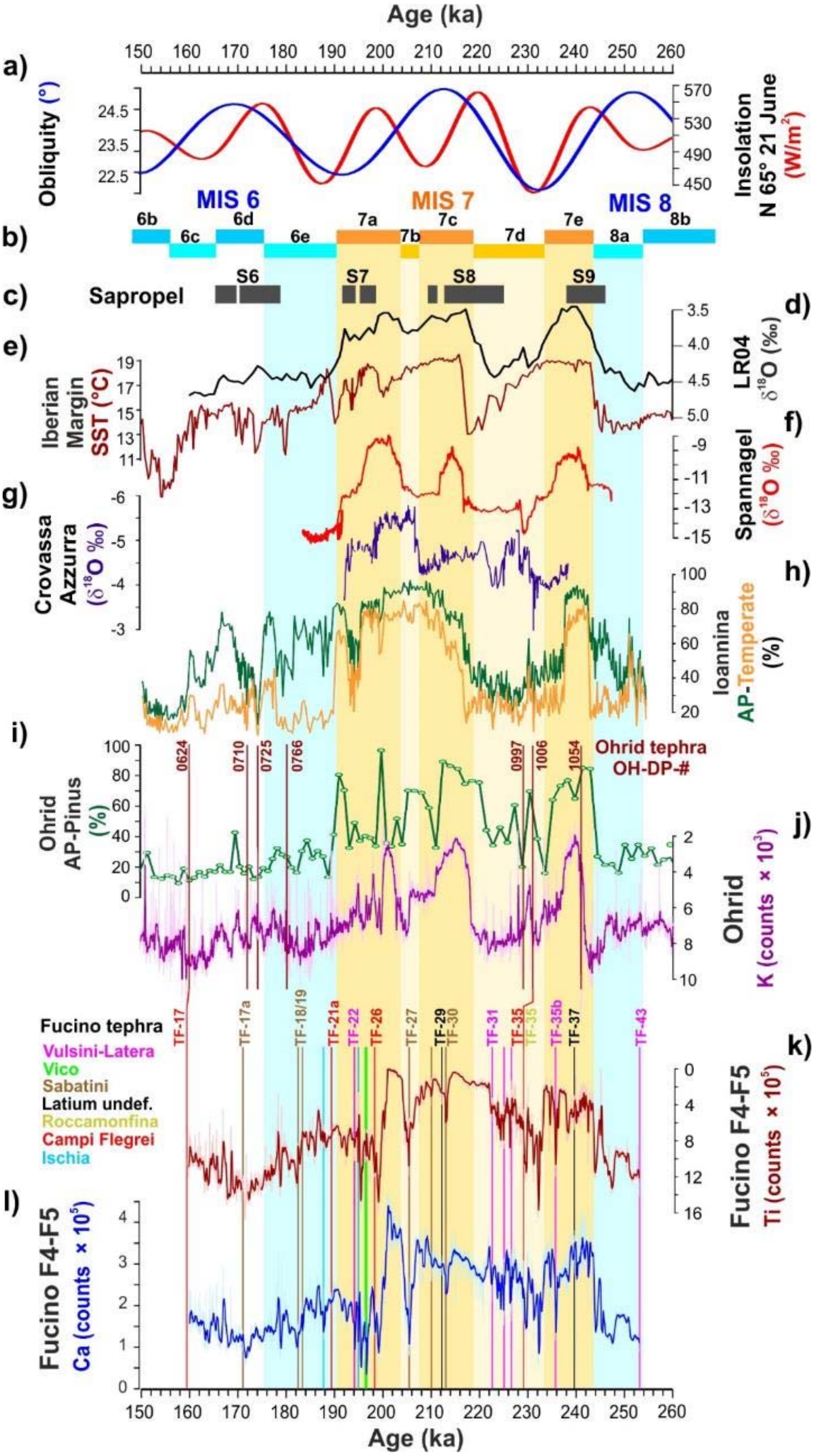

Figure 12. Comparison between Fucino and regional and extra-regional selected late MIS 8-early MIS 6 paleoclimatic records. **a)-b)** obliquity and 65°N insolation (Berger and Lutre, 1991). **c)** Mediterranean sapropel stratigraphy (Ziegler et al., 2010). **d)** LR04 Benthic Stack (Lisiecki and Raymo, 2005). **e)** Portuguese margin sea surface temperature (SST, Martrat et al., 2007). **f)** Stalagmite δ^{18}O record from Spannagel Cave (Austria; Wendt et al., 2021). **g)** Stalagmite δ^{18}O record from Crovassa Azzurra Cave (Sardinia; Columbu et al., 2019). **h)** Total arboreal pollen (AP) and Temperate tree pollen (Eurosiberian and Mediterranean taxa) percentages from Ioannina I-284 lacustrine succession (Greece, Roucoux et al., 2007). **I-j)** AP (-Pinus) percentages (Sadori et al., 2016; Donders et al., 2021) and K XRF scanning data (Wagner et al., 2019) from Lake Ohrid (Albania, North Macedonia). **k)-l)** Fucino Ti and Ca XRF scanning data (Giaccio et al., 2019).

The following MIS 7d sub-stage, containing a deep boreal summer insolation minimum, arising from the confluence of an obliquity minimum and a precession maximum, and associated with a rapid pulse of ice-sheet expansion (Ruddiman & McIntyre, 1982), is well-expressed by an abrupt increase in Ti at ~234 ka in Fucino. This interval is characterised by the occurrence of four tephras, including TF-35, likely sourced in Campi Flegrei, and the Latera series of Sovana-Grotte di Castro-Onano (TF-33, TF-32, and TF-31), from Vulsini (Fig. 12). Notably, Fucino tephra TF-35 (229.0 ± 2.2 ka) and its likely equivalent OH-DP-1006 Ohrid tephra share a similar climatostratigraphic position at the onset of an interstadial oscillation within the MIS 7d glacial sub-stage, thus supporting the tentative correlation (Fig. 12). A similar pronounced interstadial oscillation centred at ~230 ka is also evident in the high-resolution Ioannina pollen record (Fig. 12).

Among the Latera units, Onano (TF-31), here dated at 224.7 ± 2.6 ka ($^{40}Ar/^{39}Ar$ age) or 222.5 ± 2.8 ka (modelled age; Table 5), immediately precedes an abrupt decrease in Ti at ~222.0 ka, which could correspond to the wide increase in Lake Ohrid AP at ~221 ka and that, in turn, could represent the regional expression of the MIS 7d-MIS 7c, glacial-interglacial transition (Fig. 12). However, in agreement with other records, the Fucino Ca profile suggests a later onset of the MIS 7c (~218 ka; Fig. 12), leaving open the definition/chronology of this major climatic transition in Fucino record until additional multiproxy evidence (e.g., pollen analyses) is available.

The MIS 7c interglacial appears as a more stable period, according to the Ti record of Fucino, with the notable exception of a stadial oscillation at ~214-212 ka, which may be correlative with a drop of the Lake Ohrid AP at 212-210 ka (Fig. 12). This oscillation is marked by the occurrence of tephras TF-29 and TF-30 of unknown Roman and Sabatini origin, respectively, which can be thus considered as good potential markers for this event (Fig. 12). Starting from 210 ka, the Ti becomes less stable and shows a general increasing trend that culminates in an abrupt increase at ~207 ka, likely corresponding to the beginning of MIS 7b (Fig. 12). This short stadial is marked by the occurrence of the Sabatini tephra TF-27/Vigna di Valle, here precisely dated to 205.1 ± 1.4 ka (Table 5).

At ~204 ka, Ti and Ca are characterised by a rapid decrease and increase, respectively, that may represent the onset of the MIS 7a sub-stage (Fig. 12). This interpretation is in good chronological agreement with speleothem records from Austria (Wendt et al., 2021) and Sardinia (Columbu et al., 2019), which show an abrupt increase in temperature in central Europe and precipitation in the Mediterranean at ~204 ka and 206 ka, respectively (Fig. 12). Ti remains very low only up to ~200 ka, while it abruptly increases and remains generally higher and unstable between 200 ka and 190 ka, suggesting a short duration of the stable MIS 7a conditions, as previously observed in marine and terrestrial records from the Portuguese Margin and southern Europe (Tzedakis et al., 2004; Martrat et al., 2007; Roucoux et al., 2008) (Fig. 12). This is also in agreement with Austrian and Sardinian speleothem evidence, indicating a significant climatic worsening at ~197 ka and 199 ka, respectively (Fig. 12). Lake Ohrid AP and XRF records also indicate unstable conditions during the MIS 7a, with only two isolated peaks of high AP concentration, at ~192 ka and ~200 ka, the earliest one likely correlated with Fucino low-Ti at 200-204 ka (Fig. 12). The unstable phase of the late MIS 7a is marked by a series of tephra layers, including the Campi Flegrei-like TF-26, the Vico TF-24 and TF-25, the Ischia TF-23, and the Vulsini TF-22, here $^{40}Ar/^{39}Ar$ dated to 194.5 ± 2.0 ka (Fig. 7; Table 5). As far as the MIS 7/MIS 6 transition is concerned, neither the Ti nor the Ca profiles show a clear expression of this boundary in the Fucino record, which could be placed at ~190 ka, close to the CF-like tephra TF-21a (Moschiano Ignimbrite?) (Fig. 12). However, this must be considered only as a preliminary result as additional multiproxy records, especially pollen, are needed to establish the expression and the age of this transition in the Fucino record.

6. Summary and concluding remarks

In this study, we presented a new tephra record from Fucino Basin, central Italy, spanning the ~250-170 ka time interval or the late MIS 8-early MIS 6. Twenty-one Fucino tephra layers identified in this time-interval, along with one tephra from Lake Ohrid succession, thirteen pyroclastic units from near-vent sections of LVC (Vulsini Volcanic District), Vico volcano, and SVD have been characterised in terms of major, minor (EPMA-WDS) and trace element contents (LA-ICP-MS), Sr-Nd isotopic composition (TIMS), and $^{40}Ar/^{39}Ar$ dating. The results provide new data to refine the history of explosive volcanism in the peri-Tyrrhenian magmatic systems during the 250-170 ka interval and enrich the MIS 8-6 Mediterranean tephrostratigraphy. The combination of the new $^{40}Ar/^{39}Ar$ ages for Latera units (Onano, Grotte di Castro, Sovana, Farnese and Canino), which have been identified in the Fucino record, with $^{40}Ar/^{39}Ar$ ages of the Fucino tephras, allowed us to develop a robust Bayesian age-depth model that provides statistically reliable modelled ages for the investigated tephra succession. In turn, this not only yields new ages for the previously undated tephras, but also allowed us to better estimate the ages of the closely spaced Onano, Grotte di Castro and Sovana major eruptions, chronologically poorly distinguishable using $^{40}Ar/^{39}Ar$ dating of the proximal units alone. This highlights the great potential of the approach of integrating proximal and distal data for a better assessment of the dynamics and tempo of the explosive volcanism also in the perspective of hazard evaluation.

The Fucino tephrochronological record also provides the first ages for the previously undated Trevignano Romano eruptions TR-CR-1 and TR-CR-2 of the Sabatini Volcanic District, and possibly an improved age for the Upper White Trachytic Tuff of the Roccamonfina volcano. Finally, the Fucino record evidenced currently undocumented or poorly known explosive activity at Vico, Sabatini, Ischia and Campi Flegrei volcanoes, providing new fundamental insights into the eruptive history at these volcanic systems. Notably, we identified three NVA-like tephras at ~190 ka, ~198 ka and ~230 ka, i.e., preceding the already known Taurano Ignimbrite (158.8 ± 3.0 ka), which, together with other distal tephra evidence (e.g., Tyrrhenian Sea, Lake Ohrid), suggest a significant activity in the Campi Flegrei volcanic area between 160 ka and 250 ka. However, more investigations are needed in both proximal and distal setting to better define the volcanological features and history of this late Middle Pleistocene explosive activity.

Regarding the development of the Mediterranean tephrochronology, we noticed a significant paucity of records spanning the MIS 8-6 interval. Some potential correlative layers have been found only in the Adriatic Sea core PRAD 1-2, the San Gregorio Magno Basin, southern Italy, and Lake Ohrid, Albania-North Macedonia. In this regard, the rich and detailed Fucino record can provide a reference dataset for future tephra studies in the Mediterranean region of this poorly investigated period.

Finally, the preliminary analysis of the Fucino paleoclimatic proxy records (Ti and Ca XRF data), anchored to a robust radioisotopic-based chronology, indicated a coherent pattern of the late MIS 8-early MIS 6 climatic variability with respect to other regional and extraregional reference records. This sets the basis for the assemblage of high-resolution paleoenvironmental and paleoclimatic multiproxy records, which will allow exploring the timing and dynamics of climatic change independently of any assumption of the orbital tuning.

Acknowledgments

R. Jedlička is thanked for providing valuable technical assistance during EPMA analysis at Prague University. Two anonymous reviewers provided precious suggestions that allowed to greatly improve the early version. This article is a contribution to project “FUcino Tephrochronology Unites Quaternary Records (FUTURE)”, financed by the Italian Research Ministry (MUR, PRIN 2017, grant 20177TKBXZ_003, project “FUTURE”, G. Zanchetta, coordinator), issued to B.G., D.P., M.D., and G.Z. The Fucino project is co-funded by DFG (German Research Foundation) grant WA 2109/16. $^{40}Ar/^{39}Ar$ dating also received complementary contribution from the CNRS INSU-LEFE 2018-2020 action to S.N. The INGV-OV laboratories have been also financially supported by the EPOS Research Infrastructure through the contribution of the Italian Ministry of University and Research (MUR). P.C.T. acknowledges funding from NERC research grant NE/V001620/1.

References

Albert, P.G., Giaccio, B., Isaia, R., Costa, A., Niespolo, E.M., Nomade, S., Pereira, A., Renne, P.R., Hinchliffe, A., Mark, D.F., Brown, R.J., Smith, V.C., 2019. Evidence for a large-magnitude eruption from Campi Flegrei Caldera (Italy) at 29 ka. *Geology.* **47** (7), 595-599. https://doi.org/10.1130/G45805.1.

Albert, P.G., Smith, V.C., Suzuki, T., Tomlinson, E.L., Nakagawa, T., McLean, D., Yamada, M., Staff, R.A., Schlolaut, G., Takemura, T., Nagahashi, Y., Kimura, J., Suigetsu 2006 Project Members, 2018. Constraints on the frequency and dispersal of explosive eruptions at Sambe and Daisen volcanoes (South-West Japan Arc) from the distal Lake Suigetsu record (SG06 core). *Earth Sci. Rev.* **185**, 1004-1028. https://doi.org/10.1016/j.earscirev.2018.07.003.

Amato, V., Aucelli, P.P.C., Cesarano, M., Filocamo, F., Leone, N., Petrosino, P., Rosskopf, C.M., Valente, E., Casciello, E., Giralt, S., Jicha, B.R., 2018. Geomorphic response to late Quaternary tectonics in the axial portion of the Southern Apennines (Italy): A case study from the Calore River valley. *Earth Surf. Process. Landf.* **43** 2463-2480. https://doi.org/10.1002/esp.4390.

Amato, V., Aucelli, P.P.C., Cesarano, M., Jicha, B.R., Lebreton, V., Orain, R., Pappone, G., Petrosino, P., Russo Ermolli, E., 2014. Quaternary evolution of the largest intermontane basin of the Molise Apennine (Central Southern Italy). *Rend. Fis. Acc. Lincei* **25**, 197-216. https://doi.org/10.1007/s12210-014-0324-y.

Appleton, J.D., 1972. Petrogenesis of Potassium-rich Lavas from the Roccamonfina Volcano, Roman Region, Italy. *J. Petrol.* **13** (3), 425-456. https://doi.org/10.1093/petrology/13.3.425.

Arienzo, I., Civetta, L., Heumann, A., Wörner, G., Orsi, G., 2009. Isotopic evidence for open system processes within the Campanian Ignimbrite (Campi Flegrei-Italy) magma chamber. *Bull. Volcanol.* **71**, 285-300. https://doi.org/10.1007/s00445-008-0223-0.

Arienzo, I., D'Antonio, M., Di Renzo, V., Tonarini, S., Minolfi, G., Orsi, G., Carandente, A., Belviso, P., Civetta, L., 2015. Isotopic microanalysis sheds light on the magmatic endmembers feeding volcanic eruptions: The Astroni 6 case study (Campi Flegrei, Italy). *J. Volcanol. Geotherm. Res.* **304**, 24–37. https://doi.org/10.1016/j.jvolgeores.2015.08.003.

Arienzo, I., Mazzeo, F.C., Moretti, R., Cavallo, A., D'Antonio, M., 2016. Open-system magma evolution and fluid transfer at Campi Flegrei caldera (Southern Italy) during the past 5 ka as revealed by geochemical and isotopic data: the archetype of Nisida eruption. Chem. Geol. **427**, 109-124. https://doi.org/10.1016/j.chemgeo.2016.02.007.

Arienzo, I., Moretti, R., Civetta, L., Orsi, G., Papale, P., 2010. The feeding system of the Agnano-Monte Spina eruption Campi Flegrei, Italy): dragging the past into present activity and future scenarios. *Chem. Geol.* **270** (1-4), 135-147. https://doi.org/10.1016/j.chemgeo.2009.11.012.

Ascione, A., Mazzoli, S., Petrosino, P., Valente, E., 2013. A decoupled kinematic model for active normal faults: Insights from the 1980, Ms = 6.9 Irpinia earthquake, southern Italy. *Geol. Soc. Amer. Bull.* **125** (7-8), 1239-1259. https://doi.org/10.1130/B30814.1.

Balbas, A., Koppers, A.A.P., Kent, D.V., Konrad, K., Clark, P.U., 2016. Identification of the short-lived Santa Rosa geomagnetic excursion in lavas on Floreana Island (Galapagos) by $^{40}Ar/^{39}Ar$ geochronology. *Geology* **44** (5), 359-362 (2016). https://doi.org/10.1130/G37569.1.

Bear, A.N., Cas, R.A.F., Giordano, G., 2009. The implications of spatter, pumice and lithic clast rich proximal co-ignimbrite lag breccias on the dynamics of caldera forming eruptions: The 151 ka Sutri eruption, Vico Volcano, Central Italy. *J. Volcanol. Geotherm. Res.* **181** (1-2), 1-24. https://doi.org/10.1016/j.jvolgeores.2008.11.032.

Belkin, H.E., Rolandi, G., Jackson, J.C., Cannatelli, C., Doherty, A.L., Petrosino, P., De Vivo, B., 2016. Mineralogy and geochemistry of the older (>40 ka) ignimbrites in the Campanian Plain, southern Italy. *J. Volcanol. Geotherm. Res.* **323**, 1-18. https://doi.org/10.1016/j.jvolgeores.2016.05.002.

Berger, A. & Lautre, M.F., 1991. Insolation values for the climate of the last 10 million years. *Quat. Sci. Rev.* **10**, 297-317. https://doi.org/10.1016/0277-3791(91)90033-Q.

Bertagnini, A. & Sbrana, A., 1986. Il volcano di Vico: stratigrafia del complesso vulcanico e sequenze eruttive delle formazioni piroclastiche (in Italian). *Mem. Soc. Geol. It.* **35**, 699-713.

Bini M., Zanchetta G., Drysdale R.N., Giaccio B., Stocchi P., Vacchi M., Hellstrom J.C., Couchoud I., Monaco L., Ratti A., Martini, F., Sarti L., 2020. An end to the Last Interglacial highstand before 120 ka: Relative sea-level evidence from Infreschi Cave (Southern Italy). *Quat. Sci. Rev.* **250**, 106658. https://doi.org/10.1016/j.quascirev.2020.106658.

Blaauw, M., Christen, J.A., 2011. Flexible palaeoclimate age-depth models using an autoregressive gamma process. *Bayesian analysis* **6** (3), 457-474. https://doi.org/10.1214/11-BA618.

Blockley, S.P.E., Bourne, A.J., Brauer, A., Davies, S.M., Hardiman, M., Harding, P.R., Lane, C.S., MacLeod, A., Matthews, I.P., Pyne-O'Donnel, S.D.F., Rasmussen, S.O., Wulf, S., Zanchetta, G., 2014. Tephrochronology and the extended intimate (integration of ice-core, marine and terrestrial records) event stratigraphy 8-128 ka 2bk. *Quat. Sci. Rev.* **106**, 88-100. https://doi.org/10.1016/j.quascirev.2014.11.002.

Boncio, P., Lavecchia, G., Pace, B., 2004. Defining a model of 3D seismogenic sources for seismic hazard assessment applications: The case of central Apennines (Italy). *J. Seismol.* **8** (3), 407–425. https://doi.org/10.1023/B:JOSE.0000038449.78801.05.

Bourne, A.J., Albert, P.G., Matthews, I.P., Trincardi, F., Wulf, S., Asioli, A., Blockley, S.P.E., Keller, J., Lowe, J.J., 2015. Tephrochrunology of core PRAD 1-2 from the Adriatic Sea: insights into Italian explosive volcanism for the period 200-80 ka. *Quat. Sci. Rev.* **116**, 28-43. https://doi.org/10.1016/j.quascirev.2015.03.006.

Bourne, A.J., Lowe, J.J., Trincardi, F., Asioli, A., Blockley, S.P.E., Wulf, S., Matthews, I.P., Piva, A., Vigliotti, L., 2010. Distal tephra record for the last ca 105,000 years from core PRAD 1-2 in the central Adriatic Sea: implications for the marine tephrostratigraphy. *Quat. Sci. Rev.* **29**, 3079-3094. https://doi.org/10.1016/j.quascirev.2010.07.021.

Brown, R.J., Civetta, L., Arienzo, I., D'Antonio, M., Moretti, R., Orsi, G., Tomlinson, E.L., Albert, P.G., Menzies, M.A., 2014. Geochemical and isotopic insights into the assembly, evolution and disruption of a magmatic plumbing system before and after cataclysmic caldera-collapse eruption at Ischia volcano (Italy). *Contirb. Mineral. Petrol.* **168**: 1035. https://doi.org/10.1007/s00410-014-1035-1.

Brown, R.J., Orsi, G., de Vita, S., 2008. New insights into Late Pleistocene explosive volcanic activity and caldera formation on Ischia. *Bull. Volcanol.* **70**, 583-603. https://doi.org/10.1007/s00445-007-0155-0.

Casalini, M., Heumann, A., Marchionni, S., Conticelli, S., Avanzinelli, R., Tommasini, S., 2018. Inverse modelling to unravel the radiogenic isotope signature of mantle sources from evolved magmas: the case-study of Ischia volcano. *Ital. J. Geosci.* **137**, pp. 00. https://doi.org/:103301/IJG.2018.05.

Cavinato, G.P., Carusi, C., Dell'Asta, M., Miccadei, E., Piacentini T., 2002. Sedimentary and tectonic evolution of Plio-Pleistocene alluvial and lacustrine deposits of Fucino Basin (central Italy). *Sediment. Geol.* **148**, 29-59. https://doi.org/10.1016/S0037-0738(01)00209-3.

Chen, X.-Y., Blockley, S.P.E., Fletcher, R., Zhang, S., Kim, J.-H., Park, M.-O., Chen, C., Yin, J., Xu, Y.-G., 2022. Holocene tephrostratigraphy in the East-Sea/Japan Sea: Implications for eruptive history of Ulleungdo volcano and potential for hemispheric synchronization of sedimentary archives. *J. Geophys. Res. Solid Earth* **127**, e2021JB023243. https://doi.org/10.1029/2021JB023243.

Cox, S.E., Hemming, S.R., Tootell, D., 2020 The Isotopx NGX and ATONA Faraday amplifiers. *Geochronology* **2**, 231-243. https://doi.org/10.5194/gchron-2-231-2020.

Colucci, S., Palladino, D.M., Mulukutla, G.K., Proussevitch, A.A., 2013. 3-D Reconstruction of ash vesicularity: insights into the origin of ash-rich explosive eruptions. J. *Volcanol. Geotherm. Res.* **255**, 98-107. https://doi.org/10.1016/j.jvolgeores.2013.02.002.

Columbu, A., Spötl, C., De Waele, J., Yu, T.-L., Shen, C.-C., Gázquez, F., 2019. A long record of MIS 7 and MIS 5 climate ane environment from a western Mediterranean speleothem (SW Sardinia, Italy). *Quat. Sci. Rev.* **220**, 230-243. https://doi.org/10.1016/j.quascirev.2019.07.023.

D'Agostino, N., Jackson, J. A., Dramis, F., Funiciello, R., 2001. Interactions between mantle upwelling, drainage evolution and active normal faulting: an example from the central Apennines (Italy). *Geophys. J. Inter.* **147** (2), 475–497. https://doi.org/10.1046/j.1365-246X.2001.00539.x.

D'Antonio, M., Tonarini, S., Arienzo, I., CIvetta, L., Dallai, L., Moretti, R., Orsi, G., Andria, M., Trecalli, A., 2013. Mantle and crustal processes in the magmatism of the Campania region: inferences from mineralogy, geochemistry, and Sr-Nd-O isotopes of young hybrid volcanics of the Ischia island (South Italy). *Contrib. Mineral. Petrol.* **165**, 1173-1194. https://doi.org/10.1007/s00410-013-0853-x.

D'Antonio, M., Tonarini, S., Arienzo, I., Civetta, L., Di Renzo, V., 2007. Components and processes in the magma genesis of the Phlegrean Volcanic District, southern Italy. In: Beccaluva, L., Bianchini, G., Wilson, M. (eds.) Cenozoic Volcanism in the Mediterranean Area. *Geol. Soc. Am. Special Paper* **418**, 203-220.

Davies, S.M., Wastegård, S., Abbott, P.M., Barbante, C., Bigler, M., Johnsen, S.J., Rasmussen, T.L., Steffensen, J.P., Svensson, A., 2010. Tracing volcanic events in the NGRIP ice-core and synchronising North Atlantic marine records during the last glacial period. *Earth Planet. Sci. Lett.* **294** (1-2), 69-79. https://doi.org/10.1016/j.epsl.2010.03.004.

de Fontaine, C.S., Kaufman, D.S., Anderson, R.S., Werner, A., Waythomass, C.F., Brown, T.A., 2007. Late Quaternary distal-fall deposits in lacustrine sediments, Kenai Peninsula, Alaska. Quaternary Research, 68, 1, 64-78. https://doi.org/10.1016/j.yqres.2007.03.006.

De Maisonneuve, C.B. & Bergal-Kuvikas, O., 2020. Timing, magnitude and geochemistry of major Southeast Asian volcanic eruptions: identifying tephrochronologic markers. Journal of Quaternary Science, 35, 1-2, 272-287. https://doi.org/10.1002/jqs.3181.

de Rita, D., Funiciello, R., Parotto, M., 1988. Carta geologica del complesso vulcanico dei Colli Albani (Vulcano Laziale) (in Italian). C.N.R.-Gruppo Nazionale Vulcanologia.

De Vivo, B., Rolandi, G., Gans, P.B., Calvert, A., Bohrson, W.A., Spera, F.J., Belkin, H.E., 2001. New constraints on the pyroclastic eruptive history of Campanian volcanic Plain (Italy). *Mineral. Petrol*. **73**, 47-65. https://doi.org/10.1007/s007100170010.

Del Carlo, P., Smedile, A., Petrelli, M., Di Roberto, A., 2020. Evidence of an unknown explosive eruption of Mt. Etna volcano (Italy) during the Late Glacial. *J. Volcanol. Geotherm. Res.* **402**, 106992. https://doi.org/10.1016/j.jvolgeores.2020.106992.

Deino, A.L., Orsi, G., de Vita, S., Piochi, M., 2004. The age of the Neapolitan Yellow Tuff-caldera forming eruption (Campi Flegrei caldra - Italy) assessed by ^{40}Ar/^{39}Ar dating method. *J. Volcanol. Geotherm. Res.* **133** (1-4), 157-170. https://doi.org/10.1016/S0377-0273(03)00396-2.

Di Battistini, G., Montanini, A., Vernia, L., Bargossi, G.M., Castorina, F., 1998. Petrology and geochemistry of ultrapotassic rocks from the Montefiascone VOlcanic Complex (Central Italy): magmatic evolution and petrogenesis. *Lithos* **43** (3), 169-195. https://doi.org/10.1016/S0024-4937(98)00013-9.

Di Renzo, V., Arienzo, I., Civetta, L., D'Antonio, M., Tonarini, S., Di Vito, M.A., Orsi, G., 2011. The magmatic feeding system of the Campi Flegrei caldera: Architecture and temporal evolution. *Chem. Geol.* **281** (3-4), 227-241. https://doi.org/10.1016/j.chemgeo.2010.12.010.

Di Renzo, V., Di Vito, M.A., Arienzo, I., Carandente, A., Civetta, L., D'Antonio, M., Tonarini S., 2007. Magmatic history of Somma–Vesuvius on the basis of new geochemical and isotopic data from a deep borehole (Camaldoli della Torre). *J. Petrol.* **48**, 753-784. https://doi.org/10.1093/petrology/egl081.

Di Roberto, A., Smedile, A., Del Carlo, P., De Martini, P.M., Iorio, M., Petrelli, M., Pantosti, P., Pinzi, S., Todrani, A., 2018. Tephra and cryptotephra in a ~60,000-year old lacustrine sequence from the Fucino Basin: new insights into the major explosive events in Italy. *Bull. Volcanol.* **80**:20. https://doi.org/10.1007/s00445-018-1200-x.

Di Vito, M.A., Sulpizio, R., Zanchetta, G., D'Orazio M., 2008 The late Pleistocene pyroclastic deposits of the Campanian Plain: New insights into the explosive activity of the Neapolitan volcanoes. *J. Volcanol. Geotherm. Res.* **177**, 19-48. https://doi.org/10.1016/j.jvolgeores.2007.11.019.

Doglioni, C., Harabaglia, P., Martinelli, G., Mongelli, F., Zito, G., 1996. A geodynamic model of the Southern Apennines accretionary prism. *Terra Nova* **8** (6), 540-547. https://doi.org/10.1111/j.1365-3121.1996.tb00783.x.

Donders, T., Panagiotopoulos, K., Koutsodendris, A., Bertini, A., Mercuri, A.M., Masi, A., Combourieu-Nebout, N., Joannin, S., Kouli, K., Kousis, I., Peyron, O., Torri, P., Florenzano, A., Francke, A., Wagner, B., Sadori, L., 2021. 1.36 million years of Mediterranean forest refugium dynamics in response to glacial-interglacial cycle strenght. *PNAS* **118** (34), e2026111118. https://doi.org/10.1073/pnas.2026111118.

Freda, C., Gaeta, M., Karner, D.B., Marra, F., Renne, P.R., Taddeucci, J., Scarlato, P., Christensen, J.N., Dallai, L., 2006. Eruptive history and petrologic evolution of the Albano multiple maar (Alban Hills, Central Italy). *Bull. Volcanol*. **68**, 567-591. https://doi.org/10.1007/s00445-005-0033-6.

Froggat, P.C. & Gosson, G.J., 1982. Techniques for the preparation of tephra samples for mineral and chemical analysis and radiometric dating. *Geology Department, Victoria University of Wellington Publication* 23, 1-12.

Galadini, F. & Galli, P., 2000. Active tectonics in the Central Apennines (Italy) - Input Data for Seismic Hazard Assessment. *Nat. Haz.* **22**, 225-270. https://doi.org/10.1023/A:1008149531980.

Gaeta, M., Freda, C., Marra F., Arienzo, I., Gozzi, F., Jicha, B., Di Rocco, T., 2016. Paleozoic metasomatism at the origin of Mediterranean ultrapotassic magmas: Constraints from time-dependent geochemistry of Colli Albani volcanic products (Central Italy). *Lithos* **244**, 151-164. https://doi.org/10.1016/j.lithos.2015.11.034.

Galli, P., Giaccio, B., Messina, P., Peronace, E., Amato, V., Naso, G., Nomade, S., Pereira, A., Piscitelli, S., Bellanova, J., Billi, A., Blamart, D., Galderisi, A., Giocoli, A., Stabile, T., Thil, F., 2017. Middle to Late Pleistocene activity of the Matese fault system (southern Apennines, Italy). *Tectonophysics* **699**, 61-81. https://doi.org/10.1016/j.tecto.2017.01.007.

Gasperini, D., Bilchert-Toft, J., Bosch, D., Del Moro, A., Macera, P., Albarède, F., 2002. Upwelling of deep mantle material through a plate window: Evidence from the geochemistry of Italian basaltic volcanics. *J. Geophysic. Res.* **107** (B12), 2367. https://doi.org/10.1029/2001JB000418.

Giaccio, B., Galli, P., Messina, P., Peronace, E., Scardia, G., Sottili, G., Sposato, A., Chiarini, E., Jicha, B., Silvestri, S., 2012a. Fault and basin depocentre migration over the last 2Ma in the L'Aquila 2009 earthquake region, central Italian Apennines. *Quat. Sci. Rev.* **56**, 69–88. https://doi.org/10.1016/j.quascirev.2012.08.016.

Giaccio, B., Galli, P., Peronace, E., Arienzo I., Nomade, S., Cavinato, G.P., Mancini, M., Messina, P., Sottili, G., 2014. A 560-440 ka tephra record from the Mercure Basin, Southern Italy: volcanological and tephrostratigraphic implications. *J. Quat. Sci.* **29**, 232-248. https://doi.org/10.1002/jqs.2696.

Giaccio, B., Haydas, I., Isaia, R., Deino, A., Nomade, S., 2017b. High-precision ^{14}C and ^{40}Ar/^{39}Ar dating of Campanian Ignimbrite (Y-5) reconciles the time-scales of climatic cultural processes at 40 ka. *Sci. Rep.* **7**, 45940. https://doi.org/10.1038/srep45940.

Giaccio, B., Leicher, N., Mannella, G., Monaco, L., Regattieri, E., Wagner, B., Zanchetta, G., Gaeta, M., Marra, F., Nomade, S., Palladino, D.M., Pereira, A., Scheidt, S., Sottili, G., Wonik, T., Wulf, S., Zeeden, C., Ariztegui, D., Cavinato, G.P., Dean, R.J., Florindo, F., Leng, M.J., Macrì, P., Niespolo, E., Renne, P.R., Rolf, C., Sadori, L., Thomas, C., Tzedakis, P.C., 2019. Extending the tephra and paleoenvironmental record of the Central Mediterranean back to 430 ka: A new core from Fucino Basin, central Italy. *Quat. Sci. Rev.* **225**, 106003. https://doi.org/10.1016/j.quascirev.2019.106003.

Giaccio, B., Marra, F., Hajdas, I., Karner, D.B., Renne, P.R., Sposato, A., 2009. ^{40}Ar/^{39}Ar and ^{14}C geochronology of the Albano maar deposits: Implications for defining the age and eruptive style of the most recent explosive activity at Colli Albani Volcanic District, Central Italy. *J. Volcanol. Geotherm. Res.* **185**, 203-213. https://doi.org/10.1016/j.jvolgeores.2009.05.011.

Giaccio, B., Niespolo, E.M., Pereira, A., Nomade, S., Renne, P.R., Albert, P.G., Arienzo, I., Regattieri, E., Wagner, B., Zanchetta, G., Gaeta, M., Galli, P., Mannella, G., Peronace, E., Sottili, G., Florindo, F., Leicher, N., Marra, F., Tomlinson, E.L., 2017a. First integrated tephrochronological record for the last ∼190 kyr from the Fucino Quaternary lacustrine succession, central Italy. *Quat. Sci. Rev.* **158**, 211-234. https://doi.org/10.1016/j.quascirev.2017.01.004.

Giaccio, B., Nomade, S., Wulf, S., Isaia, R., Sottili, G., Cavuoto, G., Galli, P., Messina, P., Sposato, A., Sulpizio, R., Zanchetta, G., 2012b. The late MIS 5 Mediterranean tephra markers: a reappraisal from peninsular Italy terrestrial records. *Quat. Sci. Rev.* **56**, 31-45. https://doi.org/10.1016/j.quascirev.2012.09.009.

Giaccio, B., Isaia, R., Fedele, F.G., Di Canzio, E., Hoffecker, J., Ronchitelli, A., Sinitsyn, A.A., Anikovich, M., Lisitsyn, S.N., Popov, V.V., 2008. The Campanian Ignimbrite and Codola tephra layers: Two temporal/stratigraphic markers for the Early Upper Palaeolithic in southern Italy and eastern Europe. *J. Volcanol. Geotherm. Res.* **177** (1), 208-226. https://doi.org/10.1016/j.jvolgeores.2007.10.007.

Giannetti, B. & De Casa, G., 2000. Stratigraphy, chronology, and sedimentology of ignimbrites from the white trachytic tuff, Roccamonfina Volcano, Italy. *J. Volcanol. Geotherm. Res.* **96**, 3-4, 243-295. https://doi.org/10.1016/S0377-0273(99)00144-4.

Giannetti, B., 1996. The geology of the Yellow Trachytic Tuff, Roccamonfina Volcano. *J. Volcanol. Geotherm. Res.* **71** (1), 53-72. https://doi.org/10.1016/0377-0273(95)00030-5.

Giordano, G. & the CARG Team, 2010. Stratigraphy, volcano tectonics and evolution of the Colli Albani volcanic field. In: Funicello, R. & Giordano, G. (Eds.): The Colli Albani volcano. *Spec. Pub. IAVCEI* **3**, 43-97, *Geol. Soc., Lond.* (2010).

Goldstein, S.L., Denis, P., Oelkers, E.H., Rudnick, R.L., Walter, L.M., 2003. Standards for publication of isotope ratio and chemical data in chemical geology. *Chem. Geol.* **202**, 1-4. https://doi.org/10.1016/j.chemgeo.2003.08.003.

Hays, J.D., Imbrie, I., Shackleton, N.J., 1976. Variations in the Earth's orbit: pacemaker of the ice ages. *Science* **194**, 1121-1131. https://doi.org/10.1126/science.194.4270.1121.

Hayward, C., 2011. High spatial resolution electron probe microanalysis of tephras and melt inclusion without beam-induced chemical modification. *The Holocene* **22** (1), 119-125. https://doi.org/10.1177%2F0959683611409777.

Irvine, T.N. & Baragar, W.R.A., 1971. A guide to the chemical classification of the common volcanic rocks. *Canad. J. Earth Sci.* **8 (5)**, 523-548. https://doi.org/10.1139/e71-055.

Jarosewich, E., Nelen, J.A., Norberg, J.A., 1980. Reference samples for elctron microprobe analysis. *Geostand. Newsl.* **4 (1)**, 43-47. https://doi.org/10.1111/j.1751-908X.1980.tb00273.x.

Jicha, B.R., Singer, B.S., Sobol, P., 2016. Re-evaluation of the ages of $^{40}Ar/^{39}Ar$ sanidine standards and supereruptions in the western U.S. using a Noblesse multi-collector mass spectrometer. *Chem. Geol.* **431**, 54-66. https://doi.org/10.1016/j.chemgeo.2016.03.024.

Jochum, K.P., Stoll, B., Herwig, K., Willbold, M., Hofmann, A.W., Amini, M., Aarbug, S., Abouchami, W., Hellebrand, E., Mocek, B., Raczek, I., Stracke, A., Alard, O., Bouman, C., Becker, S., Dücking, M., Brätz, H., Klemd, R., de Bruin, D., Canil, D., Cornell, D., de Hoog, C.-S., Dalpé, C., Danyushevsky, L., Eisenhauer, A., Gao, Y., Snow, J.E., Groschopf, N., Günther, D., Latkoczy, C., Guillong, M., Hauri, E.K., Höfer, H.E., Lahaye, Y., Horz, K., Jacob, D.E., Kasemann, S.A., Kent, A.J.R., Ludwig, T., Zack, T., Mason, P.R.D., Meixner, A., Rosner, M., Kisawa, K., Nash, P.B., Pfänder, J., Premo, W.R., Sun, W.D., Tiepolo, M., Vannucci, R., Vennemann, T., Wayne, D., Woodhead, J.D., 2006. MPI-DING reference glasses for in situ microanalysis: New reference values for element concentrations and isotope ratios. *Geochem. Geophys.* **7**:2. https://doi.org/10.1029/2005GC001060.

Keller, J., Ryan, W.B.F., Ninkovich, D., Altherr, R., 1978. Explosive volcanic activity in the Mediterranean over the last 200,000 yr as recorded in deep-sea sediments. *Geol. Soc. Am. Bull.* **89**, 591-604. https://doi.org/10.1130/0016-7606(1978)89%3C591:EVAITM%3E2.0.CO;2.

Koppers, A.A.P., 2002. ArArCALC e software for $^{40}Ar/^{39}Ar$ age calculations. *Comput. Geosci.* **28**, 605-619. https://doi.org/10.1016/S0098-3004(01)00095-4.

Kuehn, S.C., Froese, D.G., Shane, P.A.R. 2011. The INTAV intercomparison of electron-beam microanalysis of glass by tephrochronology laboratories: Results and recommendations. *Quat. Int.* **246 (1-2)**, 19-47. https://doi.org/10.1016/j.quaint.2011.08.022.

Kutterolf, S., Schindlbeck, J.C., Jegen, M., Freundt, A., Straub, S.M., 2019. Milankovitch frequencies in tephra records at volcanic arcs: The relation of kyr-scale cyclic variations in volcanism to global climatic changes. *Quat. Sci. Rev.* **204**, 1-16. https://doi.org/10.1016/j.quascirev.2018.11.004.

Lane, C.S., Brauer, A., Blockley, S.P.E., Dulski, P., 2013. Volcanic ash reveals time-transgressive abrupt climate change during the Younger Dryas. *Geology* **41** (12), 1251-1254. https://doi.org/10.1130/G34867.1.

Lane, C.S., Cullen, V.L., White, D., Bramham.Law, C.W.F., Smith, V.C., 2014. Cryptotephra as a dating and correlation tool in archaeology. *J. Archaeol. Sci.* **42**, 42-50. https://doi.org/10.1016/j.jas.2013.10.033.

Lane, C.S., Lowe, D.J., Blockley, S.P.E., Suzuki, T., Smith, V.C., 2017. Advancing tephrochronology as a global dating tool: Applications in volcanology, archaeology and palaeoclimatic research. *Quat. Geochronol.* **40**, 1-7. https://doi.org/10.1016/j.quageo.2017.04.003.

Laurenzi, M.A. & Villa, I.M., 1987. $^{40}Ar/^{39}Ar$ chronostratigraphy of Vico ignimbrites. *Period. Mineral.* **56**, 285-293.

Le Maitre, R.W., Streckeisen, A., Zanettin, B., Le Bas, M.J., Bonin, B., Bateman, P., Bellieni, G., Dudek, A., Efremova, S., Keller, J., Lameyre, J., Sabine, P.A., Schmid, R., SØrensen, H., Woolley, A.R., 2002. Igneous Rocks: A Classification and Glossary of Terms. Reccomendation of the International Union of Geological Sciences Subcommission on the Systematics of Igneous Rocks, 2nd Edition. Cambridge University Press, Cambridge. 236 pages.

Lee, J.Y., Marti, K., Severinghaus, J.P., Kawamura, K., Yoo, H.S., Lee, J.B., Kim, J.S., 2006. A redetermination of the isotopic abundances of atmospheric Ar. *Geochim. Cosmochim. Acta* **70** (17), 4507-4512. https://doi.org/10.1016/j.gca.2006.06.1563.

Leicher, Giaccio, B., Zanchetta, G., Sulpizio, R., Albert, P.G., Tomlinson, E.L., Lagos, M., Francke, A., Wagner, B., 2021. Lake Ohrid's tephrochronological dataset reveals 1.36 Ma of Mediterranean explosive volcanic activity. *Sci. Data* **8**, 231. https://doi.org/10.1038/s41597-021-01013-7.

Leicher, N., Giaccio, B., Zanchetta, G., Wagner, B., Francke, A., Palladino, D.M., Sulpizio, R., Albert, P.G., Tomlinson, E.L., 2019. Central Mediterranean explosive volcanism and tephrochronology during the last 630 ka based on the sediment record from Laker Ohrid, *Quat. Sci. Rev.* **226**, 106021. https://doi.org/10.1016/j.quascirev.2019.106021.

Leicher, N., Zanchetta, G., Sulpizio, R., Giaccio, B., Wagner, B., Nomade, S., Francke, A., Del Carlo, P., 2016. First tephrostratigraphic results of the DEEP site record from Lake Ohrid (Macedonia and Albania). *Biogeosciences* **13**, 2151-2178. https://doi.org/10.5194/bg-13-2151-2016.

Lisiecki, L.E. & Raymo, M.E., 2005. A Pliocene-Pleistocene stack of 57 globally distributed benthic d18O records. *Palaeoceanogr. Palaeoclimatol.* **20** (1), PA1003. https://doi.org/10.1029/2004PA001071.

Lowe, D.J., 2011. Tephrochronology and its application: A review. *Quat. Geochronol.* **6**, 107-153. https://doi.org/10.1016/j.quageo.2010.08.003.

Lowe, D.J., Pearce, N.J.G., Jorgensen, M.A., Kuhen, S., Tyron, C.A., Hayward, C.L., 2017. Correlating tephras and cryptotephras using glass compositional analyses and numerical and statistical methods: Review and evaluation. *Quat. Sci. Rev.* **175**, 1-44. https://doi.org/10.1016/j.quascirev.2017.08.003.

Ludwig, K.R., 2012. User's Manual for Isoplot Version 3.75-4.15: A Geochronological Toolkit for Microsoft Excel. *Berkley Geochronological Centre Special Publication* **5**.

Mannella, G., Giaccio, B., Zanchetta, G., Regattieri, E., Niespolo, E.M., Pereira, A., Renne, P.R., Nomade, S., Leicher, N., Perchiazzi, N., Wagner, B., 2019. Paleoenvironmental and paleohydrological variability of mountain areas in the central Mediterranean region: A 190-ka-long chronicle from the independently dated Fucino paleolake record (central Italy). *Quat. Sci. Rev.* **210**, 190-210. https://doi.org/10.1016/j.quascirev.2019.02.032.

Marianelli, P. & Sbrana, A. Risultati di misure standard di minerali e di vetri naturali in microanalisi a dispersione di energia (In Italian). *Atti Soc. Tosc. Sci. Nat. Resid. Pisa, Mem. Serie A* **105**, 57-63 (1998).

Marra, F., Castellano, C., Cucci, L., Florindo, F., Gaeta, M., Jicha, B., Palladino, D.M., Sottili, G., Tertulliani, A., Tolomei, C., 2020. Monti Sabatini and Colli Albani: the dormant twin volcanoes at the gates of Rome. *Sci. Rep.* **10**:8666. https://doi.org10.1038/s41598-02-65394-2.

Marra, F., Freda, C., Scarlato, P., Taddeucci, J., Karner, D.B., Renne, P.R., Gaeta, M., Palladino, D.M., Triglia, R., Cavaretta, G., 2003. Post-caldera activity in the Alban Hills volcanic district (Italy): ^{40}Ar/^{39}Ar geochronology and insights into magma evolution. *Bull. Volcanol.* **65**, 227-247. https://doi.org/10.1007/s00445-002-0255-9.

Marra, F., Gaeta, M., Giaccio, B., Jicha, B.R., Palladino, D.M., Polcari, M., Sottili, G., Taddeucci, J., Florindo, F., Stramondo, S., 2016. Assessing the volcanic hazard for Rome: ^{40}Ar/^{39}Ar and In-SAR constraints on the most recent eruptive activity and present-day uplift at Colli Albani Volcanic District. *Geophys. Res. Lett.* **43**, 6898-6906. https://doi.org/10.1002/2016GL069518.

Marra, F., Karner, D.B., Freda, C., Gaeta, M., Renne, P., 2009. Large mafic eruptions at Alban Hills Volcanic District (Central Italy): chronostratigraphy, petrography and eruptive behavior. *J. Volcanol. Geotherm. Res.* **179**, 217-232. https://doi.org/10.1016/j.jvolgeores.2008.11.009.

Marra, F., Nomade, S., Pereira, A., Petronio, C., Salari, L., Sottili, G., Bahain, J.J., Boschian, G., Di Stefano, G., Falguères, C., Florindo, F., Gaeta, M., Giaccio, B., Masotta, M., 2018. A review of the geological sections and the faunal assemblages of Aurelian Mammal Age of Latium (Italy) in the light of a new chronostratigraphic framework. *Quat. Sci. Rev.* **181**, 173-199. https://doi.org/10.1016/j.quascirev.2017.12.007.

Martrat, B., Grimalt, J.O., Shackleton, N.J., de Abreu, L., Hutterli, M.A., Stocker, T.F., 2007. Four climate cycles of recurring deep and surface water destabilizations on the Iberian margin. *Science* **317**, 502-507. https://www.science.org/doi/10.1126/science.1139994.

McDonough, W.F. & Sun, S.-s., 1995. The composition of the Earth. *Chem. Geol.* **120** (3-4), 223-253. https://doi.org/10.1016/0009-2541(94)00140-4.

Mixon, E.E., Jicha, B.R., Tootell, D., Singer, B.S., 2022. Optimizing 40Ar/39Ar analyses using the Isotopx NGX-600 mass spectrometer. *Chem. Geol.* **593**, 120753. https://doi.org/10.1016/j.chemgeo.2022.120753.

Monaco, L., Palladino, D.M., Albert, P.G., Arienzo, I., Conticelli, S., Di Vito, M., Fabbrizio, A., D'Antonio, M., Isaia, R., Manning, C.J., Nomade, S., Pereira, A., Petrosino, P., Sottili, G., Sulpizio, R., Zanchetta, G., Giaccio, B., 2022. Linking the Mediterranean MIS 5 tephra markers to Campi Flegrei (southern Italy) 109-92 ka explosive activity and refining the chronology of MIS 5c-d millennial-scale climatic variability. *Glob. Pla. Che.* **211**, 103785. https://doi.org/10.1016/j.gloplacha.2022.103785.

Monaco, L., Palladino, D.M., Gaeta, M., Marra, F., Sottili, G., Leicher, N., Mannella, G., Nomade, S., Pereira, A., Regattieri, E., Wagner, B., Zanchetta, G., Albert, P.G., Arienzo, I., D'Antonio, M., Petrosino, P., Manning, C., Giaccio, B., 2021. Mediterranean tephrostratigraphy and peri-Tyrrhenian explosive activity revaluated in light of the 430-365 ka record from Fucino Basin (central Italy). *Earth Sci. Rev.* **220**, 103706. https://doi.org/10.1016/j.earscirev.2021.103706.

Munno, R. & Petrosino, P., 2007. The late Quaternary tephrostratigraphical record of the San Gregorio Magno basin (southern Italy). *J. Quat. Sci*. **22**, 247-266. https://doi.org/10.1002/jqs.1025.

Nappi, G., Capaccioni, B., Mattioli, M., Mancini, F., & Valentini, L., 1994. Plinian fall deposits from Vulsini Volcanic District (Central Italy). *Bull. Volcanol.* **56**, 502-515. https://doi.org/10.1007/BF00302831.

Niespolo, E.M., Rutte, D., Deino, A.L., Renne, P.R., 2017. Intercalibration and age of the Alder Creek Sanidine ^{40}Ar/^{39}Ar standard. *Quat. Geochronol.* **39**, 205-213. https://doi.org/10.1016/j.quageo.2016.09.004.

Pabst, S., Wörner, G., Civetta, L., Tesoro, R., 2007. Magma chamber evolution prior to the Campanian Ignimbrite and Neapolitan Yellow Tuff eruptions (Campi Flegrei, Italy). *Bull. Volcanol.* **70**, 961-976. https://doi.org/10.1007/s00445-007-0180-z.

Palladino, D.M. & Agosta, E., 1997. Pumice fall deposits of the Western Vulsini Volcanoes (Central Italy). *J. Volcanol. Geotherm. Res.* **78** (1-2), 77-102. https://doi.org/10.1016/S0377-0273(96)00107-2.

Palladino, D.M. & Simei, S., 2005. Eruptive dynamics and caldera-collapse during the Onano eruption, Vulsini, Italy. *Bull. Volcanol.* **67**, 423-440. https://doi.org/10.1007/s00445-004-0385-3.

Palladino, D.M. & Taddeucci, J., 1998. The basal ash deposit of the Sovana Eruption (Vulsini Volcanoes, central Italy): the product of a dilute pyroclastic density current. J. *Volcanol. Geotherm. Res.* **87** (1-4), 233-254. https://doi.org/10.1016/S0377-0273(98)00095-X.

Palladino, D.M. & Valentine, G.A., 1995. Coarse-tail vertical and lateral grading in pyroclastic flow deposits of the Latera Volcanic COmples (Vulsini, central Italy): origin and implications for flow dynamics. *J. Volcanol. Geotherm. Res.* **69** (3-4), 343-364. https://doi.org/10.1016/0377-0273(95)00036-4.

Palladino, D.M., Gaeta, M., Giaccio, B., Sottili, G., 2014. On the anatomy of magma chamber and caldera collapse: the example of trachyphonolite explosive eruptions of the Roman province (Central Italy). *J. Volcanol. Geotherm. Res.* **281**, 12-26. https://doi.org/10.1016/j.jvolgeores.2014.05.020.

Palladino, D.M., Simei, S., Sottili, G., Trigila, R., 2010. Integrated approach for the reconstruction of stratigraphy and geology of Quaternary volcanic terrains: an application to the Vulsini Volcanoes (central Italy). In: Groppelli, G., Viereck, e L. (Eds.), Stratigraphy and Geology in Volcanic Areas. *Geol. Soc. Am. Spec. Pap.* **464**, 66–84.

Palladino, D.M., Simei, S., Triglia, R., 2016. Note Illustrative della Carta geologica d'Italia alla scala 1:50.000, foglio 344 Tuscania, *ISPRA-Servizio Geologico d'Italia* (In Italian). https://www.isprambiente.gov.it/Media/carg/note_illustrative/344_Tuscania.pdf.

Pappalardo, L., Civetta, L., D'Antonio, M., Deino, A., Di Vito, M., Orsi, G., Carandente, A., de Vita, S., Isaia, R., Piochi, M., 1999. Chemical and Sr-isotopical evolution of the Phlegrean magmatic system before the Campanain Ignimbrite and the Neapolitan Yellow Tuff eruptions. *J. Volcanol. Geotherm. Res.* **91** (2-4), 141-166. https://doi.org/10.1016/S0377-0273(99)00033-5.

Past Interglacials Working Group of PAGES, 2016. Interglacials of the last 800,000 years. *Rev. Geophys.* **54**, 162-219. https://doi.org/10.1002/2015RG000482.

Patacca, E., Scandone, P., Di Luzio, E., Cavinato, G.P., Parotto, M., 2008. Structural architecture of the central Apennines: Interpretation of the CROP 11 seismic profile from the Adriatic coast to the orographic divide. *Tectonics* **27**, TC3006. https://doi.org/10.1029/2005TC001917.

Paterne, M., Guichard, F., Duplessy, J.C., Siani, G., Sulpizio, R., Labeyrie, J., 2008. A 90,000-200,000 yrs marine tephra record of Italian volcanic activity in the Central Mediterranean Sea. J. *Volcanol. Geotherm. Res.* **177**, 187-196. https://doi.org/10.1016/j.jvolgeores.2007.11.028.

Paterne, M., Guichard, F., Labeyrie, J., 1988. Explosive activity of the south Italian volcanoes during the past 80,000 years as determined by marine tephrochronology. *J. Volcanol. Geotherm. Res.* **34**, 153-172. https://doi.org/10.1016/0377-0273(88)90030-3.

Paterne, M., Guichard, F., Labeyrie, J., Gillot, P.Y., Duplessy, J.C., 1986. Tyrrhenian Sea tephrochronology of the oxygen isotope record for the past 60,000 years. *Mar. Geol.* **72**, 259-285. https://doi.org/10.1016/0025-3227(86)90123-4.

Pearce, N.J.G., Alloway, B., Wickham, C., 2019. Correlating weathered, microphenocryst-rich, intermediate tephra: An approach combining bulk and single shard analyses from the Lepué Tephra, Chile and Argentina. *Quat. Internat.* **500**, 71-82. https://doi.org/10.1016/j.quaint.2019.01.017.

Pearce, NJ.G., Perkins, W.T., Westgate, J.A., Gorton, M.P., Jackson, S.E., Neal, C.R., Chenery, S.P., 1997. A Compilation of New and Published Major and Trace Element Data for NIST SRM 610 and NIST SRM 612 Glass Reference Materials. *Geostand. Newslett.* **21** (1), 115-144. https://doi.org/10.1111/j.1751-908X.1997.tb00538.x.

Peccerillo, A., 2017. Cenozoic Volcanism in the Tyrrhenian Sea Region. In: IAVCEI, Advances in Volcanology, 2 ed. Springer, p. 400.

Pelullo, C., Cirillo, G., Iovine, R.S., Arienzo, I., Aulinas, M., Pappalardo, L., Petrosino P., Fernandez-Turiel, J.L., D'Antonio, M., 2020. Geochemical and Sr-Nd isotopic features of the Zaro volcanic complex: insights on the magmatic processes triggering a small-scale prehistoric eruption at Ischia island (south Italy). *Int. J. Earth Sci.* **109** (8), 2829-2849. https://doi.org/10.1007/s00531-020-01933-6.

Pereira, A., Nomade, S., Moncel, M.-H., Voinchet, P., Bahain, J.-J., Biddittu, I., Falguères, C., Giaccio, B., Manzi, G., Parenti, F., Scardia, G., Scao, V., Sottili, G., Vietti, A., 2018. Geochronological evidences of a MIS 11 to MIS 10 age for several landmark Acheulian sites from the Frosinone province (Lazio, Italy): Archaeological implications. *Quat. Sci. Rev.* **187**, 112-129. https://doi.org/10.1016/j.quascirev.2018.03.021.

Perini, G., Conticelli, S., Francalanci, L., 1997. Inferences on the volcanic history of the Vico volcano, Roman Magmatic Province, central Italy: stratigraphic, petrographic and geochemical data. *Mineral. Petrograph. Acta* **40**, 67-93.

Perini, G., Francalanci, L., Davidson, J.P., Conticelli, S., 2004. Evolution and Genesis of Magmas from Vico Volcano, Central Italy: Multiple Differentiation Pathways and Variable Parental Magmas. *J. Petrol.* **45** (1), 139-182. https://doi.org/10.1093/petrology/egg084.

Petrelli, M., Laeger, K., Perugini, D., 2016. High spatial resolution trace element determination of geological samples by laser ablation quadrupole plasma mass spectrometry: implications for glass analysis in volcanic products. *Geosci. J.* **20** (851-863. https://doi.org/10.1007/s12303-016-0007-z.

Petrosino, P., Arienzo, I., Mazzeo, F.C., Natale, J., Petrelli, M., Milia, A., Perugini, D., D'Antonio, M., 2019. The San Gregorio Magno lacusrine basin (Campania, southern Italy): improved characterization of the tephrostratigraphic markers based on trace elements and isotopic data. *J. Quat. Sci.* **34**, 393-404. https://doi.org/10.1002/jqs.3107.

Petrosino, P., Morabito, S., Jicha, B.R., Milia, A., Sprovieri, M., Tamburrino, S., 2016. Multidisciplnary tephrochronological correlation of marker events in the eastern Tyrrhenian Sea between 48 and 105 ka. *J. Volcanol. Geotherm. Res.* **315**, 79-99. https://doi.org/10.1016/j.jvolgeores.2016.02.001.

Poli, S., Chiesa, S., Gillot, P.-Y., Gregnanin, A., Guichard, F., 1987. Chemistry versus time in the volcanic complex of Ischia (Gulf of Naples, Italy): evidence of successive magmatic cycles. *Contrib. Mineral. Petrol.* **95**, 322-335.

Ponomareva, V.V., Portnyagin, M., Davies, S.M., 2015. Tephra without borders: far-reaching clues into past explosive eruptions. *Front. Earth Sci.* **3** (83). https://doi.org/10.3389/feart.2015.00083.

Regattieri, E., Giaccio, B., Zanchetta, G., Drysdale, R.N., Galli, P., Nomade, S., Peronace, E., Wulf, S., 2015. Hydrological variability over the Apennines during the Early Last Glacial precession minimum, as revelated by a stable isotope record from Sulmona basin, Central Italy. J. *Quat. Sci.* **30**, 19-31. https://doi.org/10.1002/jqs.2755.

Reimer, P.J., Austin, W.E.N., Bard, E., Bayliss, A., Blackwell, P.G., Bronk Ramsey, C., Butzin, M., Cheng, H., Edwards, R.L., Friedrich, M., Grootes, P.M., Guilderson, T.P., Hajdas, I., Heaton, T.J., Hogg, A.G., Hughen, H.A., Kromer, B., Manning, S.W., Muscheler, R., Palmer, J.G., Pearson, C., van der Plicht, J., Reimer, R.W., Richards, D.A., Scott, E.M., Southon, J.R., Turney, C.S.M., Wacker, L., Adolphi, F., Büntgen, U., Capano, M., Fahrni, S.M., Fogtmann-Schulz, A., Friedrich, R., Köhler, P., Kudsk, S., Miyake, F., Olsen, J., Reinig, F., Sakamoto, M., Sookdeo, A., Talamo, S., 2020. The Intcal20 northern hemisphere radiocarbon age calibration curve (0-55 cal kBP). Radiocarbon 62 (4), 725-757. https://doi.org/10.1017/RDC.2020.41.

Renne, P.R., Balco, G., Ludwig, K.R., Mundil, R., Min, K., 2011. Response to the comment by WH Schwarz et al. on "Joint determination of 40 K decay constants and ^{40}Ar*/^{40}K for the Fish Canyon sanidine standard, and improved accuracy for ^{40}Ar/^{39}Ar geochronology" by PR Renne et al. (2010). *Geochim. Cosmochim. Acta* **75**, 5097-5100.

Rolandi, G., Bellucci, F., Heizler, M.T., Belkin, H.E., De Vivo, B., 2003. Tectonic controls on the genesis of ignimbrite from the Campanian Volcanic Zone, southern Italy. *Mineral. Petrol.* **79**, 3-31. https://doi.org/10.1007/s00710-003-0014-4.

Ross, J., 2019. NMGRL/pychron v18.2: *Zenodo.* https://doi.org/10.5281/zenodo.3237834.

Rouchon, V., Gillot, P.Y., Quidelleur, X., Chiesa, S., Floris, B., 2008. Temporal evolution of the Roccamonfina volcanic complex (Pleistocene), Central Italy. *J. Volcanol. Geotherm. Res.* **177**, 500-514. https://doi.org/10.1016/j.jvolgeores.2008.07.016.

Roucoux, K.H., Tzedakis, P.C., Frogley, M.R., Lawson, I.T., Preece, R.C., 2008. Vegetation history of the marine isotope stage 7 interglacial complex at Ioannina, NW Greece. *Quat. Sci. Rev*. **27**, 1378-1395. https://doi.org/10.1016/j.quascirev.2008.04.002.

Ruddiman, W.F., McIntyre, A., 1982. Severity and speed of Northern Hemisphere glaciation pulses: The limiting case? *Geol. Soc. Am. Bull*. **93**, 1273–1279. https://doi.org/10.1130/0016-7606(1982)93%3C1273:SASONH%3E2.0.CO;2.

Sadori, L., Koutsodendris, A., Panagiotopoulos, K., Masi, A., Bertini, A., Combourieu-Nebout, N., francke, A., Koull, K., Joannin, S., Mercuri, A.M., Peyron, O., Torri, P., Wagner, B., Sinopoli, G., Donders, T.H., 2016. Pollen-based paleoenvironmental and paleoclimatic change at Lake Ohrid (south-eastern Europe) during the past 500 ka. Biogeosciences 13, 1423-1437. https://doi.org/10.5194/bg-13-1424-2016.

Sadori, L., Koutsodendris, A., Panagiotopoulos, K., Masi, A., Bertini, A., Combourieu-Nebout, N., francke, A., Koull, K., Kousis, I., Joannin, S., Mercuri, A.M., Peyron, O., Torri, P., Wagner, B., Sinopoli, G., Donders, T.H., 2018. Pollen data of the last 500 ka BP at Lake Ohrid (south-eastern Europe). PANGAEA. https://doi.org/10.1594/PANGAEA.892362.

Satow, C., Tomlinson, E.L., Grant, K.M., Albert, P.G., Smith, V.C., Manning, C.J., Ottolini, L., Wulf, S., Rohling, E.J., Lowe, J.J., Blockley, S.P.E., Menzies, M.A., 2015. A new contribution to the Late Quaternary tephrostratigraphy of the Mediterranean: Aegean Sea core LC21. *Quat. Sci. Rev.* **117**, 96-112. https://doi.org/10.1016/j.quascirev.2015.04.005.

Sbrana, A., Marianelli, P., Pasquini, G., 2018. Volcanology of Ischia. *J. Maps* **14** (2) 494-503. https://doi.org/10.1080/17445647.2018.1498811.

Shane, P., 2000. Tephrochronology, a New Zealand case study. Earth-Science Reviews, 49, 1-4, 223-259. https://doi.org/10.1016/S0012-8252(99)00058-6.

Smith, D.G.W. & Westgate, J.A., 1968. Electron probe technique for characterising pyroclastic deposits. *Earth Planet. Sci. Lett.* **5**, 313-319. https://doi.org/10.1016/S0012-821X(68)80058-5.

Snyder, C.W., 2016. Evolution of global temperature over the past two million years. *Nature* **538**, 226-228. https://doi.org/10.1038/nature19798.

Sollevanti, F., 1983. Geologic, volcanologic, and tectonic setting of the Vico-Cimino area, Italy. *J. Volcanol. Geotherm. Res.* **17** (1-4), 203-217. https://doi.org/10.1016/0377-0273(83)90068-9.

Sottili, G., Arienzo, I., Castorina, F., Gaeta, M., Giaccio, B., Marra, F., Palladino, D.M., 2019. Time-dependent Sr and Nd isotope variations during the evolution of ultrapotassic Sabatini Volcanic District (Roman Province, Central Italy). *Bull. Volcanol.* **81**:67. https://doi.org/10.1007/s00445-019-1324-7.

Sottili, G., Palladino, D.M., Gaeta, M., Masotta, M., 2012. Origins and energetics of maar volcanoes: examples from the ultrapotassic Sabatini VOlcanic District (Roman Province, Central Italy). *Bull. Volcanol.* **74**, 163-186. https://doi.org/10.1007/s00445-011-0506-8.

Sottili, G., Palladino, D.M., Marra, F., Jicha, B., Karner, D.B., Renne, P., 2010. Geochronology of the most recent activity in the Sabatini volcanic district, Roman Province, central Italy. *J. Volcanol. Geotherm. Res.* **196**, 20-30. https://doi.org/10.1016/j.jvolgeores.2010.07.003.

Sparks, R.S.J., 1975. Stratigraphy and geology of the ignimbrites of Vulsini Volcano, central Italy. *Geologische Rundschau* **64** (1), 497-523. https://doi.org/10.1007/BF01820680.

Sunyé-Puchol, I., Hodgetts, A.G.E., Watt, S.F.L., Arce, J.L., Barfod, D.N., Mark, D.F., Sosa-Ceballos, G., Siebe, C., Dymock, R.C., Blaauw, M., Smith, V.C., 2022. Reconstructing the middle to late Pleistocene explosive eruption histories of Popocatépetl, Itzaccíhuatl and Tláloc-Telapón volcanoes in central México. *J. Volcanol. Geotherm. Res.* 421, 107413. https://doi.org/10.1016/j.jvolgeores.2021.107413.

Taddeucci, J. & Palladino, D.M., 2002. Particle size-density relationships in pyroclastic deposits: inferences from emplacement processes. *Bull. Volcanol.* **64**, 273-284. https://doi.org/10.1007/s00445-002-0205-6.

Thorarinsson, S., 1944. Tefrokronologiska Studier På Island. Pjórsárdalur Och Dess Förödelse. *Geografiska Annaler* **26** (1-2), 1-217. https://doi.org/10.1080/20014422.1944.11880727.

Thorarinsson, S., 1981a. Greetings from Iceland. Geografiska Annaler: Series A, Physical Geography, 63:3-4, 109-118.

Thorarinsson, S., 1981b. Tephra studies and tephrochronology: a historical review with special reference to Iceland. In: S. Self, R.S.J., Sparks (Eds.), Tephra Studies, Reidel, Dordrecht (1981), pp. 1-12. https://doi.org/10.1007/978-94-009-8537-1_1.

Tomlinson, E.L., Arienzo, I., Civetta, L., Wulf, S., Smith, V.C., Hardiman, M., Lane, C.S., Carandente, A., Orsi, G., Rosi, M., Müller, W., Menzies, M.A., 2012. Geochemistry of the Phlegrean Fields (Italy) proximal sources for major Mediterranean tephras: Implications for the dispersal of Plinian and co-ignimbritic components of explosive eruptions. *Geochim. Cosmochim. Acta* **93**, 102-128. https://doi.org/10.1016/j.gca.2012.05.043.

Tomlinson, E.L., Smith, V.C., Albert, P.G., Aydar, E., Civetta, L., Cioni, R., çubukçu, E., Gertisser, R., Isaia, R., Menzies, M.A., Orsi, G., Rosi, M., Zanchetta, G., 2015. The major and trace element glass compositions of the productive Mediterranean volcanic sources: tools for correlating distal tephra layers in and around Europe. *Quat. Sci. Rev.* **118**, 48-66. https://doi.org/10.1016/j.quascirev.2014.10.028.

Tonarini, S., D'Antonio, M., Di Vito, M.A., Orsi, G., Carandente, A., 2009. Geochemical and Ba-Sr-Nd isotopic evidence for mingling and mixing processes in the magmatic system that fed the Astroni volcano (4.1-3.8 ka) within the Campi Flegrei caldera (southern Italy). *Lithos* **107** (3-4), 135-151. https://doi.org/10.1016/j.lithos.2008.09.012.

Turbeville, B.N., 1992. $^{40}Ar/^{39}Ar$ ages and Stratigraphy of the Latera caldera, Italy. *Bull. Volcanol.* **55**, 110-118. https://doi.org/10.1007/BF00301124.

Tzedakis, P.C., Crucifix, M., Mitsui, T., Wolff, E.W., 2017. A simple rule to determine which insolation cycles lead to interglacials. *Nature* **542**, 427-432. https://doi.org/10.1038/nature21364.

Tzedakis, P.C., Hooghiemstra, H., Pälike, H., 2006. The last 1.35 milion years at Tenaghi Philippon: revised chrnostratigraphy and long-term vegetation trends. *Quat. Sci. Rev.* **25** (23-24), 3416-3430. https://doi.org/10.1016/j.quascirev.2006.09.002.

Tzedakis, P.C., Roucoux, K. H., de Abreu, L., Shackleton, N. J., 2004. The duration of forest stages in southern Europe and interglacial climate variability. *Science* **306**, 2231-2235, https://doi.org/10.1126/science.1102398.

Tzedakis, P.C., Wolff, E.W., Skinner, L.C., Brovkin, V., Hodell, D.A., McManus, J.F., Raynaud, D., 2012. Can we predict the duration of an interglacial? *Clim. Past.* **8**, 1473-1485, https://doi.org/10.5194/cp-8-1473-2012.

Vakhrameeva, P., Koutsodendris, A., Wulf, S., Fletcher, W.J., Appelt, O., Knipping, M., Gertisser, R., Trieloff, M., Pross, J., 2018. The cryptotephra record of the Marine Isotope Stage 12 to 10 interval (460-335 ka) at Tenaghi Philippon, Greece: Exploring chronological markers for the Middle Pleistocene of the Mediterranean region. *Quat. Sci. Rev.* **200**, 313-333. https://doi.org/10.1016/j.quascirev.2018.09.019.

Vakhrameeva, P., Koutsodendris, A., Wulf, S., Portnyagin, M., Appelt, O., Ludwig, T., Trieloff, M., Pross, J., 2021. Land-sea correlations in the Eastern Mediterranean region over the past c. 800 kyr based on macro- and cryptotephras from ODP Site 964 (Ionian Basin). *Quat. Sci. Rev.* **255**, 106811. https://doi.org/10.1016/j.quascirev.2021.106811.

Vakhrameeva, P., Wulf, S., Koutsodendris, A., Tjallingii, R., Fletcher, W.J., Appet, O., Ludwig, T., Knipping, M., Trieloff, M., Pross, J., 2019. Eastern Mediterranean volcanism during Marine isotope stages 9 to 7e (335-235 ka): Insights based on cryptotephra layers at Tenaghi Philippon, Greece. *J. Volcanol. Geotherm. Res.* **380**, 31-47. https://doi.org/10.1016/j.jvolgeores.2019.05.016.

Valentine, G.A., Palladino, D.M., DiemKaye, K., Fletcher, C., 2019. Lithic-rich and lithic-poor ignimbrites and their basal deposits: Sovana and Sorano formations (Latera caldera, Italy). *Bull. Volcanol.* **81**, 29. https://doi.org/10.1007/s00445-019-1288-7.

Vezzoli, L., Conticelli, S., Innocenti, F., Landi, P., Manetti, P., Palladino, D.M., Trigila, R., 1987. Stratigraphy of the Latera Volcanic Complex: proposals for a new nomenclature. *Period. Mineral.* **56**, 89-110.

Villa, P., Soriano, S., Pollarolo, L., Smiriglio, C., Gaeta, M., D'Orazio, M., Conforti, J., Tozzi, C., 2020. Neandertals on the beach: Use of marine resources at Grotta dei Moscerini (Latium, Italy). *PLoS ONE* **15** (1), e0226690. https://doi.org/10.1371/journal.pone.0226690.

Wagner, B., Vogel, H., Francke, A., Friederich, T., Donders, T., Lacey, J.H., Leng, M.J., Regattieri, E., Sadori, L., Wilke, T., Zanchetta, G., Albrecht, C., Bertini, A., Combourieu-Nebout, N., Cvetkoska, A., Giaccio, B., Grazhdani, A., Hauffe, T., Holtvoeth, J., Joannin, S., Lagoos, M., Leicher, N., Levkov, Z., Lindhorst, K., Masi, A., Melles, M., Mercuri, A.M., Nomade, S., Nowaczyk, N., Panagiotopoulos, K., Peyron, O., reed, J.M., Sagnotti, L., Sinopoli, G., Stellbrink, B., Sulpizio, R., Timmermann, A., Tofilovska, S., Torri, P., Wagner-Cremer, F., Wonik, T., Zhang, X., 2019. Mediterranean winter rainfall in phase with African monsoons during the past 1.36 million years. *Nature* **573**, 256-260. https://doi.org/10.1038/s41586-019-1529-0.

Wastegård, S., Veres, D., Kliem, P., Hahn, A., Ohlendorf, C., Zolitschka, B., The PASADO Science Team, 2013. Towards a late Quaternary tephrochronological framework for the suouthernmost part of South America – the Laguna Potrok Aike tephra record. *Quat. Sci. Rev.* **71**, 81-90. https://doi.org/10.1016/j.quascirev.2012.10.019.

Wendt, K.A., Li, X., Edwards, R.L., Cheng, H., Spötl, C., 2021. Precise timing of MIS 7 substages from the Austrian Alps. Clim. Past 17, 1443-1454. https://doi.org/10.5194/cp-17-1443-2021.

Wilson, M. & Bianchini, G., 1999. Tertiary-Quaternary magmatism within the Mediterranean and surroundings regions. In: Durand, B., Jolivet, L., Horvàth, F., Séranne, M. (eds.) The Mediterranean Basins: Tertiary extension within the Alpine Orogen. *Geol. Soc. Lond. Spec. Publ.* **156**, 141-169.

Wulf, S., Hardiman, M.J., Staff, R.A., Koutsodendris, A., Appelt, O., Blockley, S.P.E., Lowe, J.J., Manning, C.J., Ottolini, L., Schmitt, A.K., Smith, V.C., Tomlinson, E.L., Vakhrameeva, P., Knipping, M., Kotthoff, U., Milner, A.M., Müller, U.C., Christanis, K., Kalaitzidis, S., Tzedakis, P.C., Schmiedl, G., Pross, J., 2018. The Marine isotope stage 1-5 cryptotephra record of Tenaghi Philippon, Greece: Towards a detailed tephrostratigraphic framework for the Eastern Mediterranean region. *Quat. Sci. Rev.* **186**, 236-262. https://doi.org/10.1016/j.quascirev.2018.03.011.

Wulf, S., Keller, J., Paterne, M., Mingram, J., Lauterbach, S., Opitz, S., Sottili, G., Giaccio, B., Albert, P.G., Satow, C., Tomlinson, E.L., Viccaro, M., Brauer, A., 2012. The 100-133 ka record of Italian explosive volcanism and revised tephrochronology of Lago Grande di Monticchio. *Quat. Sci. Rev.* **58**, 104-123. https://doi.org/10.1016/j.quascirev.2012.10.020.

Wulf, S., Keller, J., Satow, C., Gertisser, R., Kraml M., Grant, K.M., Appelt, O., Vakhrameeva, P., Koutsodendris, A., Hardiman, M., Schulz, H., Pross, J., 2020. Advancing Santorini's tephrostratigraphy: New glass geochemical data and improved marine-terrestrial tephra correlations for the past ~360 kyrs. *Earth Sci. Rev.* **200**, 102964. https://doi.org/10.1016/j.earscirev.2019.102964.

Wulf, S., Kraml., M., Brauer, A., Keller, J., Negendank, J.F.W., 2004. Tephrochronology of the 100 ka lacustrine sediment record of Lago Grande di Monticchio (Southern Italy). *Quat. Int*. **122**, 7-30. https://doi.org/10.1016/j.quaint.2004.01.028.

Wulf, S., Kraml, M., Keller, J., 2008. Towards a detailed tephrostratigraphy in the Central Mediterranean: The last 20,000 yrs record of Lago Grande di Monticchio. J*. Volcanol. Geotherm. Res.* **177**, 118-132. https://doi.org/10.1016/j.jvolgeores.2007.10.009.

Zanchetta, G., Giaccio, B., Bini, M., Sarti, L., 2018. Tephrostratigraphy of Grotta del Cavallo, Southern Italy: insights of the chronology of Middle to Upper Paleolithic transition in the Mediterranean. *Quat. Sci. Rev.* **182**, 65-77. https://doi.org/10.1016/j.quascirev.2017.12.014.

Ziegler, M., Tuenter, E., Lourens, L.J., 2010. The precession phase of the boreal summer monsoon as viewed from the eastern Mediterranean (ODP Site 968). *Quat. Sci. Rev.* **29**, 1481-1490. https://doi.org/10.1016/j.quascirev.2010.03.011.